UNIVERSITÀ DEGLI STUDI DI PADOVA

UNIVERSITÀ DEGLI STUDI DI PADOVA
Dipartimento di Ingegneria Industriale DII
Corso di Laurea Magistrale in Ingegneria Meccanica

Thermo-structural analysis of the ITER large electrical Busbars

Relatore: Prof. Giovanni Meneghetti
Correlatore: Dott. Ing. Federico Fortunato (ITER Organization)

Laureando: Francesco Chitarin
Matr.1058239

Anno Accademico 2014/15

Contents

Disclaimer

The views and opinions expressed herein do not necessarily reflect those of the ITER Organization.

Acronyms – Glossary

BBMS	Bus Bar Monitoring System
CL	Current Lead
CPSS	Coil Power Supply System
CWC	Cooling Water Collector
DC DS	DC Disconnect Switch (Disconnector)
DB	Dry Box
DS	Disconnect Switch (Disconnector)
FDU	Fast Discharge Unit
SNU	Switching Network Units
I&C	Instrumentation & Control
LCC	Local Control Cubicle
MS	Make Switch
PMS	Protective Make Switch
PSS	Power Supply System
SCC	Signal Conditioning Cubicle
DC	Direct current
SIC	Safety Important Component
CC	Correction Coils
TF	Toroidal Field
PF	Poloidal Field
CS	Central Solenoid
INB	Basic Nuclear Installation
PPEN	Pulsed Power Electrical Network
RPC&HF	Reactive Power Compensation and Harmonic Filtering
CPSS	Coil Power Supplies System
SSEN	Steady State Electrical Network
H&CD	Heating & Current Drive
PS	Power Supply
CPSDS	Coil Power Supply and Distributed System

Sommario

La fusione nucleare è il processo che avviene nelle stelle, dove collidono nuclei di idrogeno ad alta velocità e fondono formando nuclei più leggeri ed è ad oggi la più promettente tecnologia per generare grandi quantitativi di energia elettrica in modo controllato senza emissioni di carbonio. Questo processo di fusione genera energia termica secondo la nota legge di Einstein $E=mc^2$.
La reazione più efficiente per la produzione di energia è quella tra Deuterio (D) e Trizio (T), isotopi dell'idrogeno (H), la quale produce a parità di temperatura il più alto guadagno di energia. La temperatura richiesta è pari a 150 000 000 °C, dieci volte la temperatura richiesta per le reazioni H-H nel sole. La più promettente tecnica per ottenere la fusione sulla terra è quella del Tokamak che utilizza campi magnetici toroidali e poloidali per contenere e controllare il plasma. Questa soluzione è utilizzata nel reattore sperimentale ITER a Cadarache (Francia). Per ottenere il campo magnetico necessario ci sono vari tipi di bobine superconduttive. Il Coil Power Supply System (CPSS) è il sistema che serve ad alimentare le bobine con alta corrente ed alta tensione. I DC Busbar sono i conduttori che portano corrente dai convertitori AC/DC alle bobine.
Questo lavoro è fatto in collaborazione con il Coil Power Supply Team (Section) di ITER Organization durante uno stage di sei mesi e si occupa di valutare la possibilità di danneggiamento dell'isolamento dei DC Busbar a causa dei carichi termici agenti su di esso.
I differenti coefficienti di dilatazione termica dovuti alla non omogeneità dei materiali generano tensioni in presenza di gradienti termici. Tali variazioni termiche sono per di più cicliche.
Sono stati quindi creati modelli 2-D e 3-D FEM con il software ANSYS per l'analisi delle deformazioni e delle tensioni nell'isolamento. In seguito sono state effettuate le verifiche sia statiche che a fatica considerando i valori di tensione e deformazione ammissibili utilizzati in "*Properties of magnets insulation: Structural Design Criteria for ITER Magnet Components"* (SDC-MC)" [11]. I valori ammissibili non sono stati mai superati sia per verifiche statiche sia per quelle a fatica.
Studi eseguiti all'interno dell'Efremov Institute (Russia) [9] hanno dimostrato che il campo elettrico attorno al conduttore, in presenza di distacchi o bolle d'aria, supererebbe il valore limite di rigidità dielettrica e quindi produrrebbe un danneggiamento progressivo dell'isolamento.
Per questo si è quindi eseguita una analisi di contatto tra l'isolamento e le altri parti del DC Busbar considerando ancora i carichi termici. Questa analisi ha permesso di constatare che la formazione di distacchi è molto limitata.

Introduction

Nuclear fusion is the most promising option for generating large amounts of carbon-free electric energy in the future. Nuclear fusion is the process that heats the Sun, where hydrogen nuclei collide at very high speed overcoming their electrostatic repulsion and reacting the domain of heavy nuclear interaction, where they fuse into a composite nucleus that quickly breaks up into a lighter system of nuclei converting the relevant mass defect in kinetic energy, according to Einstein law. In particular, every second, our Sun turns 600 million tons of hydrogen into helium, releasing an enormous amount of thermal power.
Twentieth-century fusion science has identified the most efficient fusion reaction to be reproduced in the laboratory setting in the reaction between two hydrogen (H) isotopes deuterium (D) and tritium (T). In fact, such a reaction produces the highest energy gain at the nonetheless 'lowest' temperature. It requires temperatures of 150,000,000 °C that are ten times higher than those needed for the H-H reactions occurring at the Sun's core. The most promising device adopting this technique is the TOKAMAK that uses toroidal and poloidal magnetic fields to contain and control the hot plasma. This solution is implemented in the ITER reactor in Cadarache (France).
To provide the necessary magnetic field in the Tokamak to contain the hot plasma there are several types of superconductive coils. The Coil Power Supply System (CPSS) feeds each coil with high current and high voltage. The DC Busbars are conductors that carry the current from AC/DC convertors to the coils. The most delicate part of this DC Busbars is the insulation that must withstand high voltage and cyclical thermal load.
This thesis work was done during an internship of six months in ITER Organization in Cadarache (France) in collaboration with the Coil Power Supply Section.
The first chapter is an introduction to nuclear fusion and to the ITER project. The second chapter describes generally the ITER Electrical Power Supply and focus on the Coil Power Supply System (CPSS).
The third chapter is an accurate description of the DC Busbars and all the parts related with them.
The fourth chapter is the report of the analysis of the electrical field around the conductor done by the Efremov Institute (Russia).
The fifth chapter is about the objectives of this thesis.
The sixth chapter describes the geometry of the various types of DC Busbar cross-section, the thermal loads considered in the following analysis and the material properties known and, in some cases, assumed.
The seventh chapter explains the failure criteria and the allowable stress and strain used for the verification of the DC Busbar insulation.
The eighth and ninth chapter are respectively about the 2-D and 3-D thermo-structural analysis and verification of the results on the insulation with allowable values of chapter seven.
These are FEM analysis held with ANSYS 15.
The tenth chapter is about the contact analysis for insulation detachment study.
The eleventh chapter is the summary of the results and conclusion of the work and the advice for the manufacturers.

1. Fusion

The research in the field of nuclear processes and, in particular, in the field of fusion dates back to the first decades of the last century. During this period, the attention of scientists was directed to understanding the mechanisms that underlie the energetic emission of the stars.
In 1929 the astronomer R. Atkinson and the physicist F. Houtermans developed the hypothesis that nuclear fusion reactions between two light nuclei could lead to the formation of a helium nucleus (He4) with the release of a significant amount of energy.
After with the studies of K. Weiszäcker and H. Bethe, two possible cycles of fusion reactions, called proton-proton chain and the carbon cycle where discovered.
The "proton-proton chain" (*Fig. 1.1*), which is probably the main fusion reaction that feeds the energy emission of the stars of relatively small mass and with temperatures of the order of 10^7 K, is a process in three phases which begins with the formation of deuterium from the interaction of two protons and leads to the formation of a nucleus of helium (He4) by four protons.

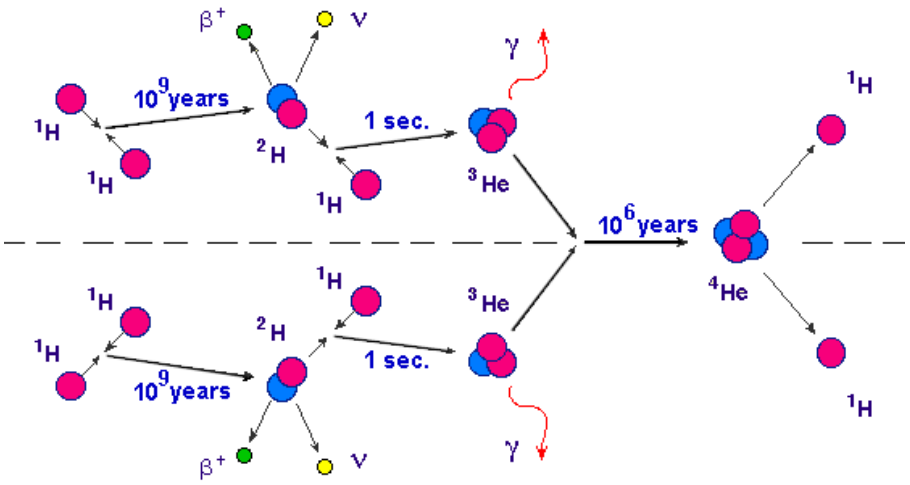

Figure 1.1 : Proton-proton chain [1]

The "carbon cycle" characteristic of the stars with relatively large mass and temperatures above 10^7 K, provides that the carbon (C12), nitrogen (N13 and N14) and oxygen (O15) act as "catalysts" in a sequence of reactions, articulated in total six stages, having as a final result the fusion of four hydrogen nuclei (H1) in a nucleus of He4. Both cycles of reaction just described are characterized by the emission of considerable amounts of energy. For example, for the carbon cycle the total energy released, dependent on the mass defect existing between the product and reagent nuclei, is equal to 26.73 MeV.
The prospect of the availability of large amounts of energy has led scientists, starting from the second half of the last century, to investigate the unresolved issues related to the implementation and control of nuclear fusion reaction.
After the completion of the first uncontrolled fusion reaction, triggered by E. Teller in the course of an experiment of war, during the sixties the efforts were mainly focused on the identification of reactions capable of being reproduced in a controlled manner, as well as the determination of the best conditions adapted to this reproduction (as evidenced by the works of L. Spitzer and L. Artsimovich).
The main fusion reactions identified are shown in *Table 1.1.*

Table 1.1: Major nuclear fusion reaction [1]

Name of the reaction		Fusion reaction	Abbreviated form	Energy released	
				MeV	Joule
D-T		${}^{2}_{1}D + {}^{3}_{1}T \rightarrow {}^{4}_{2}He\ (3.52) + {}^{1}_{0}n\ (14.06)$	$T\,(d,n)^4He$	17.58	$2.82 \cdot 10^{-12}$
D-D	D-Dn	${}^{2}_{1}D + {}^{2}_{1}D \rightarrow {}^{3}_{2}He\ (0.82) + {}^{1}_{0}n\ (2.45)$	$D\,(d,n)^3He$	3.27	$5.24 \cdot 10^{-13}$
	D-Dp	${}^{2}_{1}D + {}^{2}_{1}D \rightarrow {}^{3}_{1}T\ (1.01) + {}^{1}_{1}p\ (3.02)$	$D\,(d,p)T$	4.03	$6.46 \cdot 10^{-13}$
T-T		${}^{3}_{1}T + {}^{3}_{1}T \rightarrow {}^{1}_{0}n + {}^{1}_{0}n + {}^{4}_{2}He$	$T\,(t,2n)^4He$	11.3	$1.81 \cdot 10^{-12}$
D-^{3}He		${}^{2}_{1}D + {}^{3}_{2}He \rightarrow {}^{4}_{2}He\ (3.66) + {}^{1}_{1}p\ (14.64)$	${}^3He\,(d,p)^4He$	18.3	$2.93 \cdot 10^{-12}$
p-^{6}Li		${}^{1}_{1}p + {}^{6}_{3}Li \rightarrow {}^{4}_{2}He + {}^{3}_{2}He$	${}^6Li\,(p,\alpha)^3He$	4.02	$6.44 \cdot 10^{-13}$
p-^{11}B		${}^{1}_{1}p + {}^{11}_{5}B \rightarrow 3\,({}^{4}_{2}He)$	${}^{11}B\,(p,2\,\alpha)^4He$	8.68	$1.39 \cdot 10^{-12}$

In particular, the attention of scientists has focused more on the reactions Deuterium-Deuterium (D-D) and Deuterium-Tritium (D-T) (*Fig.1.2*) which are, at present, the best options on which it is necessary to focus for future fusion power reactors, also because of the very high energy yield.

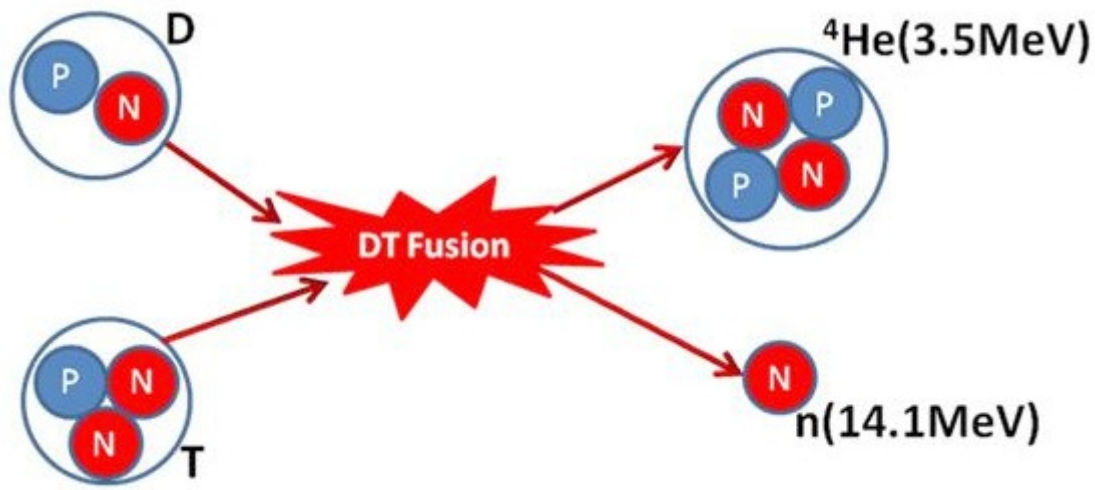

Figure 1.2: Deuterium-Tritium [14]

The nuclear fusion is a reaction in which the nuclei of two elements interact coalescing in a compound nucleus which, being generally in a metastable state, split emitting a significant amount of energy and giving rise to a system of products less massive, typically consists of a heavier nucleus and a nucleon. The energy, ΔE, liberated by the reaction is related to the mass defect, Δm, between the system of reaget nuclei and that of the products, according to the known Einstein relationship: $E=mc^2$ where c represents the speed of light in vacuum.
This energy is detectable in the form of kinetic energy of the reaction products and it is shown that, if the energy of the interacting nuclei is less than 0.1 MeV, it is distributed in a manner inversely proportional to the masses. In the case of the reaction D-T this implies that the helium nucleus assumes an energy of 3.52 MeV, while the neutron takes 14.06 MeV. The fusion reaction is favoured thermodynamically, only if the nuclear configuration of the system of the products is more stable than that of the complex of the reactants and, therefore the binding energy per nucleon of the first is greater than that of the products. Such eventuality occurs mainly when light nuclei are interacting, as is apparent from the graph shown in *Fig. 1.3*.

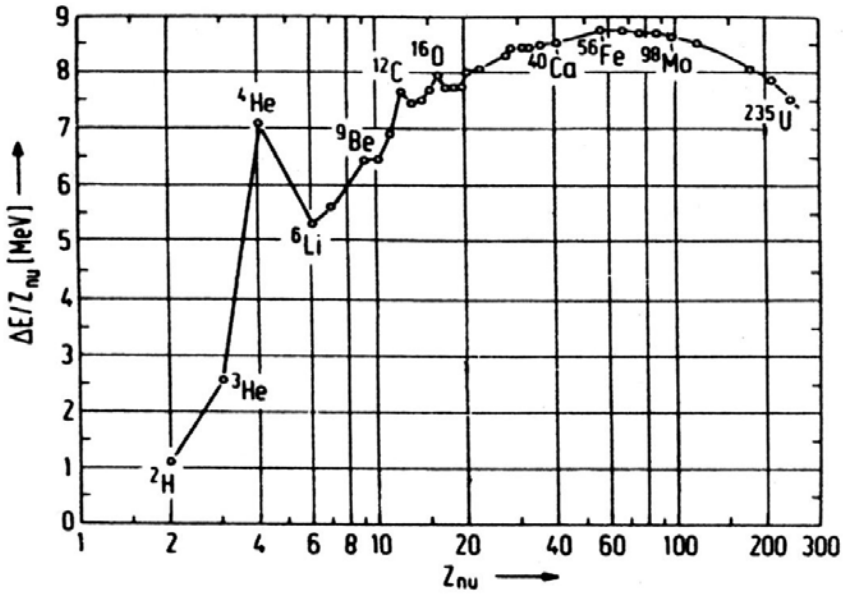

Figure 1.3: Binding energy per nucleon in function of the mass number [14]

1.1 Fusion plant for energy production

Without the benefit of gravitational forces acting within the stars in our Universe, reproducing fusion reaction on Earth for harnessing the energy of the stars requires a quite different approach and technology strategy.
Twentieth-century fusion science has identified the most efficient fusion reaction which could be reproduced in a laboratory is the reaction between two hydrogen (H) isotopes deuterium (D) and tritium (T). In fact, such a reaction produces the highest energy gain at the nonetheless 'lowest' temperature. It requires temperatures of 150,000,000°C that are ten times higher than those needed for the H-H reactions occurring at the Sun's core.
The most promising device adopting this technique is the TOKAMAK that uses toroidal and poloidal magnetic fields to contain and control the hot plasma (*Fig. 1.4*).

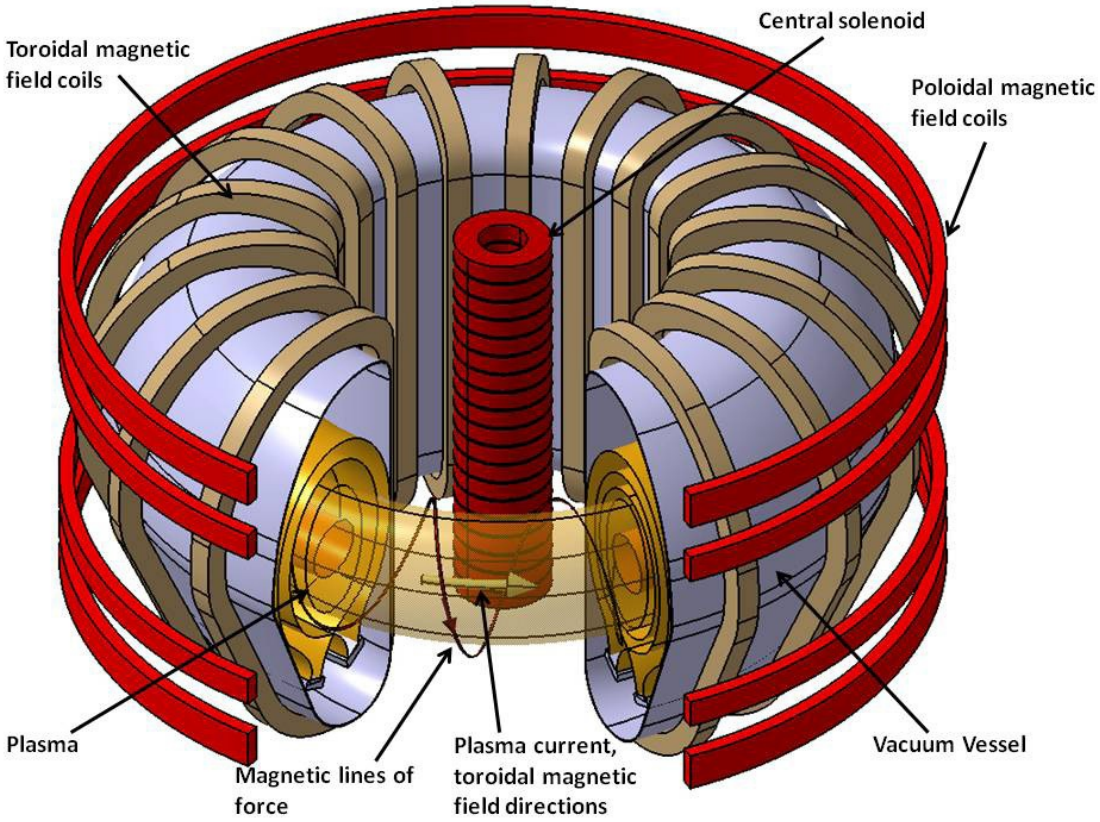

Figure 1.4 : Tokamak's coils and lines of magnetic field to contain and control the hot plasma[2]

To get the above nuclear reaction, fusion on the earth is simulated through the following steps [1]:

- Heat Deuterium + Tritium (DT) plasma to more than 100 million °C
- Keep hot plasma away from walls by strong magnetic fields (both poloidal and toroidal).
- High energy helium nuclei sustain burning plasma.
- Neutrons transfer their energy to the Blanket which works also as fuel breeding.

The advantages of this are:

- No carbon emissions. The only by-products of fusion reactions are small amounts of helium, which is an inert gas that does not contribute to atmospheric pollution.
- Abundant fuels. Deuterium can be extracted from water and tritium is produced from lithium, which is widely spread in the Earth's crust. Fuel supplies will therefore last for millions of years.
- Energy efficiency. One kilogram of fusion fuel can provide the same amount of energy as 10 million kilograms of fossil fuel.
- No long-lived radioactive waste. Only plant components become radioactive and they are estimated to be safely recycled or disposed conventionally within 100 years.
- Safety. No need of reaction chains and related reactivity accidents. The small amounts of fuel used in fusion devices (about the weight of a postage stamp at any one time)means that a large-scale nuclear accident is not possible.
- Reliable power. Fusion power plants should provide a base load supply of large amounts of electricity, at costs that are estimated to be broadly similar or even lower to the cheapest energy sources.

The fusion between deuterium and tritium (D-T) will produce one helium nucleus one neutron, and energy (*Fig. 1.2*).

The helium nucleus carries an electric charge, which will undergo the Lorentz force due to the magnetic fields and remains confined within the plasma. However, 80 percent of the energy produced is carried away from the plasma by the neutron, which has no electrical charge and is therefore unaffected by magnetic fields. The neutrons will be mainly absorbed by the surrounding walls of the TOKAMAK blanket, transferring their energy its structure in the form of thermal energy that is extracted by a coolant and proper thermo-fluid dynamic conditions needed to carry out an efficient cycle. In a fusion power plant, conventional steam generator, turbine and alternator will transform the heat into electricity (*Fig. 1.5*).

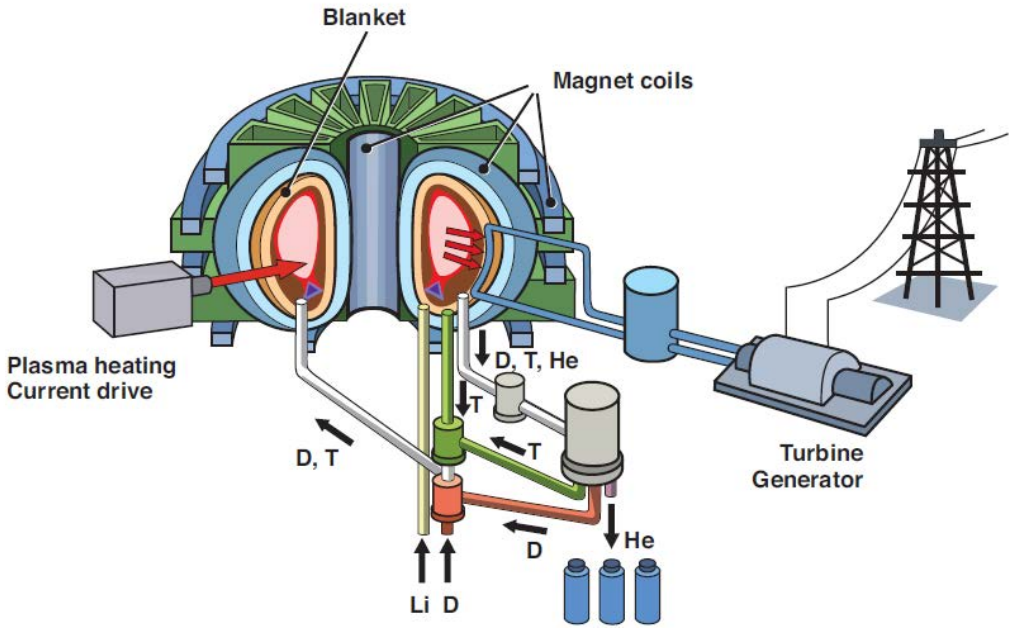

Figure 1.5: Fusion Plant for generating energy [2]

It is important to outline that 1 gram of fusion fuel is equivalent to 8 tonnes of oil.
In the DEMO fusion plant and in future Fusion Power Reactors, heat will be used to produce steam by way of turbines and alternators.

1.2 ITER: the way to new energy

ITER is an international project that aims to create an experimental nuclear fusion reactor capable of producing more energy than it consumes for the initiation and sustenance of fusion reaction.
Q ≥ 10 represents the scientific goal of the ITER project: to deliver ten times the power it consumes.
It aims to demonstrate also the engineering feasibility of a nuclear fusion reactor both in term of materials, components and safety features of the reactor. Its construction is currently underway in Cadarache (France) by an international consortium consisting of seven Nations (UE, Russia, China, Japan, USA, India and South Korea), named ITER Organization (IO). From 50 MW of input power, the ITER machine is designed to produce 500 MW of fusion power—the first of all fusion experiments to produce net energy. During its operational lifetime, ITER will test key technologies necessary for the next step: the DEMOnstration fusion power plant that will prove that it is possible to capture fusion energy for commercial use.
The science going on at ITER-and all around the world in support of ITER-will benefit all of mankind.

Nearly 30 years ago, a group of industrial nations agreed on a project to develop a new, cleaner, sustainable source of energy. At the Geneva Superpower Summit in November 1985, following discussions with President Mitterand of France and Prime Minister Thatcher of the United Kingdom, General Secretary Gorbachev of the former Soviet Union proposed to U.S. President Reagan an international project aimed at developing fusion energy for peaceful purposes.
The ITER project was born.
In the *Fig. 1.6* the phases of the ITER project.

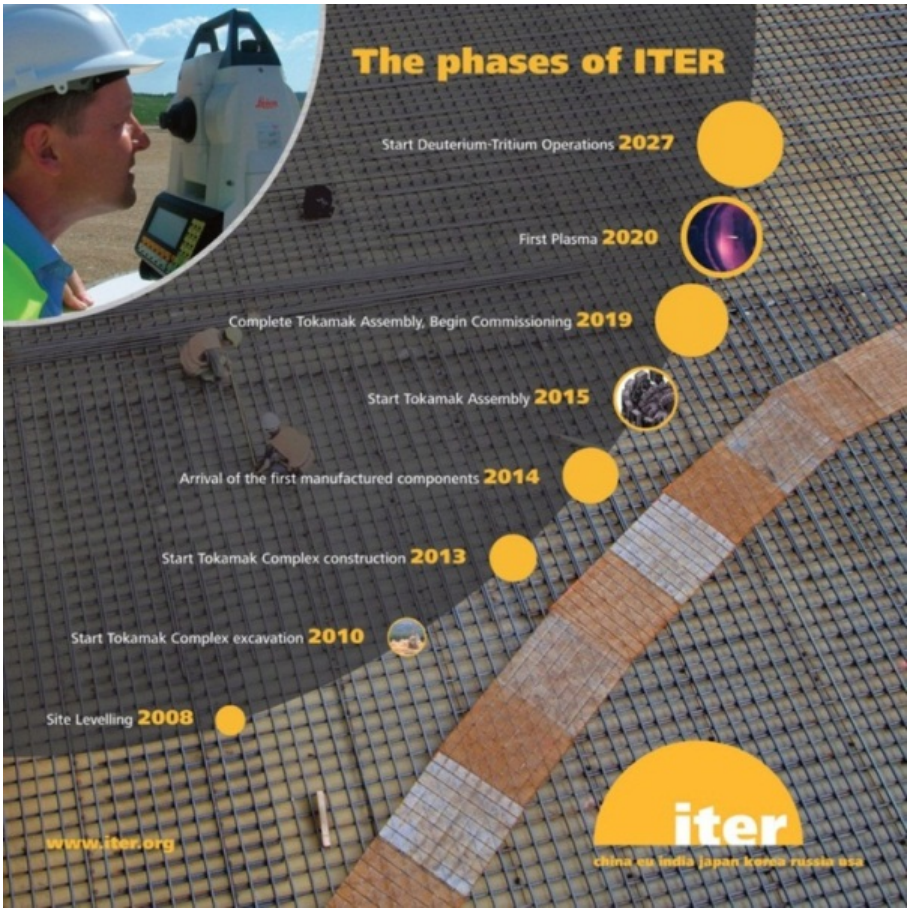

Figure 1.6-The phases of ITER [2]

The initial signatories: the former Soviet Union, the USA, the European Union (via EURATOM) and Japan, were joined by the People's Republic of China and the Republic of Korea in 2003, and by India in 2005. Together, these six nations plus Europe represent over half of the world's population.
Conceptual design work for the fusion project began in 1988, followed by increasingly detailed engineering design phases until the final design for ITER was approved by the Members in 2001.
In ITER, the fusion reaction will be achieved in a Tokamak device that uses magnetic fields to contain and control the hot plasma. In ITER, this heat will be dispersed through cooling towers. In the subsequent fusion plant prototype DEMO and in future industrial fusion installations, the heat will be used to produce steam and by way of turbines and alternators-electricity. [2]

1.3 The ITER Tokamak machine

The overall programmatic objective of ITER project is to demonstrate the scientific and technological feasibility of fusion energy for peaceful purposes. Its principal goal is to design, construct and operate a Tokamak experiment at a scale which satisfies this objective. ITER is designed to confine a Deuterium-Tritium plasma in which α-particle heating dominates all other forms of plasma heating; it means that ITER is a burning plasma experiment. As ultimate goal ITER will develop steady state fusion power production and will integrate and test all essential fusion power reactor technologies and components. ITER has to demonstrate safety and environmental acceptability of fusion . For all these reasons ITER is a necessary step on the way to commercial fusion reactor. ITER will exploit the process by magnetic confinement of plasma whereby it is contained within toroidal vessel walls by strong magnetic fields produced by superconducting coils surrounding the vessel and an electrical current driven in the plasma, a magnetic configuration called a Tokamak.(*Fig. 1.7*)

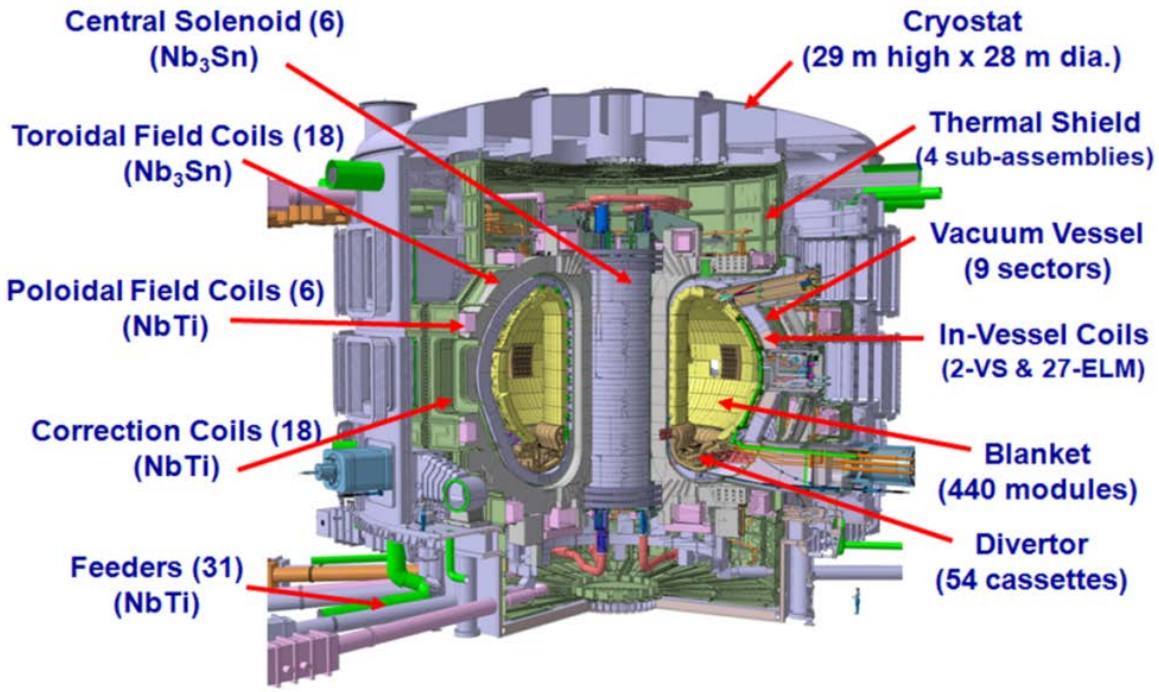

Figure 1.7: Tokamak Basic Machine [2]

The ITER Tokamak uses magnetic fields to confine plasma in the shape of a torus (donut). Stable plasma equilibrium requires magnetic field lines that move around the torus in a helical shape. The helical field is the result of adding a toroidal field (travelling around the torus in circles) and a poloidal field (travelling in circles orthogonal to the toroidal field).
In ITER, 18 superconducting electromagnet coils, surrounding the torus, will produce the Toroidal Field (TF) (*Fig. 1.8*).

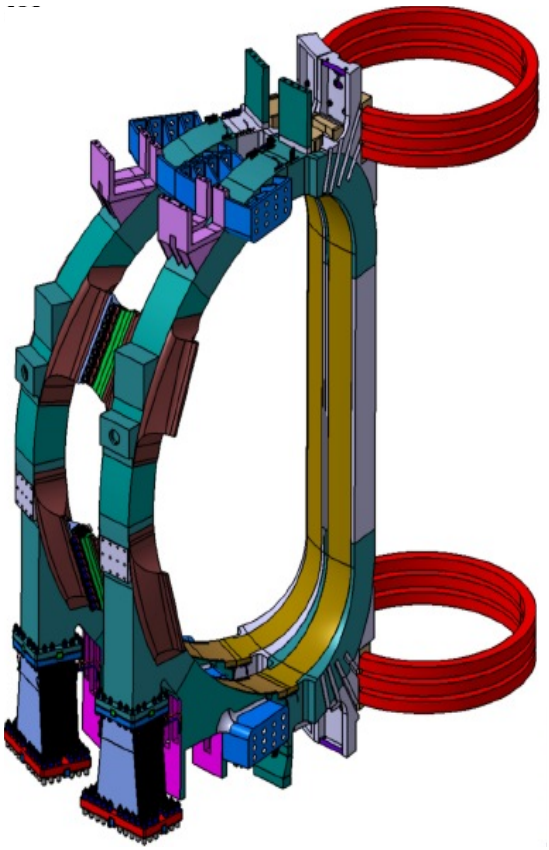

Figure 1.8: Pair of Toridal Field Coils [3]

The Poloidal Field (PF) is the result of a Toroidal electric current flowing in the plasma induced by six superconducting electromagnet coils in the Central Solenoid (CS) as per *Fig.1.9* and *Fig. 1.10*.

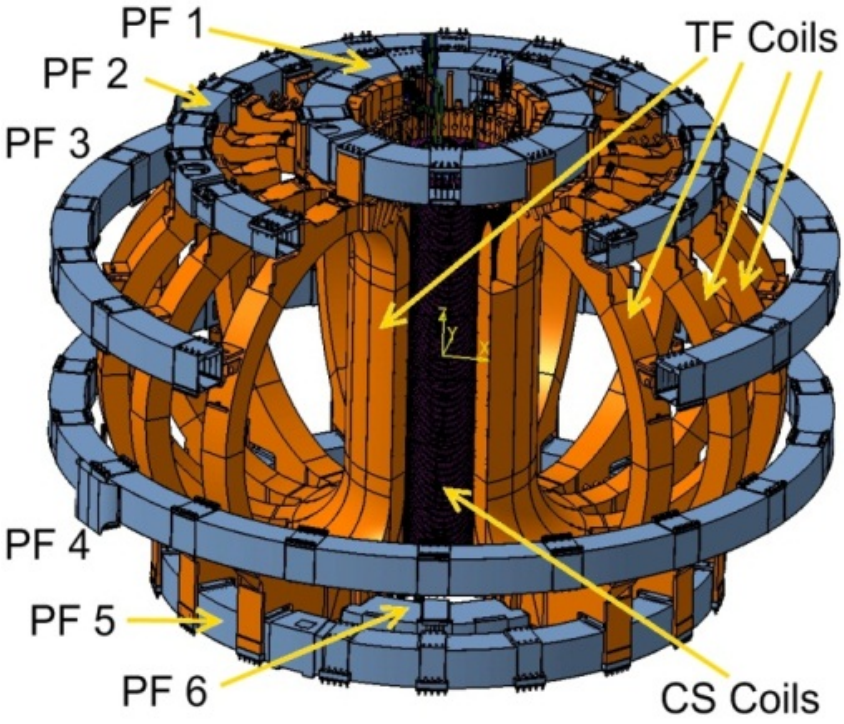

Figure 1.9 : Arrangement of Magnet Coils [3]

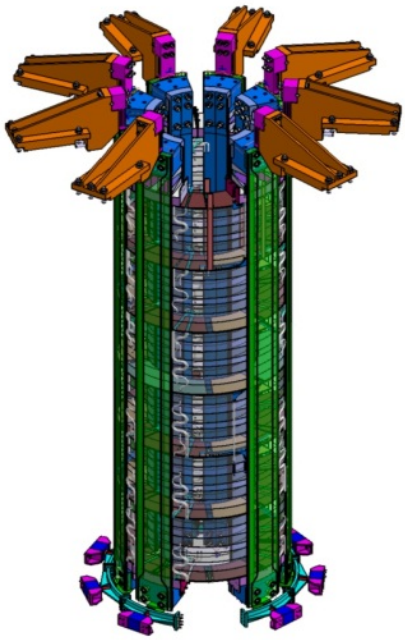

Figure 1.10: Central Solenoid [3]

In addition, six superconducting electromagnetic coils are positioned externally to permit variations of radial and vertical fields to control the plasma position and shape. In addition to these main coils, there are three sets of three Correction Coils (CC) for the fine compensation of the stray field *(Fig.1.11)*.

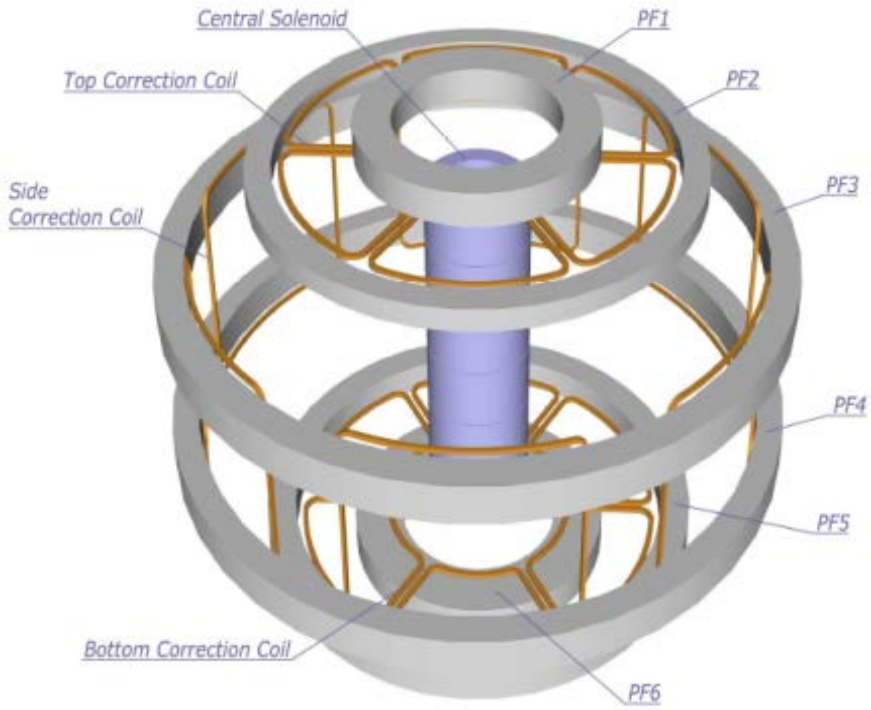

Figure 1.11: Bottom, side and top Correction Coils [3]

Further in-vessel coils are proposed for compensating possible instabilities of the plasma vertical position and for controlling edge phenomena such as Edge Localized Modes (ELM).
Plasma has to be intended as the fourth status of the matter characterized by high energy density being a warm dense matter. Non Linear phenomena and far equilibrium state characterize Plasma behaviour. The plasma comprises charged particles – positive nuclei and negative electrons that can be confined and shaped by magnetic fields, particles in the plasma will follow magnetic field lines.
The walls of the vacuum vessel (*Fig. 1.12, Fig. 1.13*), the first safety confinement barrier, will not be in contact with the plasma due to the magnetic confinement with it.

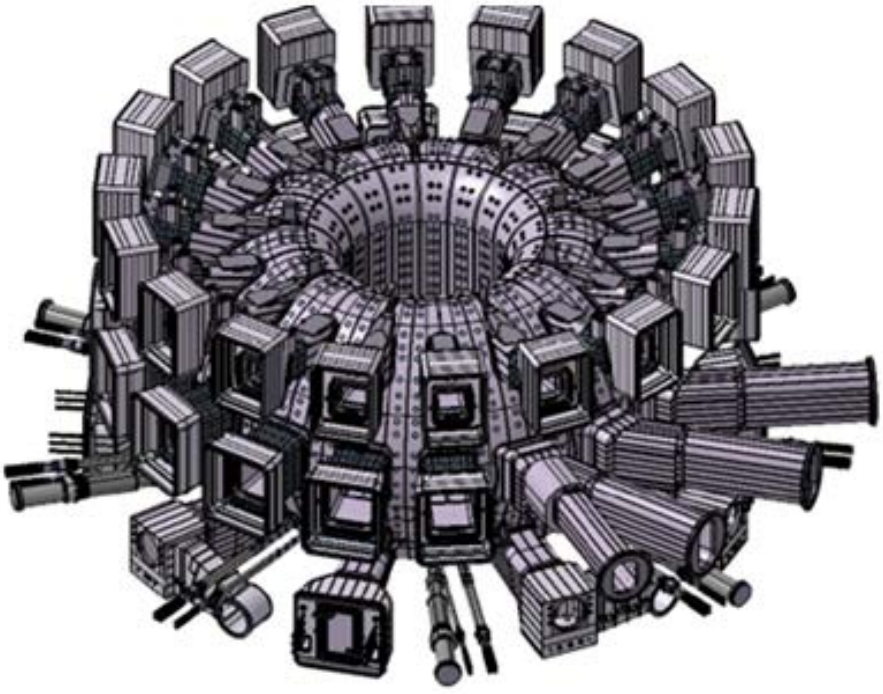

Figure 1.12: Vacuum vassel [2]

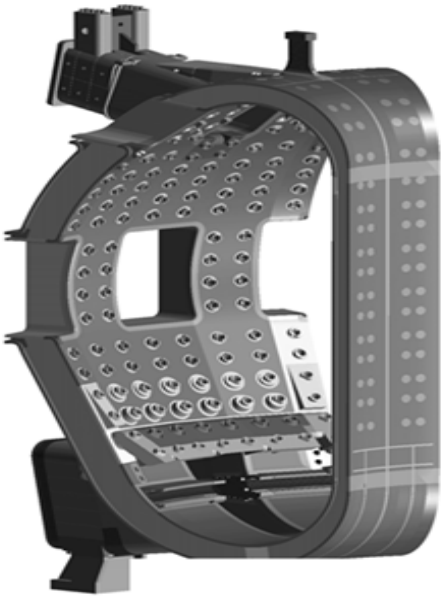

Figure 1.13: Part of Vacuum Vassel [2]

Separation of the plasma and the 'first wall' vessel wall is vital to limit heat loading, damage and plasma contamination.
All the Machine Assembly is confined into the Vacuum Barrier (named Cryostat) which has the containment function for the ITER Machine Assembly (*Fig. 1.14*).

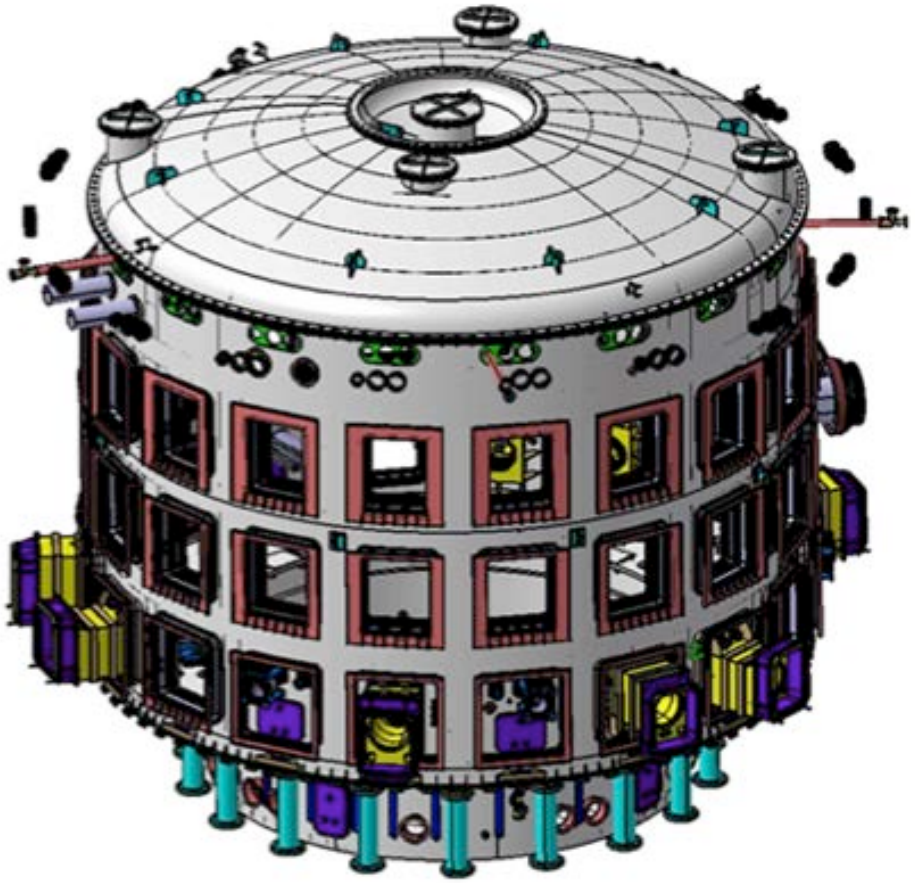

Figure 1.14: Cryostat and vacuum system [2]

Few questions have to be satisfied before closing the short overview in ITER project:

- How safe is ITER Machine [1], [3]
- Radioactivity Release and Radiological wastes for next generations [4]

Nuclear Accidents like Fukushima or Chernobyl are physically and technologically impossible because there is no reactivity factor that can diverge as for nuclear fission plants. The fusion reaction is intrinsically safe. Additionally fuel inventory is very small: less than one gram of fuel is reacting at any given moment in the reactor core. Any disturbance will stop the plasma and the nuclear fusion reaction switches off. As a consequence runaway reactions and core-meltdown are impossible. Cooling is not a safety function: if power is lost, heat evacuation happens naturally.
In the frame of the control of radiological wastes it has to be understood that ITER will not generate long-life/high activity waste.
During normal operation, ITER's radiological impact on the most exposed populations will be one thousand times less than natural background radiation. "Worst-case scenarios", such as fire in the Tritium Plant, would have a lesser impact on neighbouring populations than natural background radiation. The ITER facility is being licensed in France as a Basic Nuclear Installation (INB) and will observe French safety and security regulations. Nevertheless, as per all the other fission Nuclear reactors following Fukushima event, a stress test in the frame of WENRA and IAEA framework requirements, will be conducted by Nuclear Safety Authority to demonstrate safety margins of the ITER Machine considering beyond design basis events.

2. ITER Electrical Power Supply

The ITER Electrical Power Supplies is comprehensive of the following four major systems [5], [6], [7]:

- Pulsed Power Electrical Network (PPEN)
- Reactive Power Compensation and Harmonic Filtering (RPC&HF)
- Coil Power Supplies System (CPSS)
- Steady State Electrical Network (SSEN)

The PPEN receives power from the 400 kV Grid and distributes (at 66 kV and 22 kV level) it to the pulsed loads of Coil Power Supply Systems (CPSS) and Heating & Current Drive (H&CD) Systems. The SSEN provide AC power to various loads, primarily motors, within the plant systems such as cooling water system, cryo-plant, buildings and HVAC as well as Tritium Plant. The coil PS and the H&CD PS supply their corresponding loads – superconducting magnet coils, in-vessel coils and H&CD PS – in general with controlled Direct Current (DC) power. The PPEN and the connected coil PS are referred together as the Coil PS and Distribution System (CPSDS).

The main functions of the CPSS and SSEN are to:

- supply electrical power to the ITER machine and ITER plant systems;
- protect the ITER machine and ITER plant systems in the event of electrical fault and superconducting coil quench;
- provide proper earthing of the ITER machine and power supply components.

Electrical power requirements for the ITER plant and facilities will range from 120 MW for steady state auxiliary supplies, plus 500 MW for peak periods (pulsed) during plasma operation. As a result of the characteristics and duty cycle of the loads, the ITER power network is divided into two independent systems: the Pulsed Power Electrical Network (hereby PPEN) that supplies the pulsating loads and the Steady State Electrical Network (hereby SSEN) feeding the auxiliaries.
Both the PPEN and SSEN systems will be connected to the French 400 kV transmission network operated by RTE (Gestionnaire du Réseau de Transport d'Electricité) [14]. This is capable of providing the steady-state power required by the SSEN in addition to 500 MW, 200 Mvar pulsed power for the pre-programed PF scenarios, the plasma current, position and shape control, including vertical stabilization, the H&CD PS, the superconducting magnet coils and in the vessel coils.
This substation will be connected to the 400 kV grid by a double circuit line. For this aim, the current nearby 400 kV overhead line will be diverted and a new 5 km overhead line will be pulled.

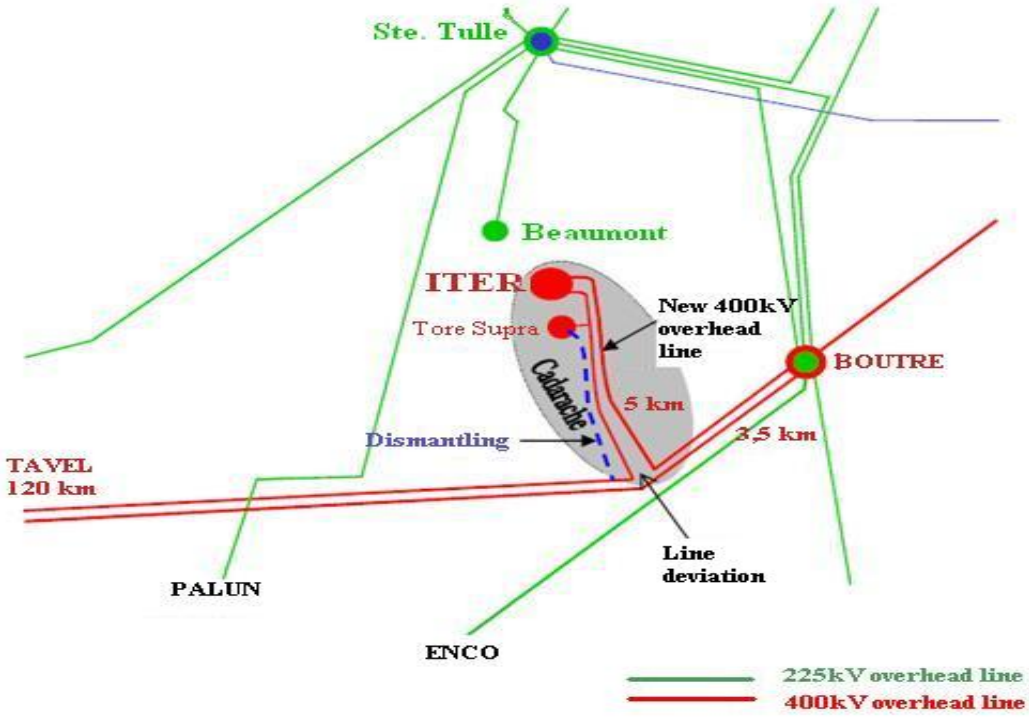

Figure 2.1: 400kV and 225kV grids in the ITER area. [6]

2.1 Coil power supply system

Function of the Coil Power Supply System (CPSS) is to receive power from the French 400 kV transmission grid and to provide controlled DC current and voltage to each coil for plasma confinement, plasma initiation, shape and position control, error field correction, as well as superconductive magnet quench protection and the earthing detection.
For this reason the Coil Power Supply System (CPSS) consists of AC/DC converter units connected in series with Switching Network Units (SNU), Fast Discharge Units (FDU) and the earthing circuits.
The Coil Power Supply System (CPSS) will include the following nine systems to supply controlled DC current to the TF and PF coils and the CS modules:

- one common Power Supply for the 18 TF coils;
- one common Power Supply system for the CS1 upper and lower modules connected in series;
- four Power Supply systems for the CS2 upper, CS2 lower, CS3 upper and CS3 lower modules;
- two Power Supply systems for individual supply of the PF1 and PF6 coils;
- one common system for the four outer PF coils, i.e. PF2, PF3, PF4 and PF5, used for plasma vertical stabilization.

In addition, nine relatively small PS systems with very similar configurations will supply the flux error Correction Coils (CC).
The whole CPSS will be interconnected between the AC/DC converters, PMS, SNU, FDU and magnets by a huge and complex DC Busbar system.
The various type of Busbar will be named in function of the name of the coil that they feed.
In *Fig. 2.2* is shown the configuration of Coil Power Supply

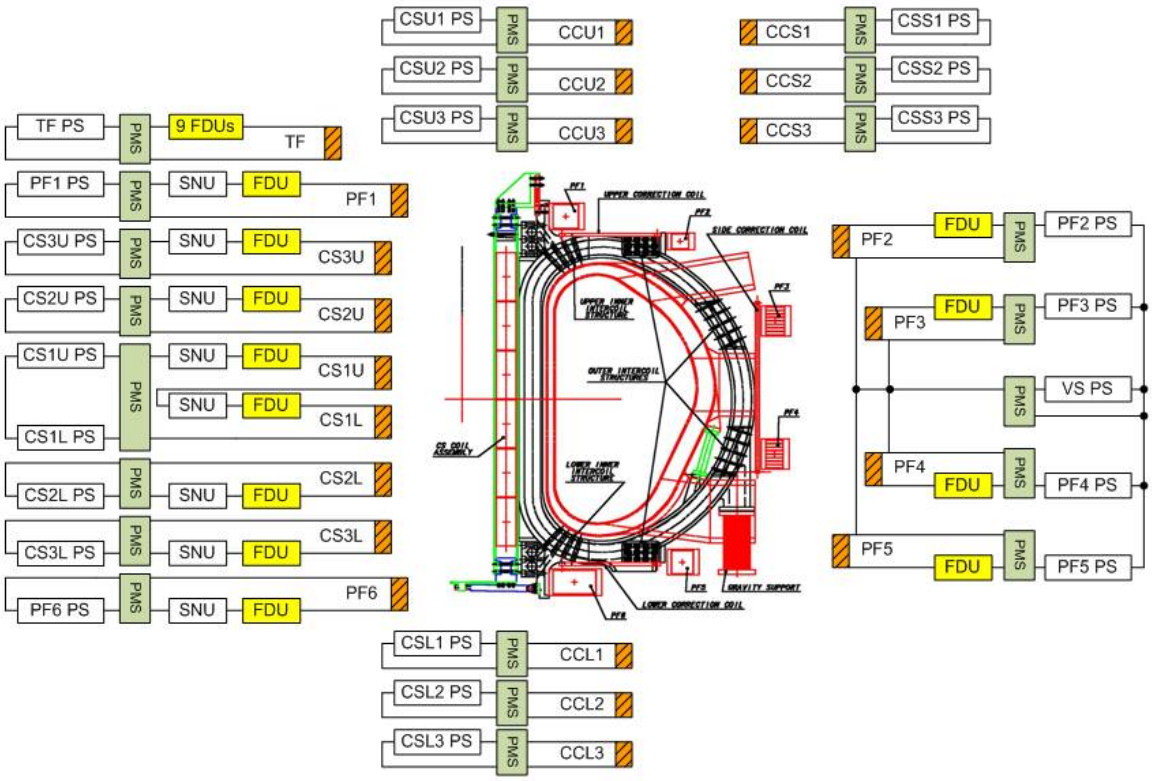

Figure 2.2: Configuration of Coil Power Supplies [6]

The Fast Discharge Units (FDUs) will protect the superconducting coils by extracting the energy stored in the magnet system in case of a quench or other abnormal events which could potentially damage the coils or power equipment. This energy will be absorbed by resistors included in series with the coils but normally bridged by circuit breakers.

The Switching Network Units (SNU) will generate a high voltage required for breakdown and plasma initiation at the beginning of each cycle. This will be realized by inserting resistors in series with the Central Solenoid (CS) modules and two PF coils, PF1 and PF6, with the help of DC circuit breakers. Make switches will be used to change by steps the voltage applied to the coils during and after the initial plasma current ramp-up phase on commands from the plasma control system.

The Protective Make Switches (PMS) will be connected in parallel to the ac/dc converters to bridge them under fault conditions and in case of the coil fast discharge. In the latter case they shall be closed prior to opening of the FDU circuit breakers but with a certain delay giving the time for the shunted ac/dc converters to be switched into inversion mode to avoid short circuit.

A more general scheme from the supply grid to the coils of the Coil Power Supply System is shown in *Fig. 2.3.*

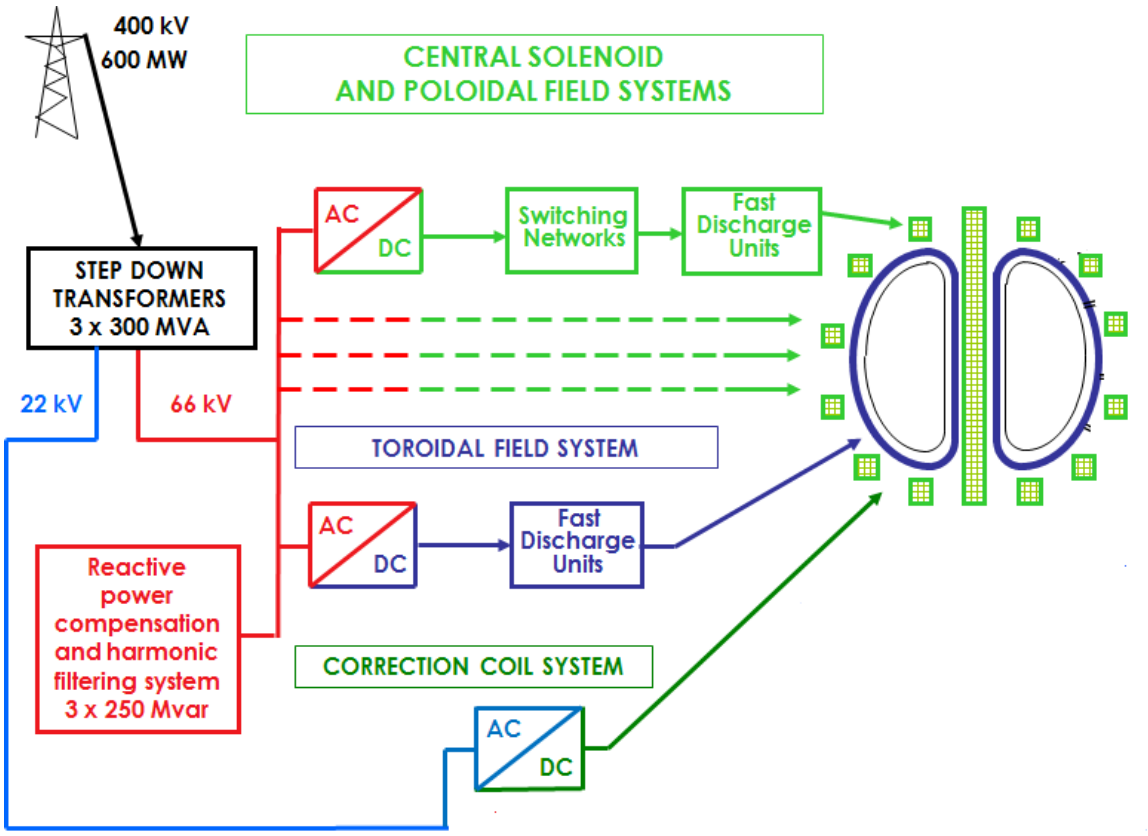

Figure 2.3-Coil Power Supply System [7]

The connection between AC/DC convertors and coils is a system of high current Busbars.
In Buildings 32-33 there are located the ac/dc convertors. Busbars start from this buildings and go to Building 74 through two bridges.
From Building 74 the Busbar goes to Building 11, the Tokamak building, to feed the coils.
In Fig. 2.4 the general view of the site.

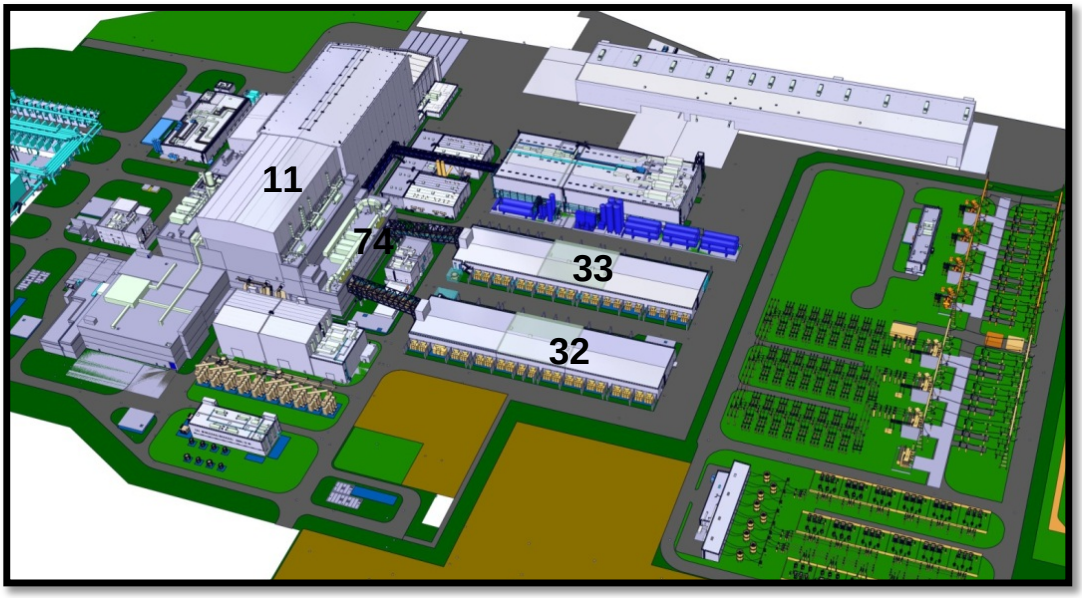

Figure 2.4-Buildings 11, 32, 33 [7]

3. DC Busbars

DC Busbars of the Coil Power Supply System (CPSS) located in the Buildings 11, 74, 31, 32 consists of separate buses. The DC Busbars will connect the superconducting coils of the Tokamak magnet system located in Building 11 to the AC/DC converters located in Buildings 32 and 33 via DC Disconnectors, Fast Discharge Units (FDUs) and Switching Network Units (SNUs) located in Building 74 (*Fig. 3.1*).
The various type of Busbar will be named in function of the name of the coil that they feed. [8]

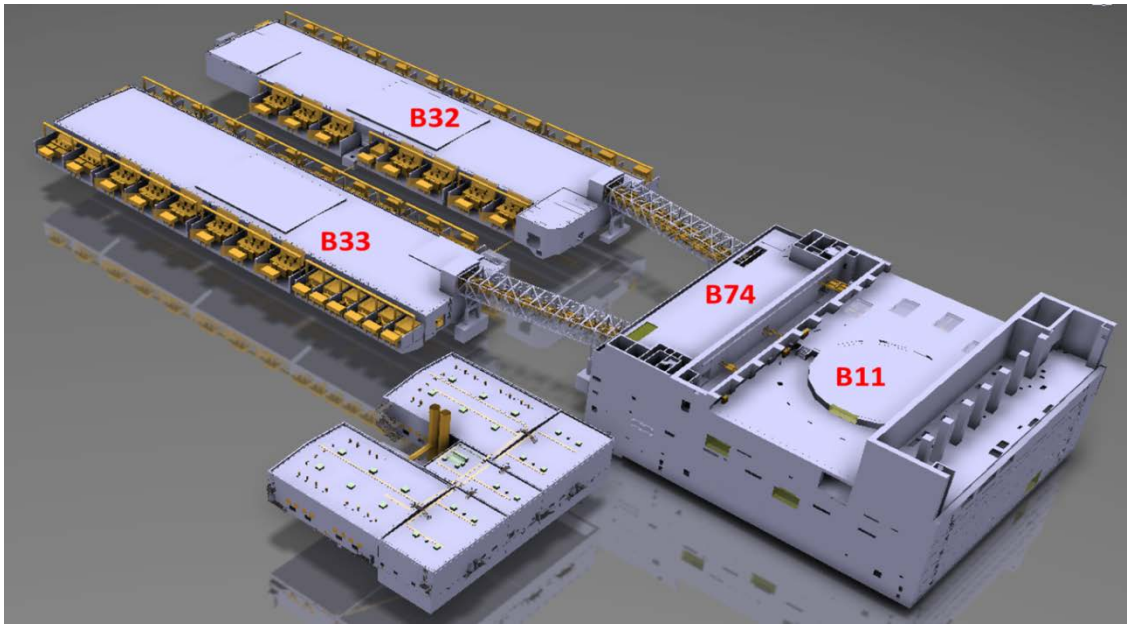

Figure 3.1. Buildings housing the CPSS equipment and Busbars [8]

Building 11 is the Tokamak Building where the reactor is located and it is the heart of the experiment. The Buildings 32-33 are called Magnet Power Conversion Buildings because inside there are the AC/DC converters for all the different kind of coils. The Building 74 is called Diagnostic Building.
In the next pages is shown the path of the Busbars through the buildings. In Fig. 3.2 and Fig. 3.3 there are the AC/DC transformers in yellow and the Busbar in black attached through connectors to the transformers and going out from this buildings to the bridges. The white boxes in certain points of the Busbars are called expansion boxes and their functionality will be explained in Cap 3.1.4 .

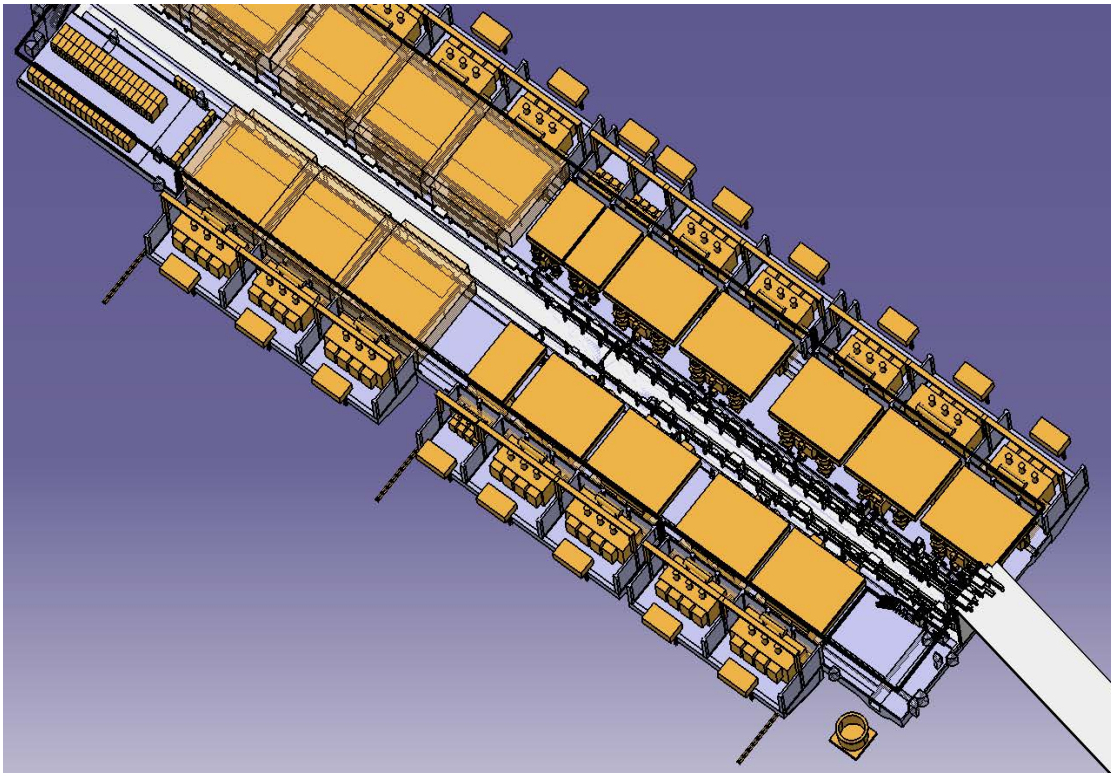

Figure 3.2: Building 32 AC/DC transformers(yellow) and Busbar (black) [8]

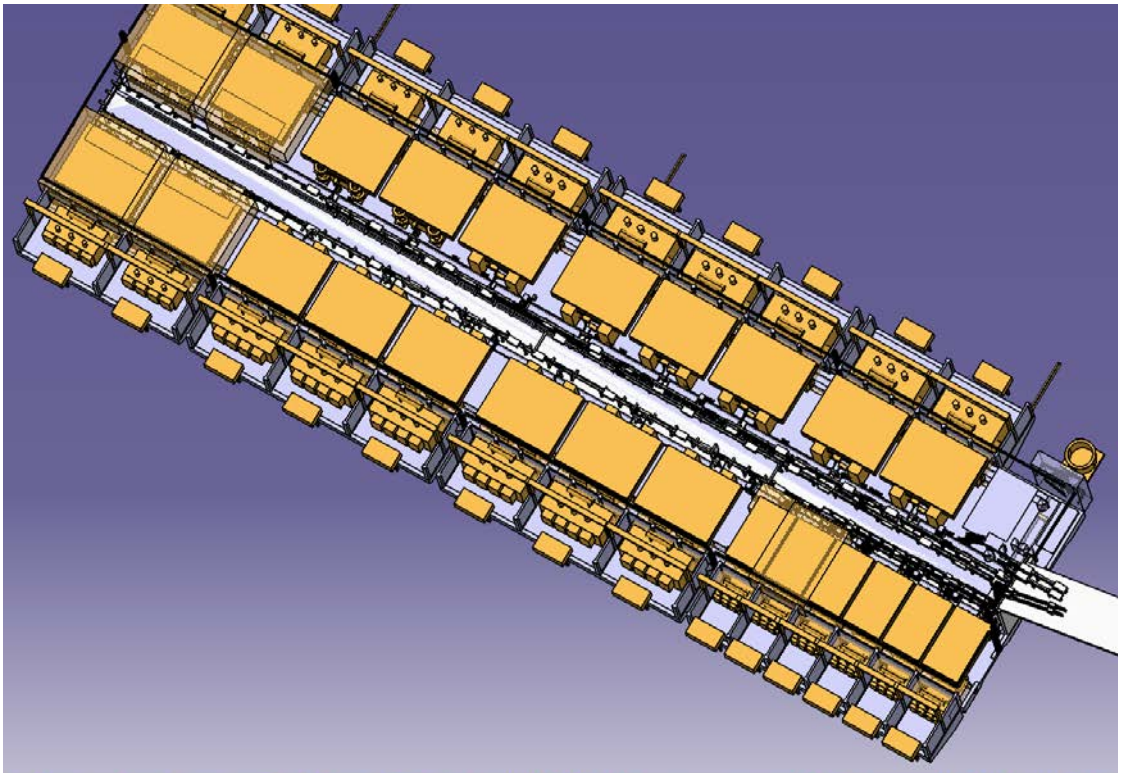

Figure 3.3: Building 33 AC/DC transformers (yellow) and Busbar (black) [8]

The Busbars going through the bridges are in *Fig. 3.4* and *Fig. 3.5*

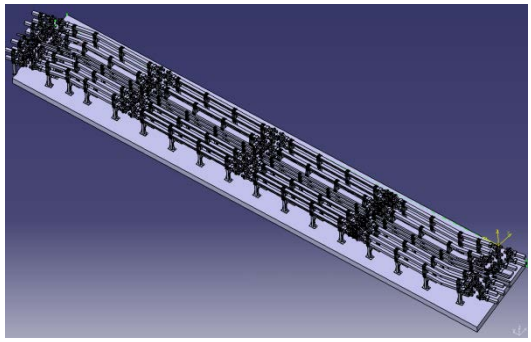

Figure 3.4: Bridge 1 [8]

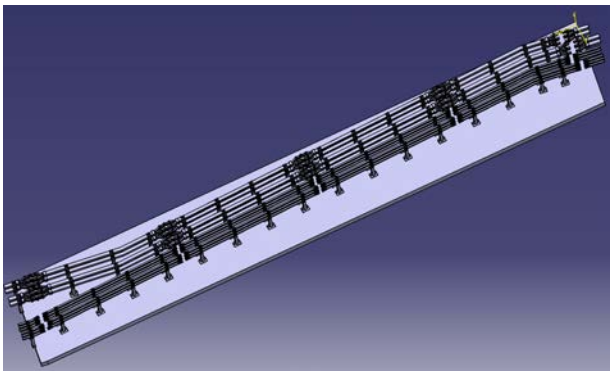

Figure 3.5: Bridge 2 [8]

The Busbars in Building 74 (Fig. 3.6 and Fig. 3.7) are ceiling embedded to leave more space for the diagnostic equipment.

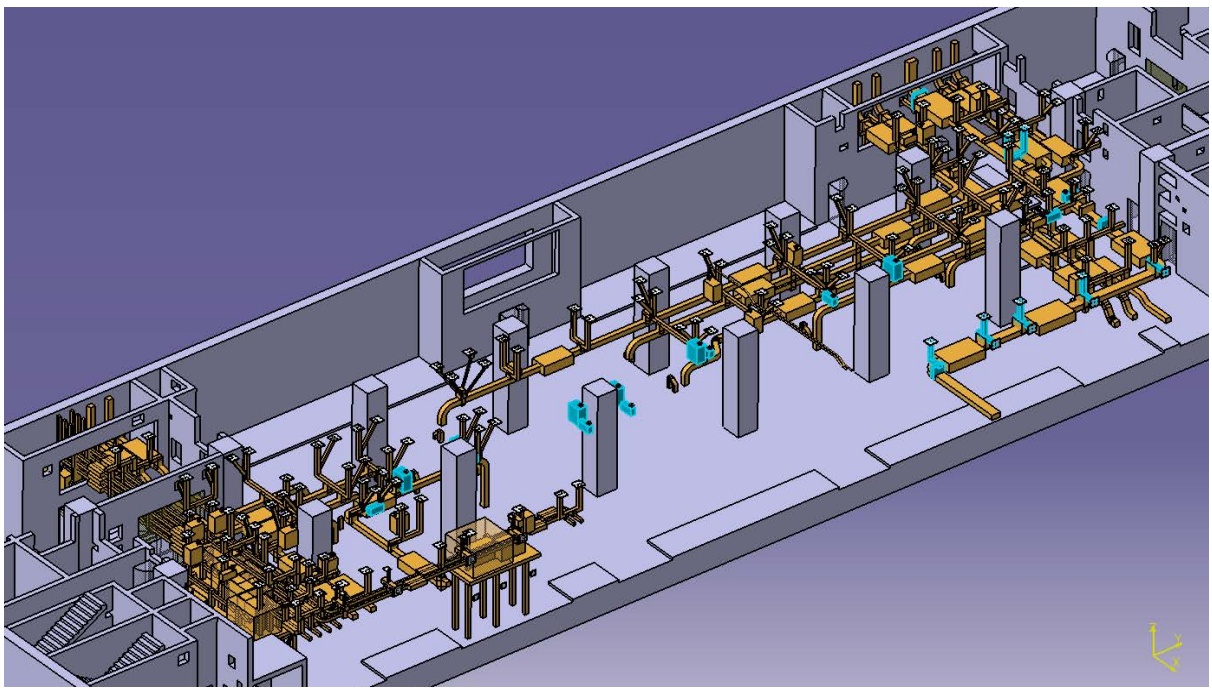

Figure 3.6: Layout of the ceiling embedded Busbars in Building 74. Level B2 [8]

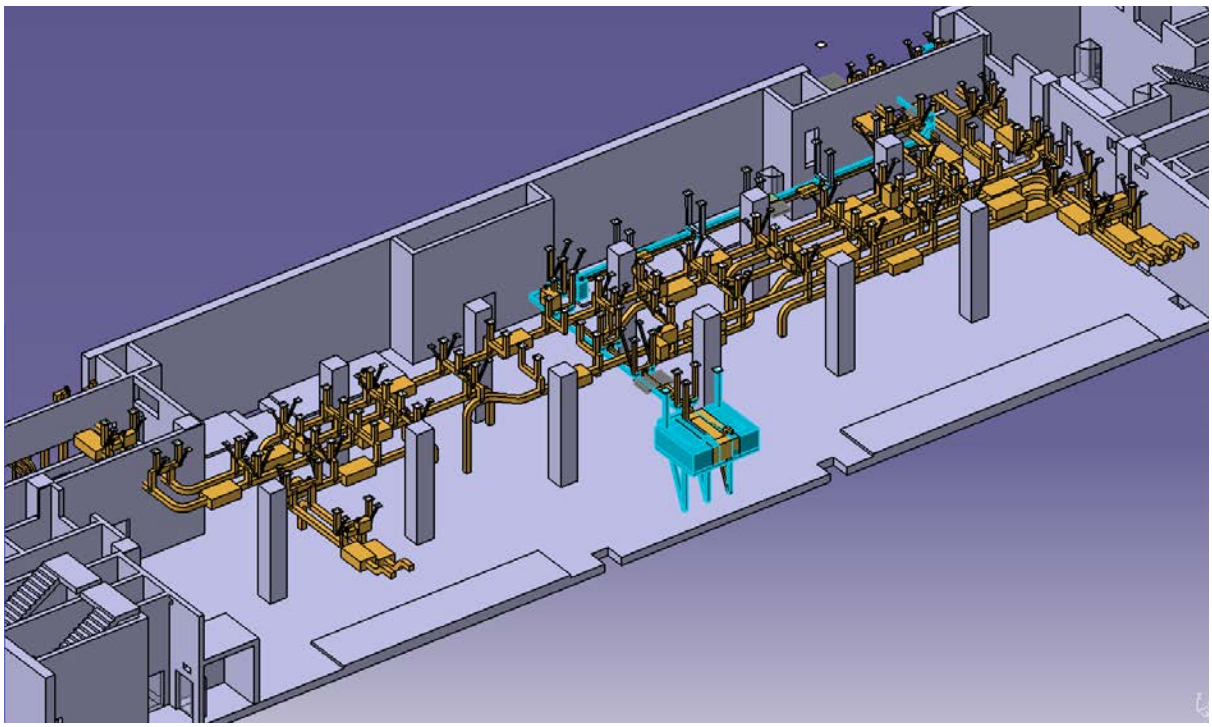

Figure 3.7. Layout of the ceiling embedded Busbars in Building 74. Level L3 [8]

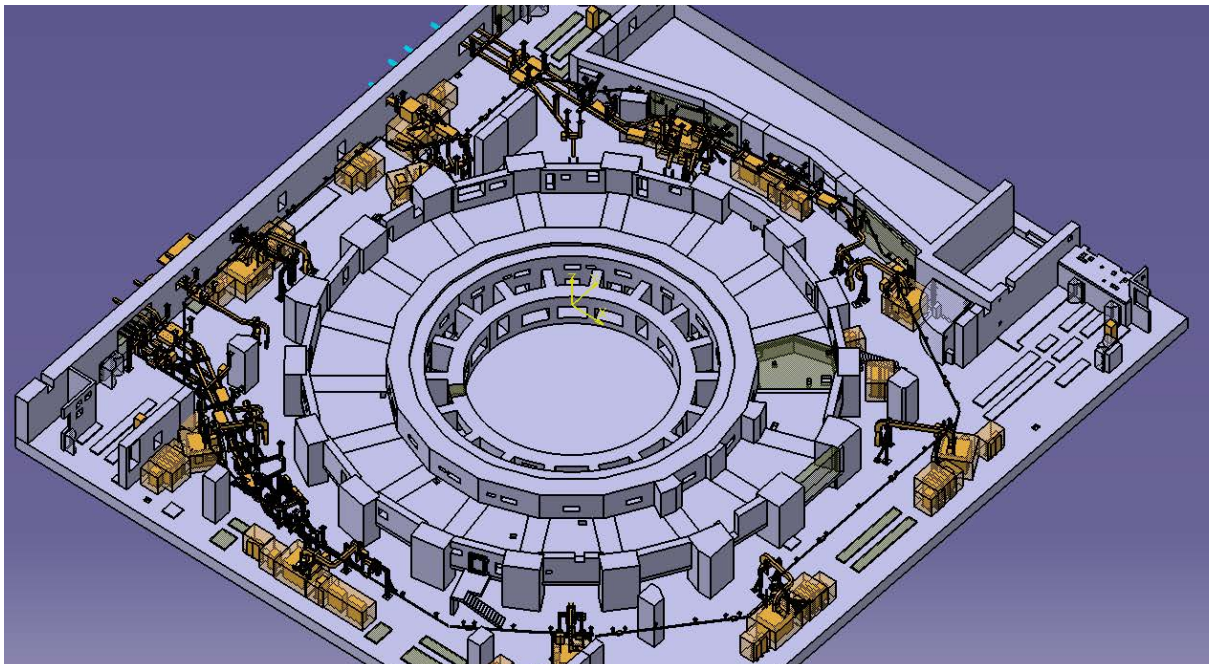

Figure 3.8. Layout of the Busbars in Building 11.Level B2. [8]

3.1.1 Main Specification

DC Busbars and bus links are designed for continuous duty at rated current and must be able to withstand the short-circuit fault current of the respective AC/DC converter.
The main ratings of the DC Busbars are presented in Table 2. [8]

Table 3.1 [8]

Characteristic	Unit	TF	CS	PF1, PF6	PF2–PF4	PF5	CC
Rated continuous current	kA DC	68	45	48	55	52	10
Rated insulation level according to IEC 60034	kV AC	13.2	13.2	13.2	13.2	13.2	2.3
Rated peak withstand current (100 ms)	kA DC	350	300	350	350	350	80
Rated withstand voltage according to IEC 60034-1	kV DC*	48	48	48	48	48	-
Rated withstand voltage according to IEC 60034-1	kV AC	-	-	-	-	-	6

3.1.2 Design

Because of their considerable length and rated current, each DC Busbar system requires active cooling and consist of the following parts: Busbars (sections) (*Fig. 3.9*), thermal expansion compensators (TEC) (*Fig. 3.10*) and rigid inserts, supports (*Fig. 3.11*) and cooling water collectors (CWC).

Figure 3.9: DC Busbars [8]

Figure 3.10. Thermal expansion compensators (TEC) [8]

Figure 3.11: Busbar Supports [8]

The designs of the Busbars for the PF&CS, TF and CC coil PSS has been developed by the Russian Domestic Agency (Efremov Institute) for ITER Organization. They are based on the common principles and have a high degree of unification. The current-carrying parts of the Busbars, referred to below as “conductors”, are all made of two types of rectangular Busbars: 24000 mm^2 in cross-section for PF and CS systems and 5000 mm^2 in cross-section for CC systems. In the TF Busbars the current carrying element is composed of two PF/CS conductors, and hence, is 48000 mm^2 in total cross-section (*Fig. 3.12*).

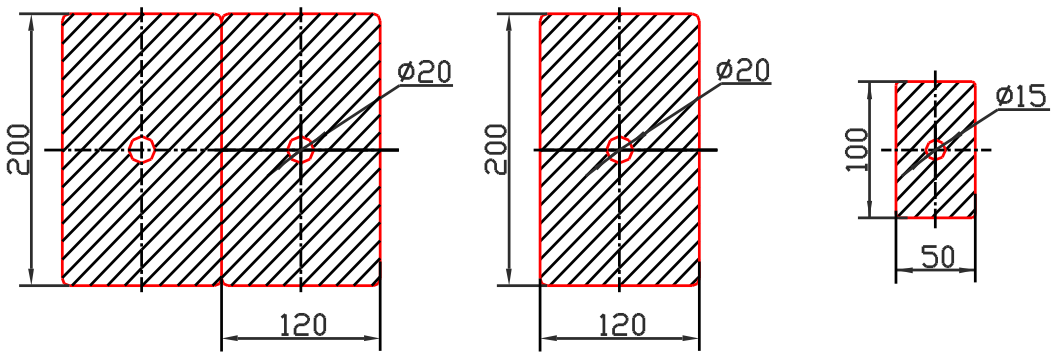

TF Busbar **PF/CS Busbar** **CC Busbar**

Figure 3.12: Busbar conductor cross-sections [8]

The conductors will be made of АД0 GOST 4784-97 commercially pure aluminum. A cooling water channel 20 mm or 15 mm in diameter is provided in the centre of the Busbar for the PF/CS and CC Busbars, respectively. The current density with account taken of the cooling channels is 1.4 A/mm^2, 2.3 A/mm^2 and 2.07 A/mm^2 in the TF, PF/CS and CC Busbars, respectively.

Due to their length, the Busbars are subdivided in several pieces (sections) in series.

The length of a piece (section) of the Busbars should not exceed 12 m, with the length of the bent part being no more than 2.3 m. At two ends, each Busbar is a bent for connection with flexible or rigid inserts. Moreover, the conductor can be bent in horizontal or vertical plane depending on the expected location of the Busbars.

The basic high-voltage insulation is made of a glass mica tape impregnated with heat-resistant epoxy resin. The LSM-type tape used for the Busbar insulation is a three-layer composition of fiberglass, mica paper and Lavsan polyester (biaxially-oriented polyethylene naphthalate) film pre-impregnated with a modified epoxy-novolac binder during manufacturing of the tape. The insulation is formed, when the binder goes to hardened state during the curing (“molding”) process at a MICAFIL facility. Before applying the insulation, the conductor surface is degreased with white spirit, coated with epoxy compound. The TF Busbars is additionally wound by one layer of glass tape to provide reliable adhesion of the insulation to the conductor.

Then, the basic insulation is wrapped on the conductor half-overlapped. The basic insulation of the TF/PF/CS Busbars consists of 11 layers of LSM tape 0.16 mm in thickness and 30 mm in width. The total thickness is 3.0-4.0 mm. The CC Busbar insulation is similar, with 6 layers of the LSM tape and a total thickness of 1.9-2.2 mm.

The bent ends of the TF conductors have the same basic insulation as the PF/CS Busbars. The straight parts of two equipotential parallel conductors, which form the TF one-pole Busbar, are wrapped together with 11 layers of LSM tape similar to the PF Busbars. Prior to wrapping the basic insulation, each single conductor is wound by one layer of epoxy-impregnated glass

tape to avoid uncontrollable current flow from one conductor to another. Besides, in the zone of transition from the straight part to the bent one, an additional layer of 40μm polyimide film tape is wound half-overlapped between 2 layers of LSM tape.
The insulated Busbar is loaded into a autoclave for hydrostatic pressing of the insulation with hot bitumen at a pressure of 10 kg/cm² and for polymerization of Epoxy-Novolac binder within 12-14 hours at a temperature of 155-165°C.
Finally, one or two (at the bent ends) layers of fiberglass tape impregnated with cold polymerized epoxy compound are wound over the basic insulation to prevent mechanical damage. The curing process lasts 24 hours under pressure provided by metallic mending plates pressed by G-cramps.
The two-pole Busbar is composed of two symmetrical single buses for the forward and reverse current. A 5mm aluminum plate (separator) is inserted between two single Busbars of different polarities. At both ends of the separator there are terminals for connection to the earthed parts with the aim to prevent inter-pole short circuits and to provide conditions for indication of single insulation breakdowns.
The Busbars are bonded to the separator by high viscosity epoxy resin, so as to reduce the through-thickness stresses acting on the insulation at a short current to negligible values. This also allows avoiding gaps between the insulation and separator. The exception is made for the area of transition from straight to bent part, where the separator is wounded by a layer of polyamide tape to avoid adhesion to the Busbars. The Busbars and separator, when put together, are additionally wrapped with 6 layers of epoxy-impregnated glass tape (4 layers in the CC Busbars), which form a strong bandage providing mechanical protection of the insulation.
A double Busbar is laid in a thin steel casing 1 mm in thickness. The casing consists of two parts joined together by a polyester tape. Fiberglass laminate spacers are placed between the bandage and casing. The spacers are glued to the bandage and can slip relative to the casing at a temperature expansion of the Busbar. [8]

Figure 3.13: PF Busbar [8]

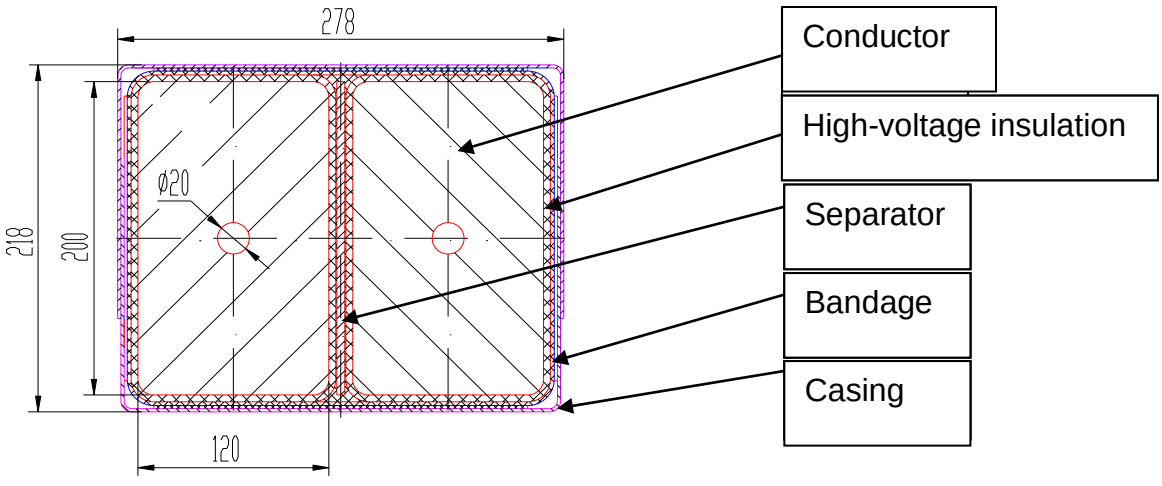

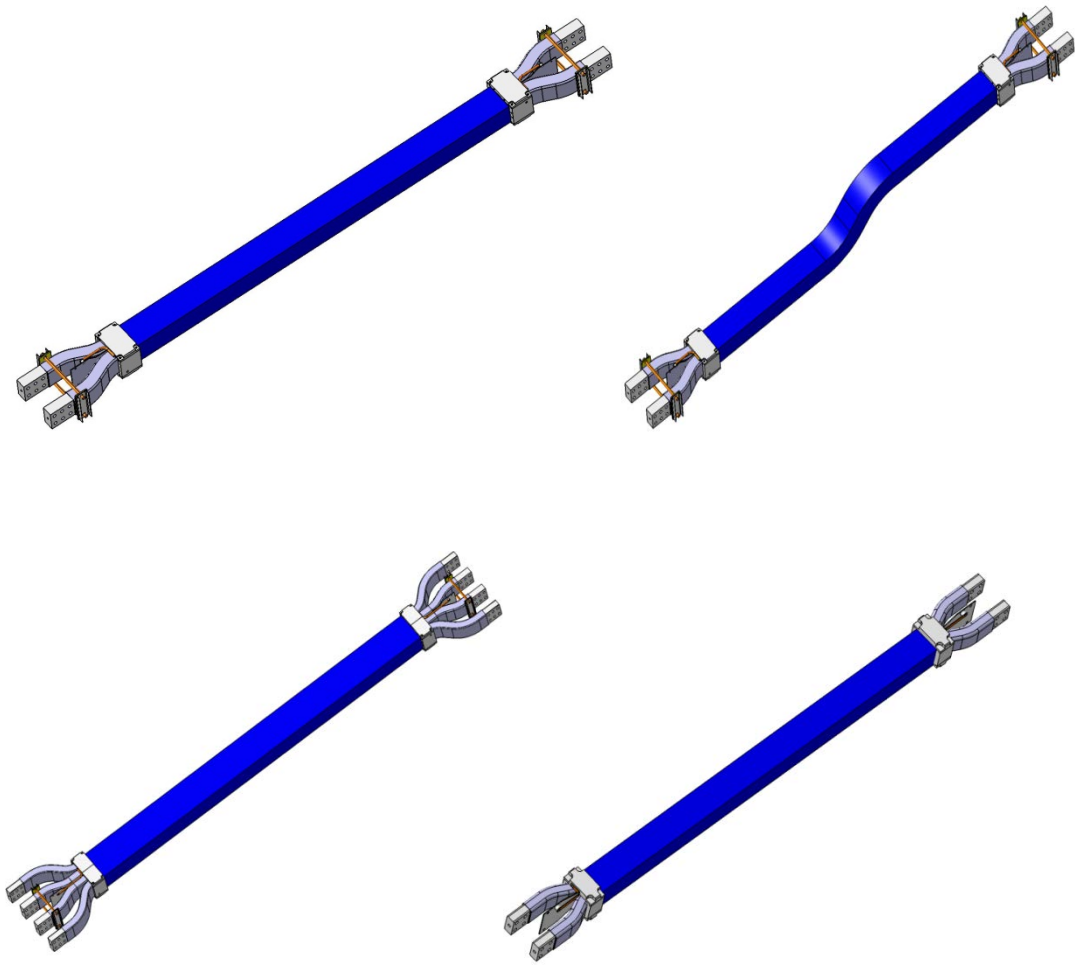

Figure 3.14:Straight Busbar and bend Busbar [8]

More details can be seen in *Fig. 3.15* showing the bent part of the PF/CS Busbar near connection with flexible links. The durostone stud and the calmps that are needed to contain magnetic forces effect on the Busbars.

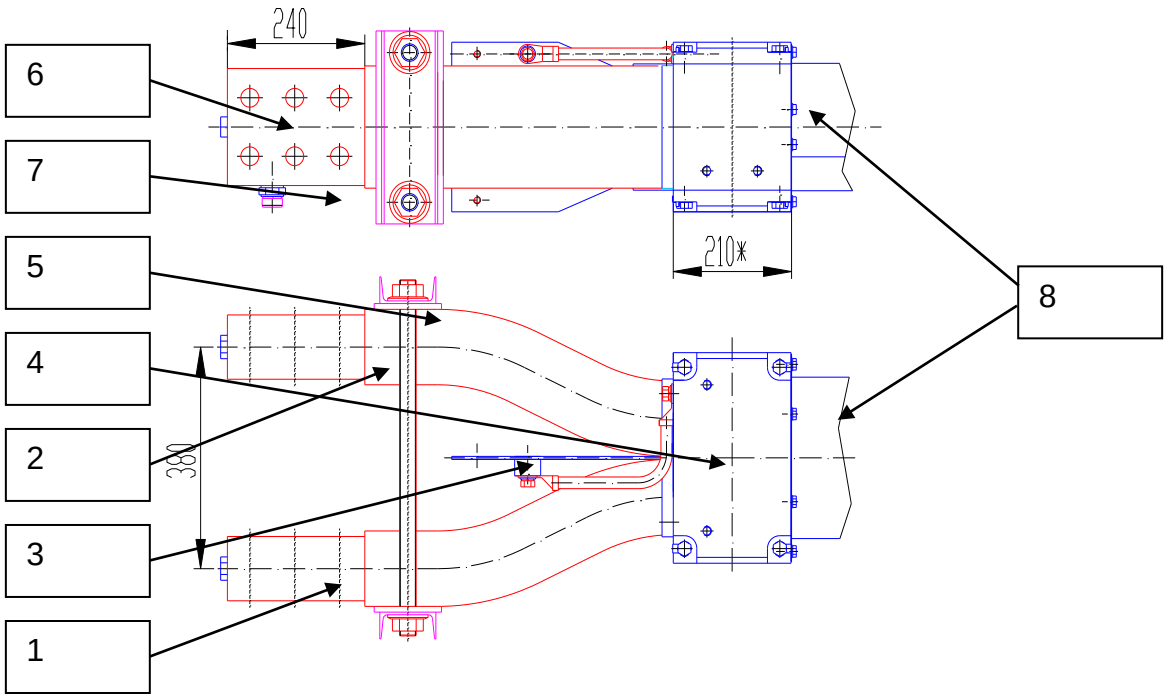

Figure 3.15 :PF/CS Busbar near the connection with flexible links. 1, 2 – one-polarity Busbars, 3 – separator, 4 - separator earthing, 5 - durostone stud, 6 – plug of axial hole, 7 - fitting for cooling water hose, 8 –clamp [8]

Table 3.2

Parameter	Unit	TF	PF/CS	CC	DL
Size of 2-pole Busbar cross-section (WxH)	mm	520x220; (272x420)	278x218	124x114	130x118
Maximum length of one piece	m	12	12	12	12
Tolerance for length	mm	±4	±4	±4	±4
Tolerance for deviation of ends from conductor axis	mm	±6	±6	±6	±6
Tolerance for parallelism of contact surfaces	mm	±2	±2	±2	±1
Minimal bending radius (horizontal)	m	0.55	0.43	0.18	0.18
Minimal bending radius (vertical)	m	0.6	0.6	0.3	0.3
Conductor weight per meter (2-poles)	kg	260	130	26	26
Busbar weight per meter (2-poles)	kg	316	162	39	40

3.1.3 Busbar supports

The DC Busbars are fastened to the ceiling, floor or, in some cases, to the walls of the ITER buildings with the help of metallic supports. These supports should withstand Busbar weight loads, seismic loads and electromagnetic forces emerging in the points, where the Busbars are connected with each other and with switches of the power supply systems, as well as in case of short-circuits. Location and fastening of the DC Busbars in different buildings is different. In Building 74 the Busbars are located above the power supply system equipment and are fastened to the ceilings. As the space is limited, some Busbars are arranged one above the other at two levels in height. The Busbars in Building 11 fastened either to the ceiling or to the floor are arranged. In buildings 32, 33 and on the bridges the Busbars also arranged at two or even three levels, are mainly fastened to the floor.
Two types of supports are used in the DC Busbar network independently of specific location and fastening method, namely, individual supports and group supports. The individual supports consist of the right and left halves fastened between each other with bolts and studs. Shims 2-4 mm in thickness are installed between the Busbars and supports. The supports can be rigidly fastened to the Busbars or with the possibility to slip. Rigidly fastened supports are installed on the Busbars nearby their junction with the switches and coil feeders. In the first case spacers are made of silicon rubber, which is pressed between two halves of the supports and the Busbar with a force of about 14 t using four M16 bolts of strength class 8.8. In other places the Busbars slip in the supports, when their length changes due to thermal expansion. The individual supports shall be installed on the Busbar prior to assembly so as to provide precise regulation of their positioning depending on the location of other elements of Busbar fastening (embedded plates, beams, frames, etc.). Holes for support fastening are of the oval form making it possible to position the Busbar in the direction perpendicular to their axis.
Some versions of the individual supports are shown in *Fig. 3.16*.

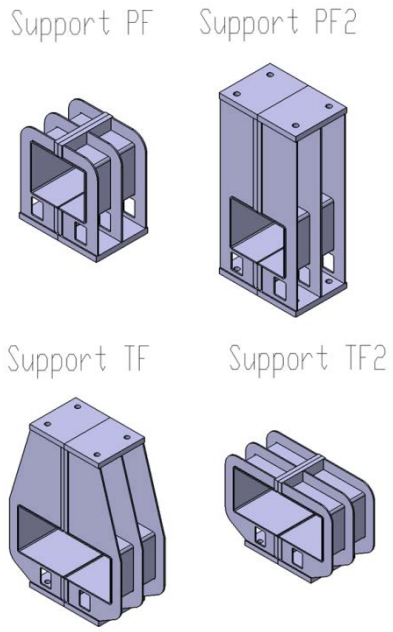

Figure 3.16: Individual supports [8]

The photographs of the supports of the TF and CC Busbar prototypes are shown in *Fig. 3.17, 3.18*.

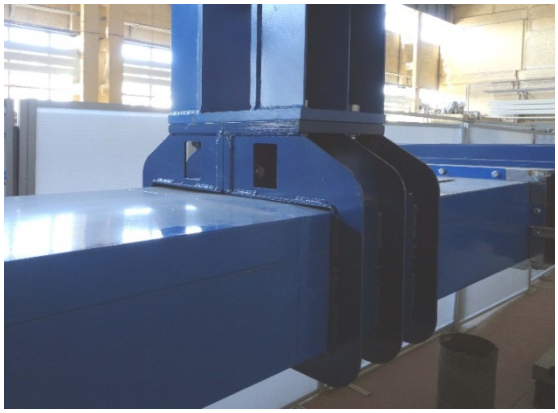

Figure 3.17 :Supports of the TF Busbar [8]

Figure 3.18: Supports of the CC Busbar [8]

The group supports carry several Busbars. As a rule, they are welded to the embedded plates in the ceilings, floor and walls of building. In buildings 32 and 33 they are installed on the concrete floor and fastened to the floor with anchor, Hilti, bolts. [8]

3.1.4 Thermal Expansion Compensators (TEC) and Rigid Inserts

Flexible links inserted between the Busbars to compensate for their thermal expansion are made of 0.6 mm copper strips. The thickness of the strips is a compromise between capabilities of the flexible links to withstand cyclic and electrodynamic loads at short circuit current.
At both ends of the flexible links the copper strips are mechanically interconnected by “diffusion bonding” (compression under very high pressure in vacuum), practically forming solid terminations. Fig. *3.19* and *Fig. 3.20* show the flexible links for the TF/PF/CS and CC Busbars. [8]

Figure 3.19: PF Busbar and CC Busbar thermal expansion compensator [8]

Figure 3.20: TF Busbar thermal expansion compensator and water cooling connections between the Busbars [8]

4. Electrical field distribution and possibility of partial discharge [9]

An analysis was developed by the Efremov Institute (Russia) for the definition of the regions of the most stressed state of the TF Busbar high-voltage insulation and the assessment of the effect of air cavities (voids) in insulation on the electrical field distribution in a TF Busbar.
The area with the highest field strength in the analysed geometrical models will be located in a place, where the distance between Busbar elements with different potentials will be minimal.
On this basis, the area between the conductor and separator inside the straight part of the Busbar shown in *Fig. 4.1* was chosen for the detailed analysis.

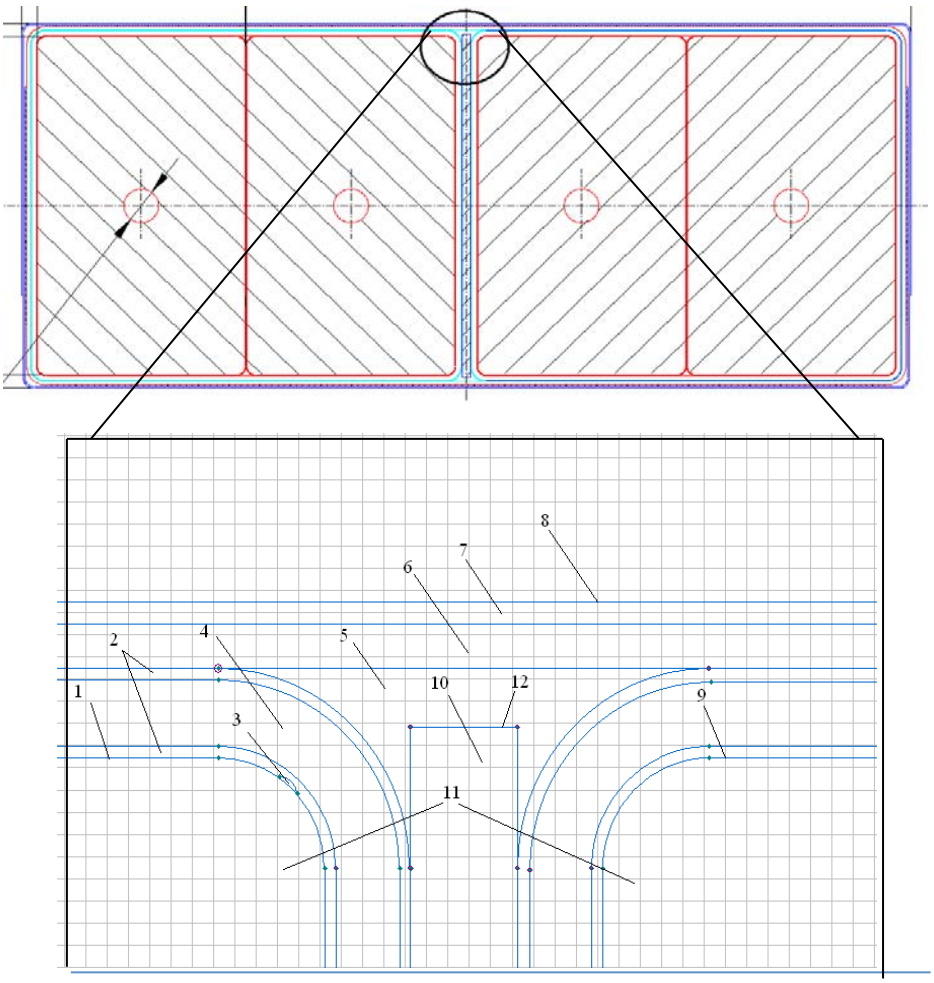

Figure 4.1: *The Busbar area around the separator inside the straight section of the Busbar, where 1, 9 – the boundary of the aluminium Busbar surface, where the value of voltage U is preset; 2 – the glass tape; 3 – the void; 4 – the basic insulation; 5 – the epoxy compound; 6– the bandage; 7 – the glass fiber plastic; 8, 12 – boundaries of casing and separator; 10 –separator; 11 – aluminium Busbars.* ***[9]***

In the *Fig. 4.2* below a plot of the electrostatic field distribution in the area showed in *Fig. 5.1* without any air gaps in the insulation between the conductor and the separator.

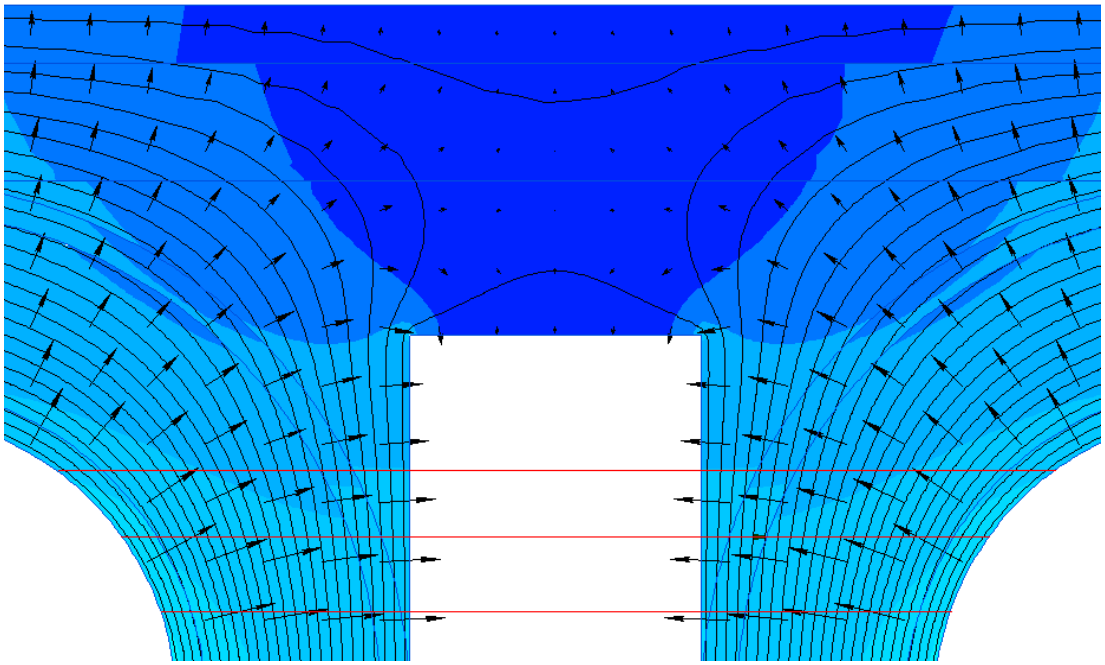

Figure 4.2: Distribution of the electrostatic field in the area around the TF Busbar separator. The lines, along which the field distribution graphs are plotted, are marked in red. [9]

The voltage between the separator and the two conductors is 10kV in normal operating conditions and 48kV for testing the insulation. Electrical field analysis was carried out in both cases.

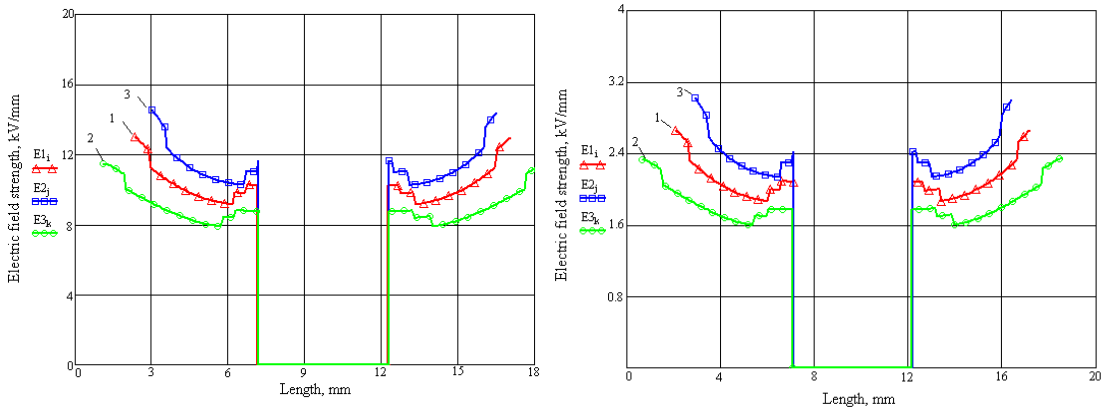

Figure 4.3: Graphs of electric field strength distribution (U=48 kV and U=10 kV): 1 – graph for the central line; 2 – graph for the upper line; 3 – graph for the lower line. [9]

One model was done to understand the entity of electric field in air gaps and it turned to be higher than the field in the insulation. The model with an air gap is in *Fig. 4.4* and *Fig. 4.5* is the plot of magnetic field strength along three paths.

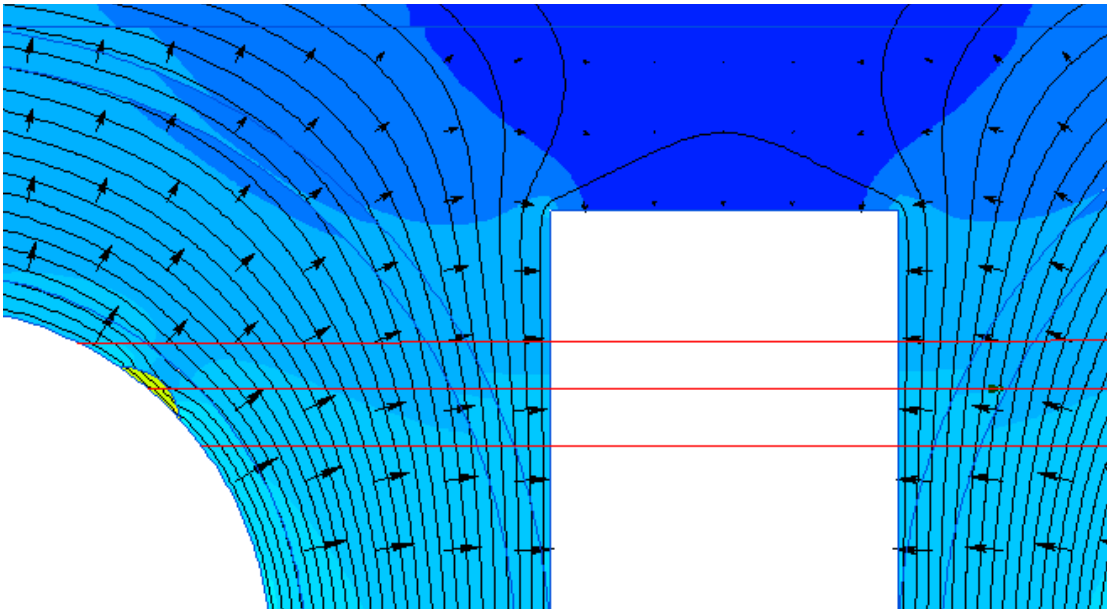

Figure 4.4: Distribution of the electrostatic field with consideration for effect of the air void near the aluminium conductor edge. [9]

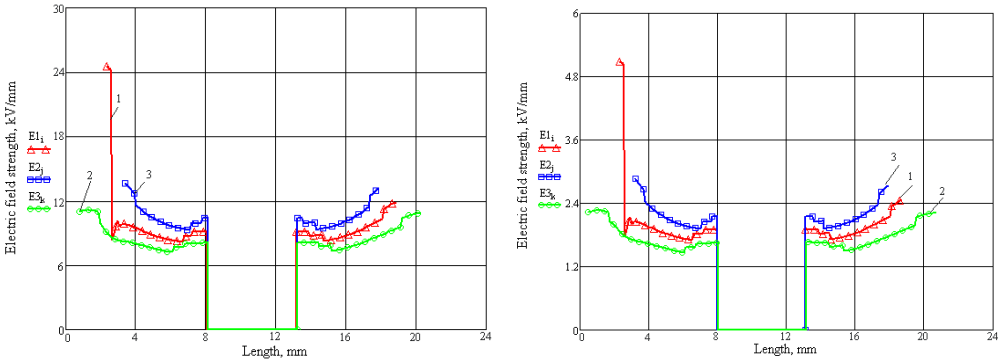

Figure 4.5: Graphs of the electric field strength distribution (U=10 kV and U=48kV): 1 – graph for the central line; 2 – graph for the upper line; 3 – graph for the lower line. [9]

The maximum electric field in normal operating condition without air gaps will be around 3.2 kV/mm, but if an air gap occurs it will be around 5 kV/mm. The most critical area is for sure the zone around the separator.

The analysis [9] of the electric field distribution in the TF Busbars has revealed that:

1. The area with the highest electric field strength inside the insulation is located on the straight-line part of the Busbar, where the separator is adjacent to the high-voltage insulation of the Busbar current-carrying parts. It is shown, that in this area the electric field strength might be as high as about 3.2 kV/mm at a voltage of 10 kV between the separator and the Busbar.

2. In all computational models, including those with a maximum applied voltage of 48 kV, the field strength inside the insulation was considerably less than the breakdown strength for this type of insulation (35 kV/mm).

3. The level of the electric field strength inside air voids can exceed air breakdown strength.

5. Objective of the thesis

Busbars are subjected to high voltage that involves a high electrical field around the conductor and between the conductor and the separator.
A model for the estimation of the electric field was done by the Efremov Institute (RUSSIA).
Also the case of air gaps was taken into account in the insulation layer and the conclusion was:
“The level of the electric field strength inside air voids can exceed the value of air breakdown strength, which might initiate partial discharges” [9].
The objective of this work is to evaluate if thermo-structural loads on the insulation, could lead, not only to the immediate failure of the insulation, but also to the formation of cracks and gaps that with time will lead to electrical failure.
A numerical evaluation of stress and strain in the insulation will be done using ANSYS Multiphysics software.
Unfortunately, no official specific design criteria is available at the moment for Busbar insulation and it was not possible to carry out experimental test to understand the properties of high voltage insulation and the bandage.
The material properties recommended by the manufacturer are used in the analysis.
The design criteria and the stress and strain limits considered for the insulation are chosen considering:

- ITER design criteria for magnets insulation; in fact for the magnets insulation materials extensive experimental tests where done.
- Scientific literature about test on similar materials (In particular the insulation of the Busbars is used for the stator windings insulation of medium-high power and high voltage generators).
- Failure criteria used by the manufacturer for the previews calculation.

The possibility of static or fatigue failure of the insulation is analyzed checking if the stress or strain exceeds the values of the various criteria. The other main possibility of failure is the possibility of debonding between the layers of insulation or easier between the insulation and the aluminum conductor. A contact analysis, to understand the possibility of gap generation between the two surfaces, will be done.
The loads applied are only thermal because extensive analysis on magnetic loads was already done [10] and no other external force is considered.

6. DC Busbars thermo-structural analysis

The DC Busbars are subjected to thermal loads generated by the current that flows in the conductor. The first part of this analysis estimates stress and strain on the insulation considering that it will bond the aluminium conductor and insulation (using GLUE command). The 2-D or 3-D volumes are meshed with thermal mass elements and a thermal analysis is performed. After this analysis the temperature distribution on the model is known and the thermal elements are switched to mechanical.
Mechanical analysis is performed using proper boundary conditions in each different model (2-D and 3-D).

6.1 Busbar section geometry

There are three main different section geometry : CC Busbar, PF Busbar, TF Busbar.
The dimension of the model for PF Busbar are in the Fig. 6.1 and Fig 6.2.

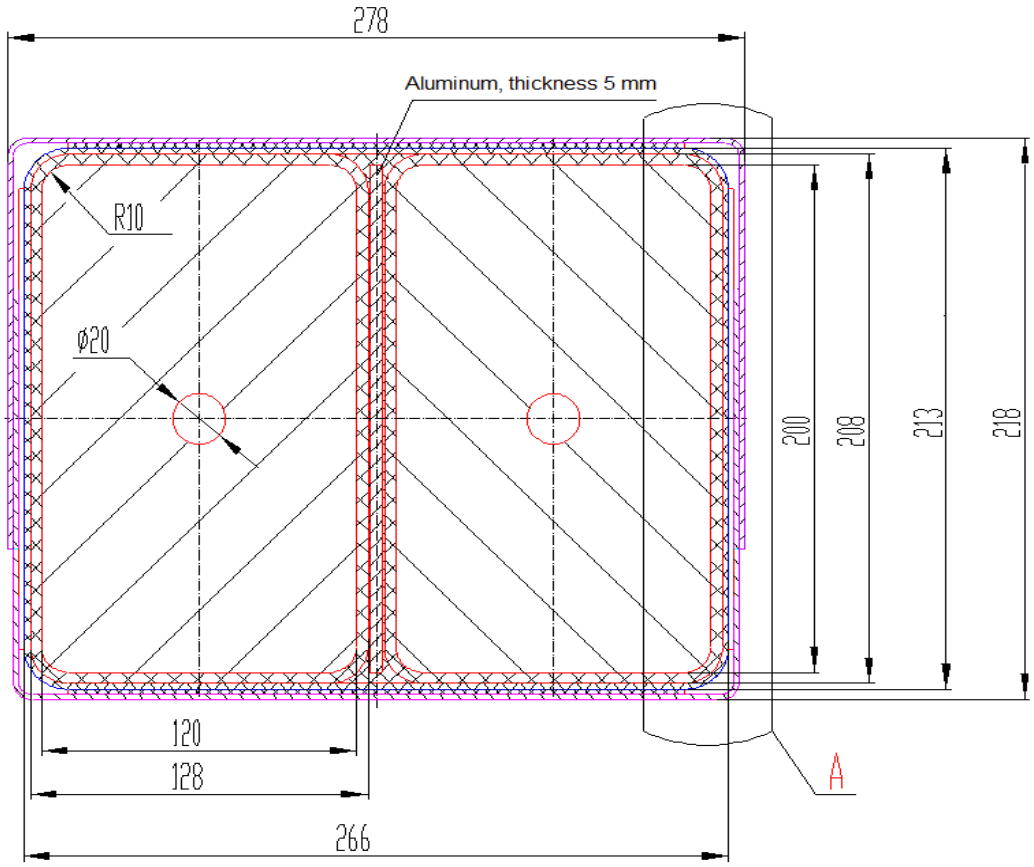

Figure 6.1: PF Busbar cross-section geometry [8]

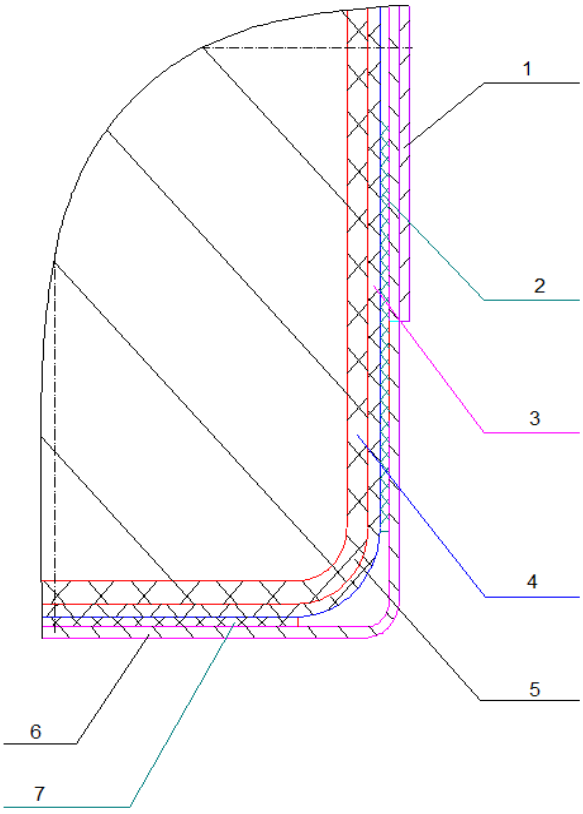

Figure 6.2 : Area A in Figure 39: 1, 6 – steel casing (δ=1 mm); 2, 7 –spacer (δ=2 mm); 3 –glass-epoxy bandage (δ= 2.5 mm); 4,5 –high voltage insulation(δ=3.5 mm); [8]

The dimension of the model for TF Busbar are in the Fig. 6.3 and Fig. 6.4.

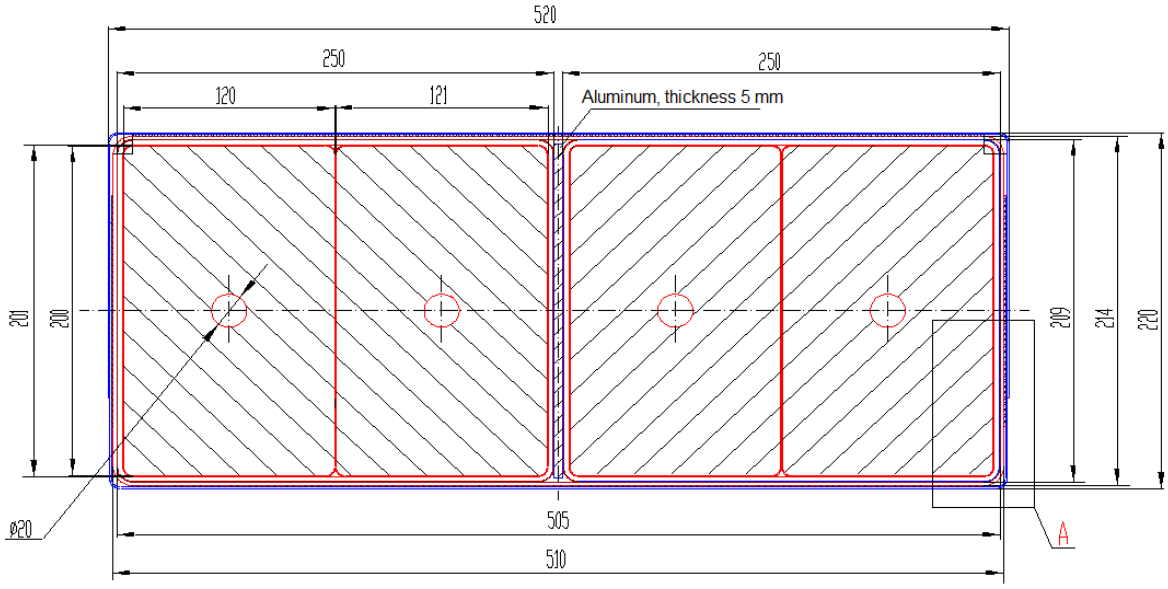

Figure 6.3: TF Busbar cross-section geometry [8]

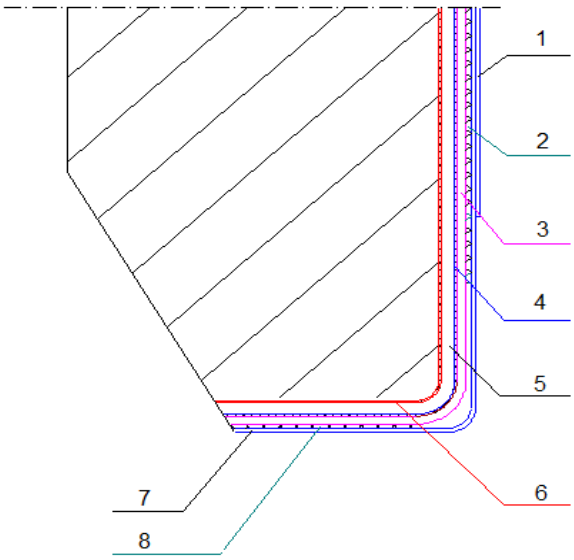

Figure 6.4: Area A in Figure 41: 1, 7 – steel casing (δ=1 mm); 2, 8 – glass-epoxy spacer (δ=2 mm); 3 – glass-epoxy bandage (δ= 2.5 mm); 4 – glass-epoxy insulation (δ=0.5 mm); 5 – high voltage insulation layer (δ=3.5 mm); 6 - glass-epoxy insulation (δ=0.5 mm); [8]

The dimension of the model for CC Busbar are in the Fig. 6.5, 6.6.

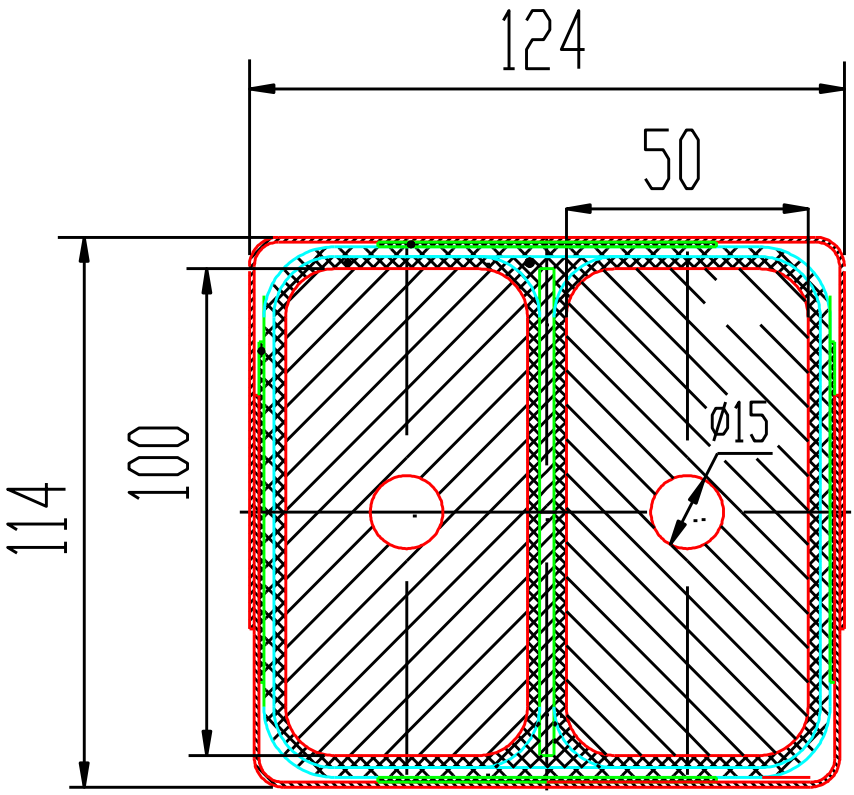

Figure 6.5: CC Busbar cross section geometry [8]

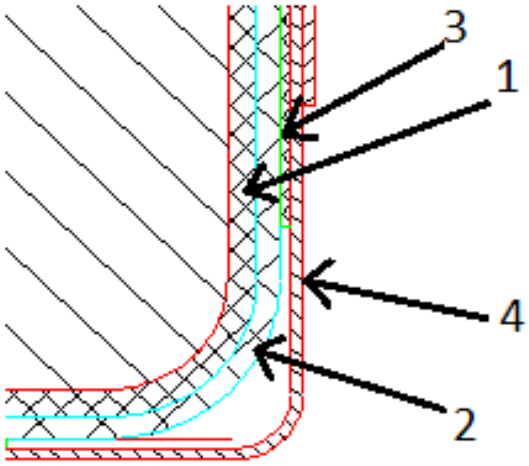

Figure 6.6: 1-high voltage insulation layer (δ=2 mm); 2-glass-epoxy bandage (δ= 2 mm); 3-spacers (δ= 2mm); 4-casing (δ= 1mm) [8]

6.2 Thermal Loads

- Heat generated by the current
- Natural air convection
- Cooling Water convection

6.2.1 Heat generated by the current

The current flows in the bus heats the conductor; this effect is described by the Joule law.

I= current intensity

ρ= Resistivity

A=Area

L=Length

V=A L= Volume

P= Power produced

p=Specific power produced

$$P = \frac{\rho L I^2}{A} \text{ [W]} \qquad (6.1)$$

$$p = \frac{\rho L I^2}{AV} = \frac{\rho L I^2}{A^2 L} = \frac{\rho I^2}{A^2} \text{ [W/m}^3\text{]} \qquad (6.2)$$

The power produced by current is written in *Table 6.1* for a temperature of 20°C.

Table 6.1.Current and Power produced 20°C

Busbar type $\rho_{(20°C)}$ =2.95 $10^{-8}\Omega$m	Current	Current density	Power Produced (20°C)
PF/CF	55 kA	2.3 A/mm^2	155204 W/m^3
TF	68 kA	1.4 A/mm^2	59311 W/m^3
CC	10 kA	2.07 A/mm^2	119020 W/m^3

The thermal analysis held highlighted that the variation of electrical resistance within a temperature variation in the aluminium conductor was not negligible. It was considered this variation of resistance with a simple approximation taking in account the temperature variation. The electrical resistance changes within temperature variation with this law:

$$R(T)=\rho_{(20°C)}\ (1+\alpha\Delta T) \qquad (6.3)$$

$$\Delta T=(T-20°C) \qquad (6.4)$$

T=temperature

α=temperature coefficient of resistance

$\rho_{(20°C)}$=resistivity at 20°C

R(T)=resistivity as a function of temperature

The variation of temperature of the aluminium conductor is around 30-40°C. For analysis purposes was used the power produced at 60°C.

The power produced by current is written in *Table 6.2* for a temperature of 60°C.

Table 6.2. Current and Power produced 60°C

Busbar type $\rho_{(20°C)}$ =2.95 $10^{-8}\Omega$m	Current	Current density	Power Produced (60°C)
PF&CF	55 kA	2.3 A/mm^2	180000 W/m^3
TF	68 kA	1.4 A/mm^2	68800 W/m^3
CC	10 kA	2.07 A/mm^2	140000 W/m^3

6.2.2 Air convection and Water cooling

Convection is related to heat flux using Newton's law of cooling:

$$q/A = h\ (t_s - t_f) \qquad (6.5)$$

where:

q/A= heat flux out of the face

h= is the film coefficient

t_s = is the temperature on the face

t_f = is the bulk fluid temperature

Air natural convection was considered on the external face of the steel casing of the Busbar and water convection in the hole of the aluminium conductor where there is the cooling water. Increase in water temperature should be about 20-25°C or less under normal operating conditions and the maximum temperature is around 50°C.
The temperature for water convection in the following analysis was considered constant and equal to 51 °C.

Table 6.3

	t_f = is the bulk fluid temperature	h= film coefficient
Air convection	31 °C	5 W/m^2K
Water convection	51 °C	10000 W/m^2K

In reality the cooling water flows in the hole through the aluminium conductor and the water temperature changes. Each pole in the Busbars has a different water channel. The water in the Busbar will flow in the same direction in each pole. The channels for water cooling of the two different polarity conductors will be in parallel in the piping circuit of the water cooling system.
This means that in each section of the Busbar we can consider the same temperature of the water in the different poles. There will be no differential thermal expansion between the two poles of a single Busbar.

6.3 Material properties

The properties of the aluminium conductor, aluminium separator and the steel casing are well known.
For the high voltage insulation layer and the bandage the values are assumed because there aren't any properties available with the exception of the electrical properties. For the electrical properties see Annex I.
The Busbars manufacturer considers the properties of superconductive magnets insulation suitable for the analysis in this work. [10]

6.3.1 Aluminium conductor

The thermal conductivity properties of the aluminium conductor are summarized in Table 6.4.

Table 6.4: aluminium conductor thermal conductivity

Temperature, ^oC	27	77	177	227
Thermal conductivity, W/(m×K)	207	210	217	222

In the range of 45-65 ^oC the variation of thermal conductivity is around 0.74%.
Thus it could be approximated to a single value in order to reduce the time of calculation in the analysis. In the following graph (Fig. 6.7) the fitting of the data of the previous Table 6.4 is shown.

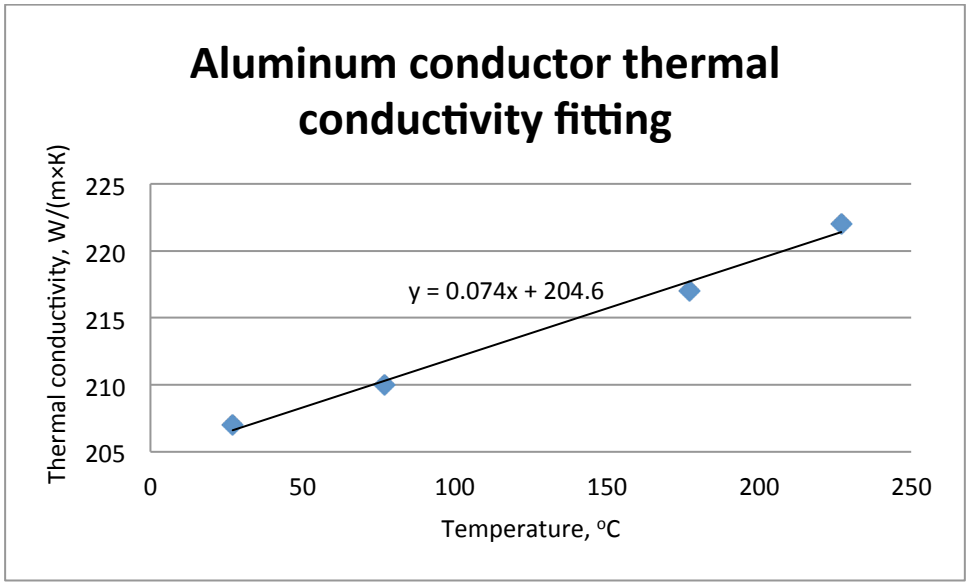

Figure 6.7

The regression equation is: λ =0.074*50+204.6
The thermal conductivity computed for a temperature of 50 ^{o}C is 208.3 W/(m×K).

The mechanical properties of the aluminium conductor are shown below (Table 6.5).

Table 6.5: Mechanical properties

v	0.32
ρ, kg/m^3	2600
E, GPa	70
CTE, 10^{-6}/K	22.2

6.3.2 Aluminum separator

The mechanical properties of the aluminium separator are reported below (Table 6.6).

Table 6.6. Aluminum alloy АМцМ5 (Russian grade)

E, GPa	71
v	0.3
ρ, kg/m^3	2730
CTE,10^{-6}	25×10^{-6}
λ, W/(m K)	180
UTS, MPa	120
YS, MPa	50
RA, %	70

6.3.3 Insulation

The high voltage insulation and the fiberglass bandage have, for this analysis purposes, the same properties. The thermal conductivity recommended by the manufacturer for this kind of analysis is λ=0.3W/(mK).
The mechanical properties of the superconductive insulation have been assumed to be same of the high voltage insulation and of the fiberglass bandage of the Busbars. [11]

Table 6.7: Properties of insulation

Component	Material	properties
TF, CS, PF turn insulation	High voltage insulation	$E_1=E_1=20GPa$ $E_3=12GPa$ G=6GPa $V_{12}=0.17$ $V_{13}=v_{23}=0.33$

These data are given for 4K and the manufacturer of the Busbar insulation inform that these properties (E, G and v) vary about 10% passing from room temperature to 4K.
In this kind of insulation material the Joung's Modulus (E) decrease with a rising temperature. All the analysis done will consider the properties at 4K. This rough approximation is done because the stiffness of the material is greater at 4K and thus using this value results in higher stresses and will be conservative (the higher the modulus the higher stresses).
The thermal expansion coefficient is given by the manufacturer and there is valid for both the high voltage insulation and the bandage (Table 6.8).

Table 6.8: Coefficient of thermal expansion

Direction	CTE 10^{-6}/K
1	3
2	3
3	9

The directions the table refers to are shown in the picture below (Fig. 6.8).

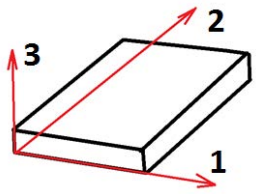

Figure 6.8: Orientation of axes. Axis 3 goes through the insulation thickness

6.3.4 Spacers

The spacers are located between Busbars and fixed-type supports. They are made of resin based on siloxane-type rubber.
The recommended modulus of material is within $2\div5\times10^3$ MPa.
For the thermal analysis the conductivity considered is λ=0.3W/(mK).

6.3.5 Casing

The casing is made of Stainless steel and it is the protection of the Busbar. In the following Table (Table 6.9) thermal and mechanical properties of the casing are shown.

Table 6.9. Stainless steel 12X18H10T (Russian grade, austenitic steel)

	Temperature, °C					
	20	**50**	**100**	**150**	**200**	**250**
E, GPa	205	202	200	195	190	185
v	0.3					
CTE,10^{-6}	16.4	16.4	16.6	16.8	17.0	17.2
λ, W/(m K)	13.9		15.1		16.5	
UTS, MPa	491	480	461	436	417	397
YS, MPa	196	191	189	186	181	176
RA, %	40	40	40	40	40	40

In the range of 45-65 ^{o}C the variation of thermal conductivity is around 2.5%.
Thus it could be approximated to a single value in order to reduce the time of calculation in the analysis. In the following graph (Fig. 6.9) the fitting of the data of the previous Table 6.9 is shown.

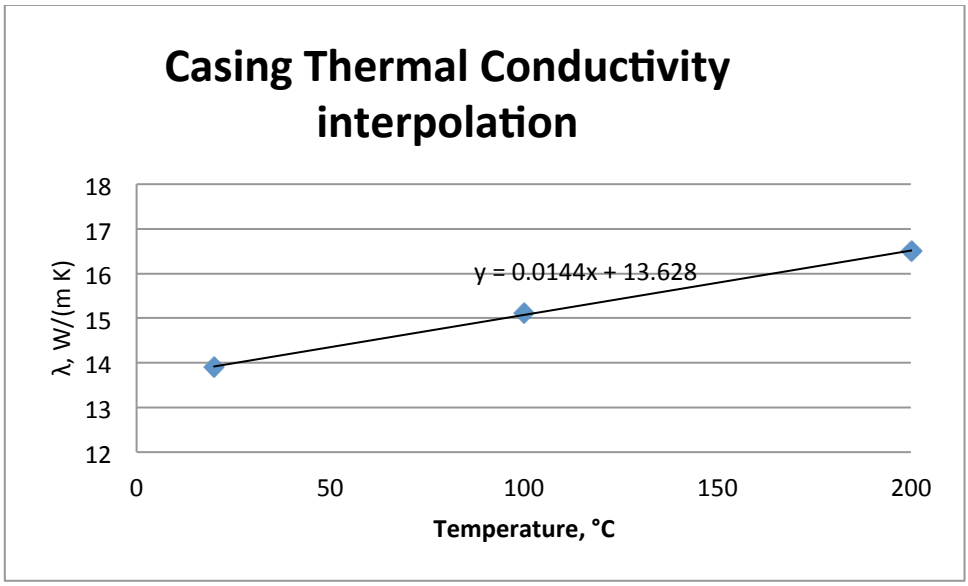

Figure 6.9

The regression equation is: λ_{casing}= 0.0144*50+13.628λ
The thermal conductivity computed for a temperature of 50 ^{o}C is 14.3 W/(m K) and will be used in the following analysis.

6.3.6 Air

Air gaps between the casing and the insulation were considered only in the thermal analysis.
The considered thermal conductivity of air was: λ_{air}=0.03 W/(m K)

6.3.7 Material properties macro

Filename: matprop.mac
!thermal conductivity
MP,KXX,1,208.3 !conductor
MP,KXX,2,180 !separator
MP,KXX,3,0.3 !insulation
MP,KXX,4,0.03 !air
MP,KXX,5,14.3 !casing
!aluminum conductor structural material properties
MP,EX,1,70E9
MP,PRXY,1,0.32
MP,ALPX,1,22.2E-6
!aluminum separator structural material properties
MP,EX,2,71E9
MP,PRXY,2,0.3
MP,ALPX,2,25E-6
!high voltage and bandage insulation structural material properties
MP,EX,3,12E9
MP,EY,3,20E9
MP,EZ,3,20E9
MP,PRXY,3,0.33
MP,PRYZ,3,0.17
MP,PRXZ,3,0.33
MP,GXY,3,6E9
MP,GYZ,3,6E9
MP,GXZ,3,6E9
MP,ALPX,3,9e-6
MP,ALPY,3,3e-6
MP,ALPZ,3,3e-6

7. Allowable stress and strain in high voltage insulation

Our main concern is to understand the behaviour of the insulation layer. This will tell us if is there the possibility of electrical failure of the insulation. The first thing is to understand if there is the possibility of mechanical static and fatigue failure under thermal loads.
Unfortunately, no official specific design criteria are available at the moment for the Busbar insulation. To ensure a good design criteria choice here there is a comparison between the design criteria for ITER magnets insulation, Efremov Institute design criteria and tests on mica/epoxy insulation of generators stator windings.
There wasn't any possibility to held experimental test on the insulation material of DC Busbars.
The main criteria used for this work will be the criteria for ITER magnets.

7.1 Allowable stress and strain for ITER magnets

Failure Modes considered for magnets insulation:

- Compressive and Tensile failure (static and fatigue)
- Shear de-lamination (static and fatigue)
- Tensile de-bonding (static and fatigue)

The insulation materials have a 2-dimensional reinforcing (in-plane directions) and mechanical failure of high voltage insulation normal to the reinforcing is assumed to eventually result in electrical breakdown. Local failure parallel to the reinforcing can be tolerated. In composites and insulation systems, the critical stresses are determined by the normal and shear stresses in a coordinate system defined by the in-plane and normal directions. (It is not usually convenient to separate the stresses into primary and secondary components, so the stresses referred to in the following sections are the total stresses, including peak stresses, except tensile stresses across the insulation layers.)

7.2 Design Criteria for High-Voltage Magnets Insulation Systems

Insulation does not undergo yielding as metallic materials do, but local stress peaks caused by geometric discontinuities are relieved by local cracking and particularly by de-bonding from the metal surface. The tensile and shear stress criteria may be locally exceeded by secondary and peak tensile and shear stresses where it can be demonstrated that cracking or surface de-bonding parallel to the insulation layer will relieve the stresses. The compressive stress criterion defined may not be exceeded by secondary or peak stresses.

7.2.1 Experimental data

The data in the Table 7.1 below are obtained from experimental tests on the insulation of superconductive magnets.

Table 7.1: Magnets insulation material properties

Components	Static Stress Limits	Fatigue Stress Limits	Ultimate compressive strength
TF, CS, PF Turn Insulation	τ_o = 85 MPa C_2 = 0.45 for $S_{c(n)}$ < 58 MPa	τ_o = 85 MPa C_2 = 0.45 for $S_{c(n)}$ < 58MPa	σ_{cs} =1200MPa
	S_{ss} = 68.6 MPa for $S_{c(n)}$ > 58 MPa	S_{sf} = 68.6 MPa for $S_{c(n)}$ > 50MPa	

Where:

σ_{cs} = minimum static compressive strength is defined as the average compressive strength minus two standard deviations (95.4% percentile) of the data set of a minimum of 10 measurements.

τ_o = the experimentally determined minimum intrinsic shear strength of the material (the subscripts s and f refer to data from static and fatigue tests, respectively) with no compressive load at the temperature and nuclear radiation dose representative of the service condition. The strength will represent the lowest of the bond shear strength or the composite interlaminar shear strength. This strength, established by testing, represents the lowest data point of at least 6 specimens or, if more than 10 specimens are tested, the mean value minus 2 standard deviations (95.4% percentile).

c_2 = an experimentally determined factor for the proposed insulating material based on combined shear and compression testing at the temperature and nuclear radiation dose level representative of the service conditions. The constant represents the slope of the dependence of shear strength on compressive stress.

$S_{c(n)}$ = the applied normal compressive stress and the subscripts s and f refer to data from static and fatigue tests, respectively.

7.2.2 Compressive-Stress Allowable Normal to Reinforcing Plane

Static

The compressive-stress allowable in the through-thickness direction of continuous sheets or plates of insulating material shall be equal to 1/2 the minimum ultimate compressive strength:
$S_c = (1/2)\sigma_{cs}$

In our case σ_{cs} for the high voltage insulation and the bandage is 1200MPa at 4K.
Considering the values in *Table 7.1* the compressive stress allowable is S_c =600MPa

Fatigue

The compressive fatigue stress allowable S_c shall be equal to the lower of: 1/2 the ultimate compressive fatigue strength σ_{cf} measured at the lifetime number of cycles or the ultimate compressive fatigue strength at 10x the lifetime cycles.
$S_{c\ (fatigue)} = (1/2)\ \sigma_{cf}$
In the absence of fatigue data, the compressive fatigue stress allowable shall be equal to 1/3 the static compressive strength σ_{cs}.
In the case of the magnets σ_{cs} for the high voltage insulation is 1200MPa at 4K.

Considering the values in *Table 7.1* the compressive fatigue stress allowable is $S_{c\ (fatigue)}$ =200MPa

7.2.3 Tensile-Strain Allowable Normal to Reinforcing Plane

In the direction normal to the adhesive bonds between metal and composite, no primary tensile strain is allowed. Secondary strain will be limited to 1/5 of the ultimate tensile strain.
In the absence of specific data, the allowable working tensile strain is 0.02% in the insulation adjacent to the bond.

7.2.4 Shear Stress Allowable

The static and fatigue shear-stress allowable (S_{ss} and $S_{sf,}$ respectively) across the reinforcing planes for an insulating material is most strongly a function of the particular material and processing method chosen, the stress-loading conditions, the temperature and the radiation exposure level. The shear strength of an insulator depends strongly on the applied compressive stress.

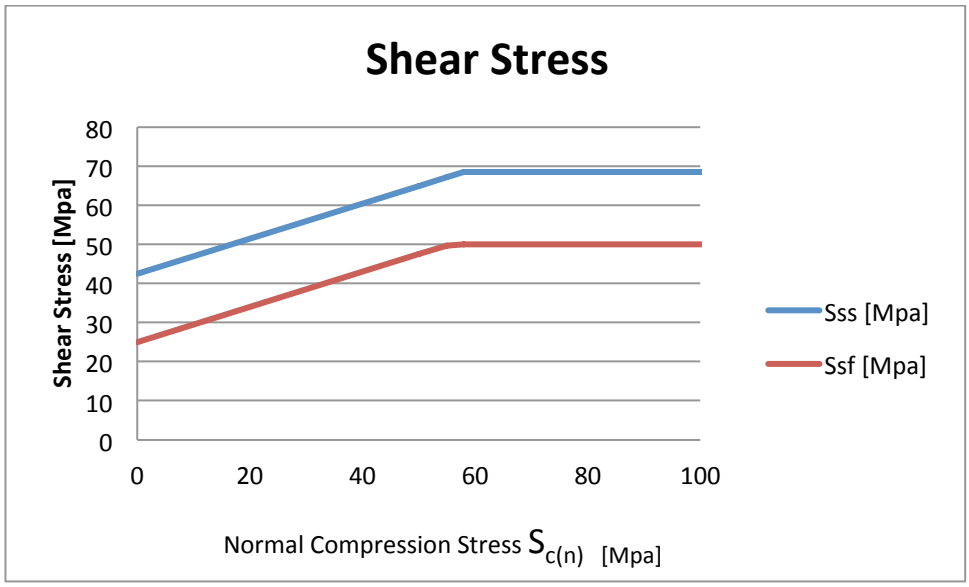

Figure 7.1: Allowable shear stress as a function of normal compression

The form of the variation of shear strength for magnets insulation material is in the data is shown in *Fig. 7.1*. At zero compression there is a so-called bonding shear strength τ_o. The shear strength increases linearly up to a limiting value and then remains constant until the compressive strength limit is reached. The linear part of the curve is expressed by the following equations, with the factor of 0.5 representing a safety factor. The value of c_2 is the experimentally determined factor, without a safety factor. The limiting value of the compression is chosen so that the corresponding limiting shear value is a factor of two below the experimental values, to provide a safety factor.

Static $S_{ss} = [0.5\ \tau_{os}] + [c_{2s} \times S_{cs(n)}]$ up to the limiting value of compression
then constant above the limiting value of compression

Fatigue $S_{sf} = [0.5\ \tau_{of}\ ] + [c_{2f} \times S_{cf(n)}]$ up to the limiting value of compression
then constant above the limiting value of compression

7.2.5 Strain Allowable in Plane of Reinforcing

The in-plane strains are usually secondary stresses, imposed by the coil structural material. The maximum tensile or compressive strain permitted in the plane of the insulation material is either +0.5% or -0.5%. This strain limitation is imposed to preclude micro cracking in the through-thickness direction of the insulation sheets. The strain limits normal to the plane of the insulation are considered to be independent of the in-plane strain.

7.3 Manufacturer criteria

7.3.1 Allowable tensile stress criteria

Allowable tensile stress along layer of high voltage insulation of DC Busbar, considered by Efremov Institute, is $\sigma_{insulation} = \sigma_u/3 = 83$ MPa.
This is the only criteria used in the ITER document : “Stress analysis of PF, CS, TF and CC Busbars” by Efremov Institute.
The value of $\sigma_u = 250$MPa was took from “Meterials in Machine Construction. Non-metallic materials.” Handbook, V.5, Moscow, “Mashinostroenie” publishing house, 1969 (In Russian). [10]

7.4 Experimental tests held on similar insulation materials

In scientific literature information about similar insulation types can be found only regarding electric medium-high power generators. This mica/epoxy insulation type is used in stator windings.
For example in [12] experiments on mechanical fatigue were conducted using the specimen which were cut from hydrogen cooled generator (rated 22kV and *500MW)* stator windings. In this article the ageing mechanism of mica/epoxy insulation systems were investigated under air or hydrogen by both the tensile and compressive loadings.
Are here written the Mica/epoxy insulation properties found in experimental test useful for checking the superconductive magnets failure criteria and understand if this criteria is applicable for LSM type tape. [12]
Tensile static characteristics in *Table 7.2*:

Table 7.2

Specimens	Young’s modulus	Max tensile strength	Max tensile strain
Sound specimen under air	18.13 GPa	94.25 MPa	0.67%
Aged specimen under air	18.11 GPa	84.34 MPa	0.58%

Young’s modulus value confirms the material properties used in our analysis. On the other side max tensile stress is lower than the one considered in *Cap.9.3.1* because this material is not reinforced with fiberglass as LSM type Tape.

Table 7.3

Specimens	Compressive strength	Compressive strain
Sound specimen under air	-110 MPa	0.1%
Aged specimen under air	-100 MPa	0.1%

All the electrical equipment must withstand at list around 30000 cycles. The fatigue characteristics took from the article are tensile fatigue characteristics at 30000 cycles.

Table 7.4

Specimens	tensile fatigue strength
Sound specimen under air	25 MPa
Aged specimen under air	25 MPa

Compressive Fatigue characteristics at 30000 cycles in *Table 7.5*.

Table 7.5

Specimens	Compressive strength
Sound specimen under air	-70 MPa
Aged specimen under air	-70 MPa

7.5 Comments

To verify the Busbar insulation all the criteria for the magnet insulation will be used:

- Compressive/Stress Allowable Normal to Reinforcing Plane
- Tensile Strain Allowable Normal to Reinforcing Plane
- Strain Allowable in Plane of Reinforcing
- Shear Stress Allowable across the reinforcing planes

The material used for the experimental test in [12] is not a reinforced tape like the LSM type tape. The young modulus is really close to the one used for the analysis. The max tensile strain in [12] confirm the limit values in the magnet insulation criteria.
The ultimate static tensile strength for the mica/epoxy material in [12] is 94.25MPa and the allowable value considered by the manufacturer for the LSM tape is $\sigma_{insulation} = \sigma_u/3 = 83$ MPa and the static tensile strength is 250MPa. The ultimate tensile strength in the article does not confirm the values considered by the manufacturer because this is due to the fact that the materials of the specimen in the article are done only of mica and epoxy without other reinforcing material.

Another possible failure criteria is using Von Mises Criteria and for the σ_{id} could be used directly the value of $\sigma_L = 83$ MPa.

8. 2-D Thermo-structural analysis

8.1 Steady state thermal analysis

The software used for thermal analysis is ANSYS Multiphysics.
The loads considered for this analysis are the uniform heat generation in the aluminium conductor, the air natural convection on the casing and the convection of cooling water.
The objective is to calculate nodal temperatures in order to have the whole field of temperature. Once computed these temperatures, a structural analysis will be done considering the variation of temperature in each part of the Busbar.
The mesh was modified step by step in order to improve the mechanical analysis results starting from a free rough mesh and improving it where possible with mapped mash.

The thermal analysis is done on a quarter of Busbar. The reasons of this choice are:

- The geometry of the Busbar cross-section is symmetric with respect to the X-Z plane and the Z-Y plane. See *Fig. 8.1*.
- Thermal loads applied are symmetric with respect to the X-Z plane and the Z-Y plane because they are uniformly applied to geometrical entities (areas and volumes). Furthermore there is no heat exchange in the planes of symmetry.

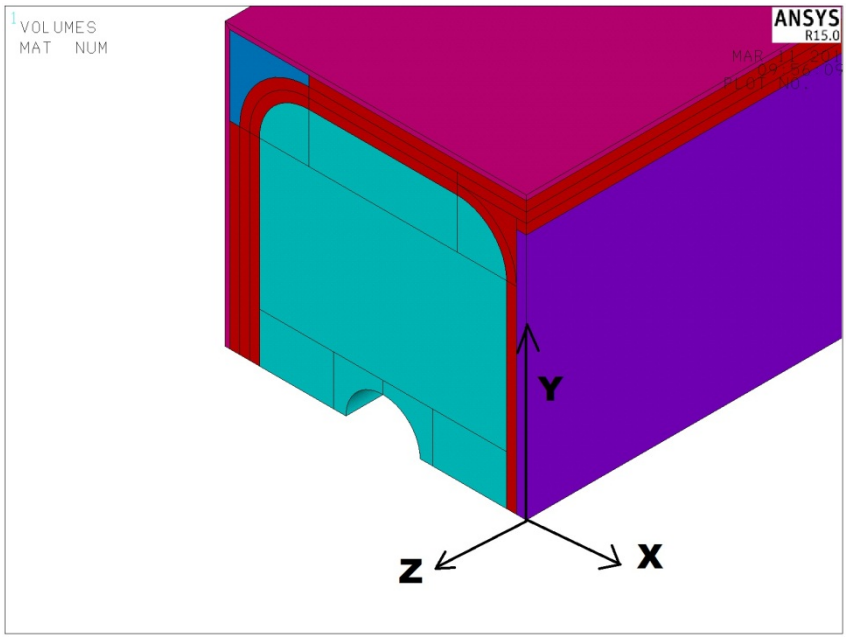

Figure 8.1: Reference system and symmetry planes

8.1.1 Element Type

Element SOLID55 was used for this analysis. This element can be used as a plane element or as an axisymmetric ring element with a 2-D thermal conduction capability. The element has four nodes with a single degree of freedom, the temperature, at each node.
The element is applicable to a 2-D, steady-state or transient thermal analysis.
Element Keyoptions are:
-k1 Evaluate film coefficient at average film temperature
-k2 Element behaviour: Plane
-k3 Element coordinate system are defined parallel to the global reference system

The element geometry is shown in Fig. 8.2

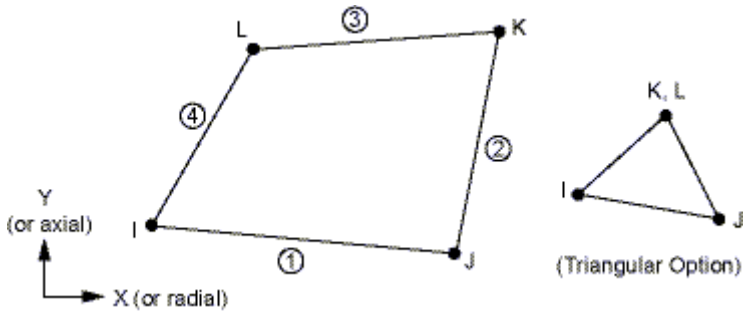

Figure 8.2 PLANE55 Geometry

8.2 CC, PF, TF Busbar 2-D FEM model

The 2-D thermal analysis model is the cross section of the Busbar.
The geometry of cross section of the CC, PF, TF Busbar is done with a “bottom–up” method starting from the definition of keypoints and than defining lines and areas. No 2-D or 3-D geometrical model was provided and thus it was built as is reported in the APDL script in Annex II. The model is a unique body with no interface/contact thermal effects.
In the figure below (Fig. 8.3) are shown the plots of the geometry and the thermal material properties.

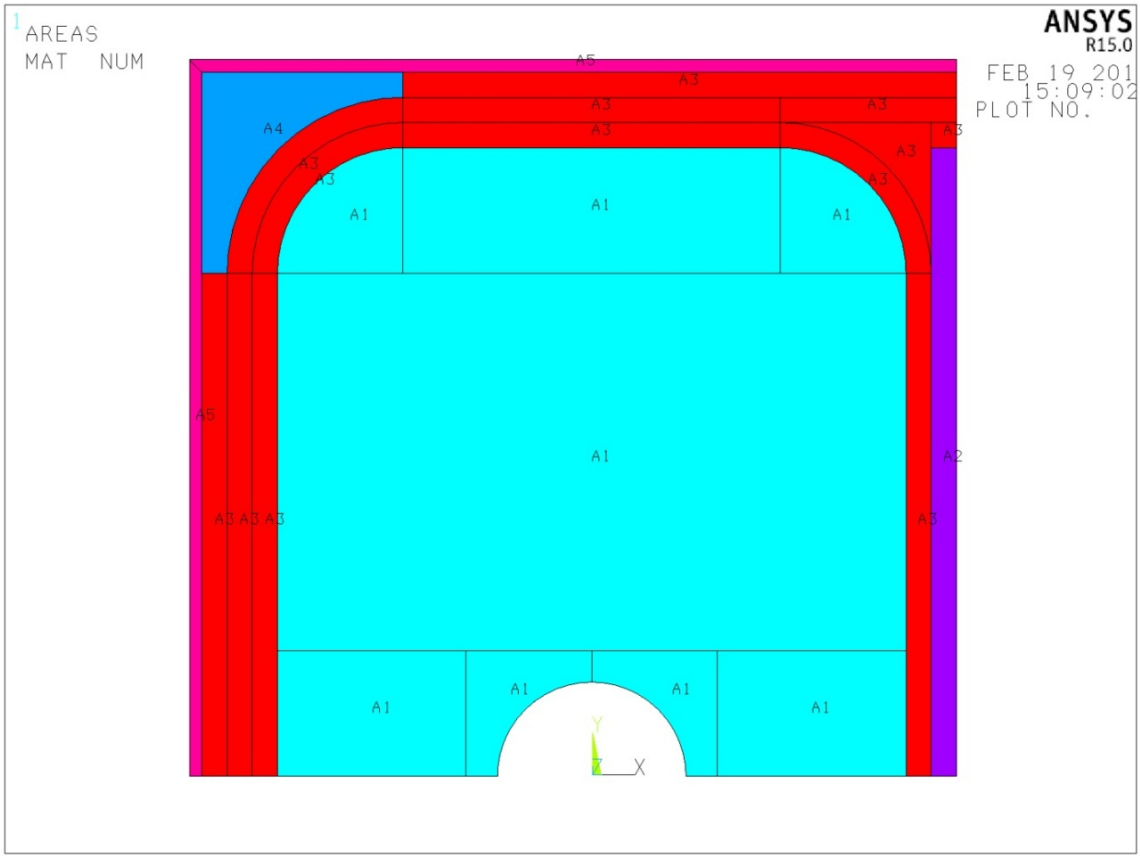

Figure 8.3: Model and material properties for CC Busbar

In the picture above Area A1 (filled in light blue) represents Material Number 1 and corresponds to the aluminium conductor in reality. Area A2 (filled in violet) is the aluminium separator (Material Number 2), Area A3 (filled in red) represents the high voltage insulation, the bandage and the spacers (Material Number 3). Area A4 (filled in blue) is an air gap between the insulation and the casing. Area A5 (magenta) is the casing (Material Number 5).
In the next figure (Fig. 8.4) the mesh of the 2-D cross section model of the CC Busbar.

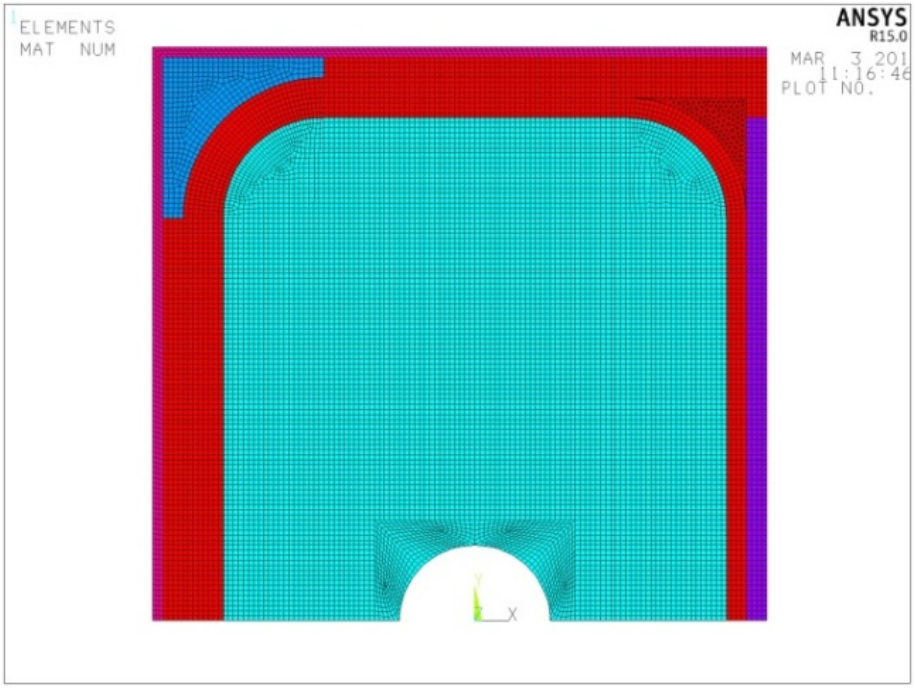

Figure 8.4: Mesh of CC Busbar model

In the following Fig. 8.5 the mesh of the PF&CS Busbar cross section.

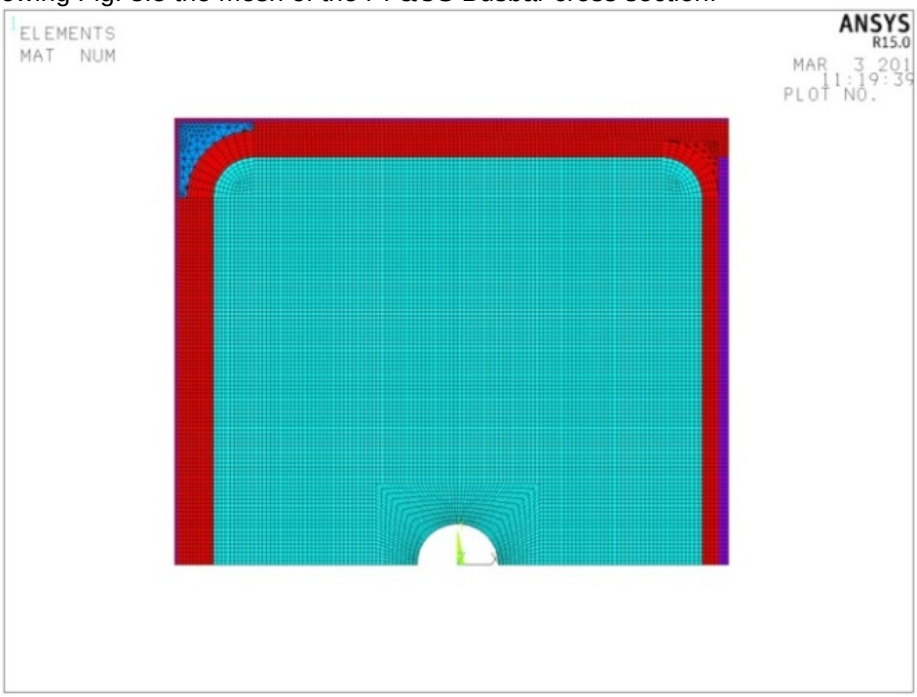

Figure 8.5: Mesh of PF Busbar model

In Fig. 8.6 the model and the mesh of TF Busbar cross section.

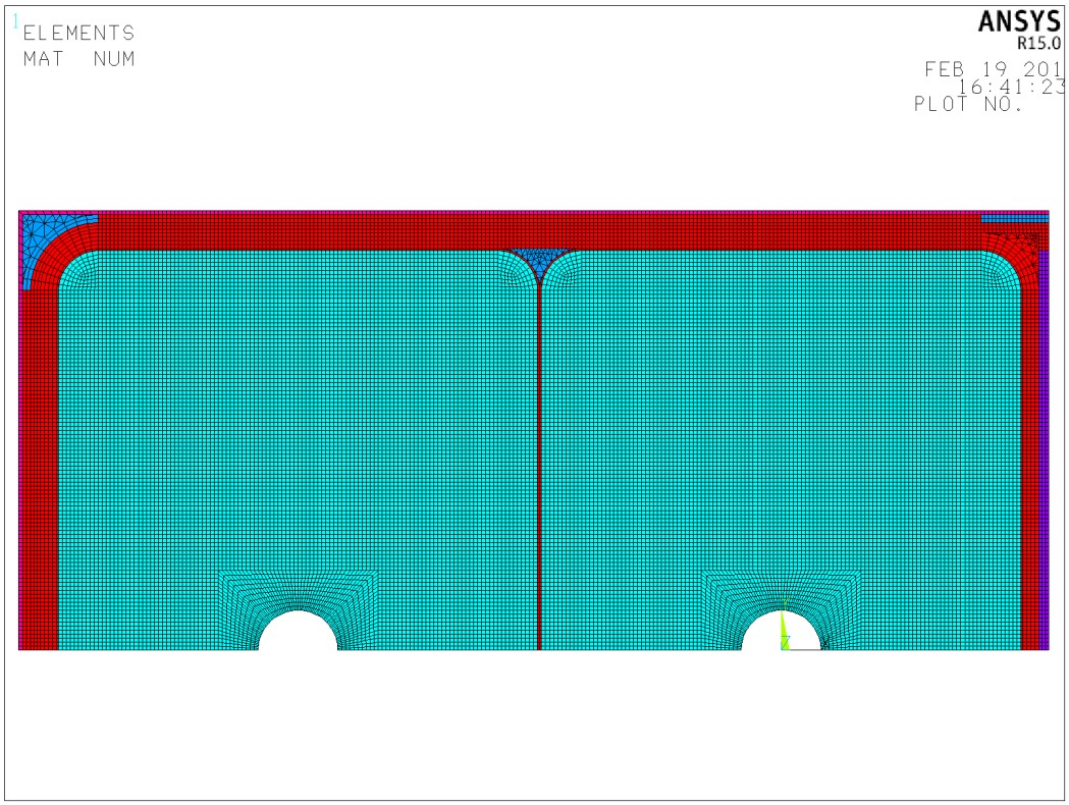

Figure 8.6: Mesh of TF Busbar model

A convergence analysis was held in order to choose the right dimension of the elements considering the throught-thickness stress results in the high voltage insulation.
This analysis was done only for the CC-Busbar model and then scaled for the other geometrys.
The number of elements in CC Busbar model is 14521, in PF Busbar is 15366, in TF Busbar is 28850.

8.2.1 Thermal loads on CC, PF/CS , TF Busbar 2-D model

As written above the thermal loads assumed are uniform heat generation, water convection and air convection.
The values of the uniform heat generation applied to the model are written in *Table 8.1* and applied to the surface that represents the aluminium conductor *Fig. 8.7* .

Table 8.1

Busbar type	Uniform Heat Generation
CC	140000 W/m^3
PF/CS	180000 W/m^3
TF	68800 W/m^3

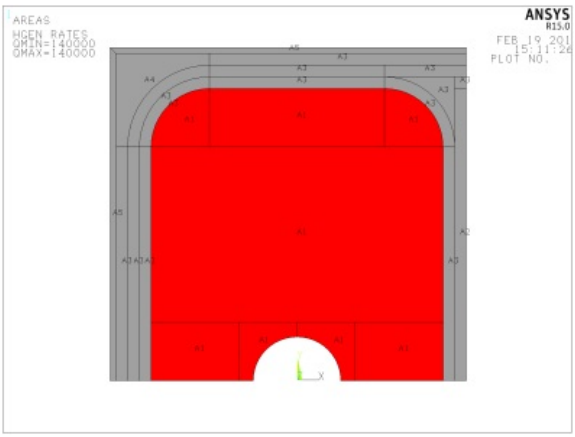

Figure 8.7: Uniform heat generation (in red) for CC Busbar

In all the types of Busbar the convection loads are the same as in *Table 8.2*.

Table 8.2 : Convection loads

	Film coefficient (W/m^2K)	Bulk Temperature (°C)
Air convection	5	31
Water convection	10000	51

The air convection load is applied to the external lines of the model representing the surfaces of the casing (blue in Fig. 8.8). The water convection is applied to the lines of the border of the hole in the aluminium conductor where the cooling water flows (red in Fig. 8.8).

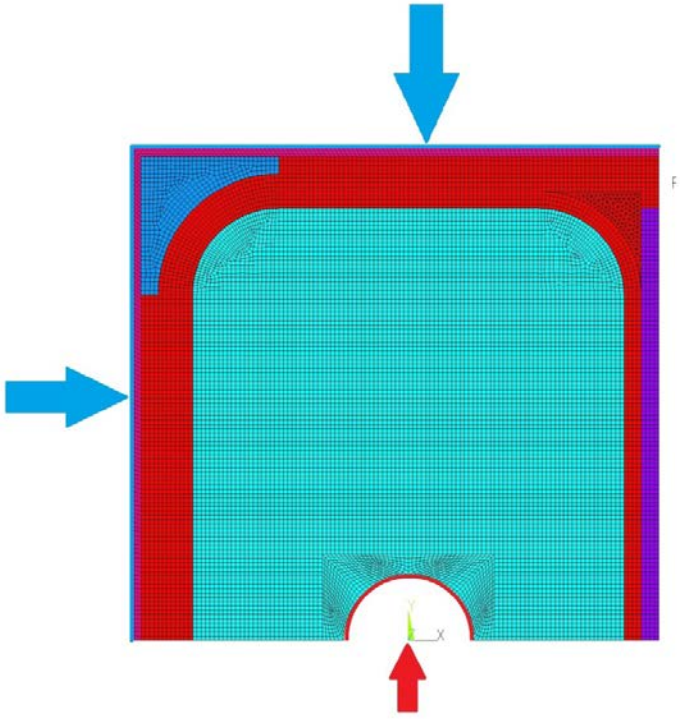

Figure 8.8 : Convection loads location in CC Busbar. Blue arrows and lines are air convection; red arrow and line represents water convection.

8.2.2 Thermal results

The thermal results are shown in figures below in terms of temperature field distribution. The gap between the maximum and minimum temperature is not really high but the difference in the thermal expansion coefficient between the different materials will lead to stresses in any case.
In the Fig. 8.9 is shown the thermal analysis solution for CC Busbar.

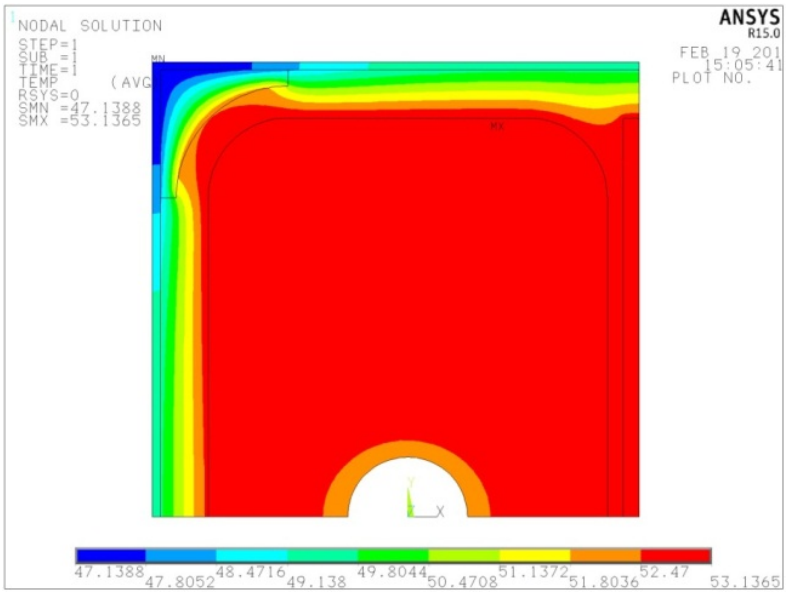

Figure 8.9: Temperature distribution in CC Busbar

In the Fig. 8.10 the temperature of the PF&CS Busbar is shown. In this Busbar the temperature are higher then the other Busbars because the current density is the highest.

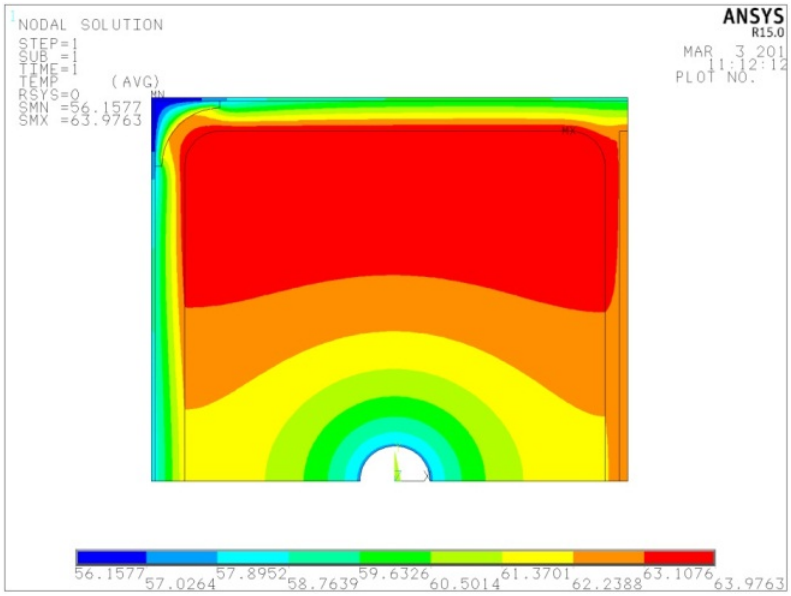

Figure 8.10: Temperature distribution in PF&CS Busbar

In the figure below (Fig. 8.11) the temperature distribution of the TF Busbar is shown.

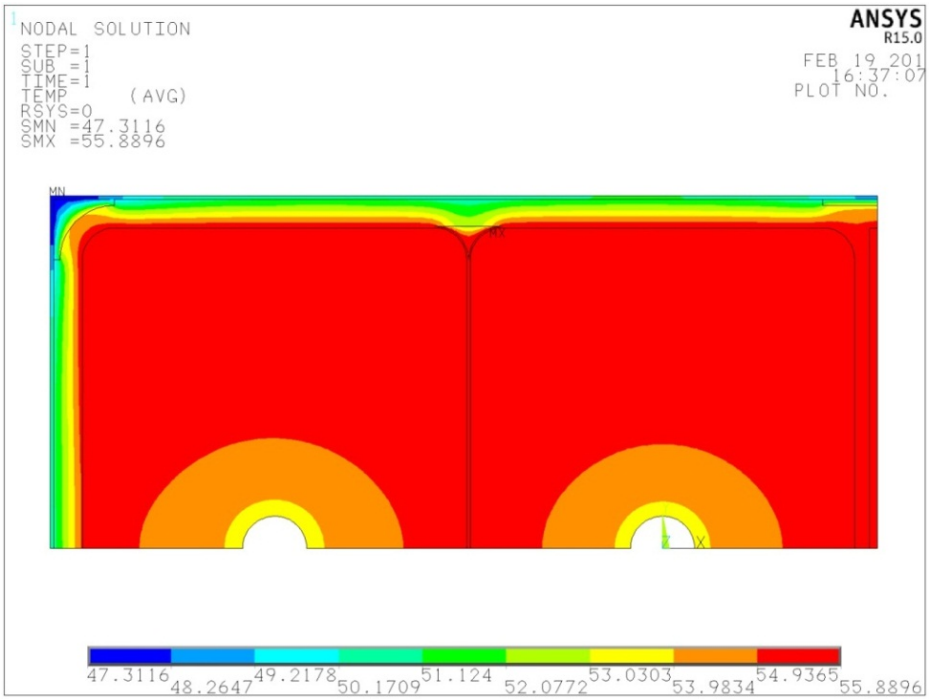

Figure 8.11: Temperature distribution in TF Busbar

A comparison of the three types of cross-section and Busbar types is given below, witch the here below, which reports the maximum and minimum table reports temperature of each analysis.

Table 8.3: Maximum and minimum Temperature

Busbar section Type	Min Temperature (°C)	Max Temperature (°C)
CC Busbar	47.1	53.1
PF Busbar	56.2	64.0
TF Busbar	47.3	55.9

8.3 Insulation and bandage element reference system in the FEM models

The high voltage insulation and the bandage have anisotropic material properties. For the correct implementation of these properties in FEM model, the reference system of the elements must be rotated according to the wrapping direction. The X-axis is defined as the throught-thickness direction of the tape; Z and Y-axis are in-plane. The throught-thickness direction will be normal to the surface where the tape and the bandage are laid. Both in 2-D and 3-D models the method described below was used in ANSYS.

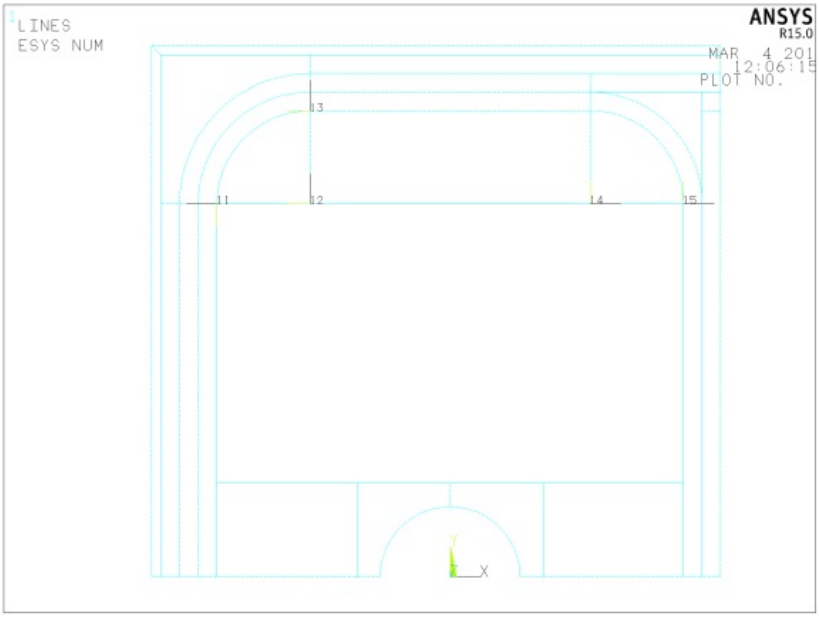

Figure 8.12: Local coordinate system

The first step is to define local reference systems for each area; these systems must be cylindrical for curved parts and Cartesian for straight parts. In Fig. 12.1 five local reference systems of 2-D CC Busbar model are plotted: reference systems number 12 and 14 are cylindrical, whereas reference systems number 11, 13 and 15 are cartesian.
In Fig. 12.2 each area associated with a different local coordinate system has a different colour. In Fig. 12.2b the elements and the element reference systems are plotted, the black lines indicate the X-axis of each element. In the FEM model the reference system of the element must be correctly rotated. Figure 12.3 shows the local reference systems used to obtain the appropriate rotation.

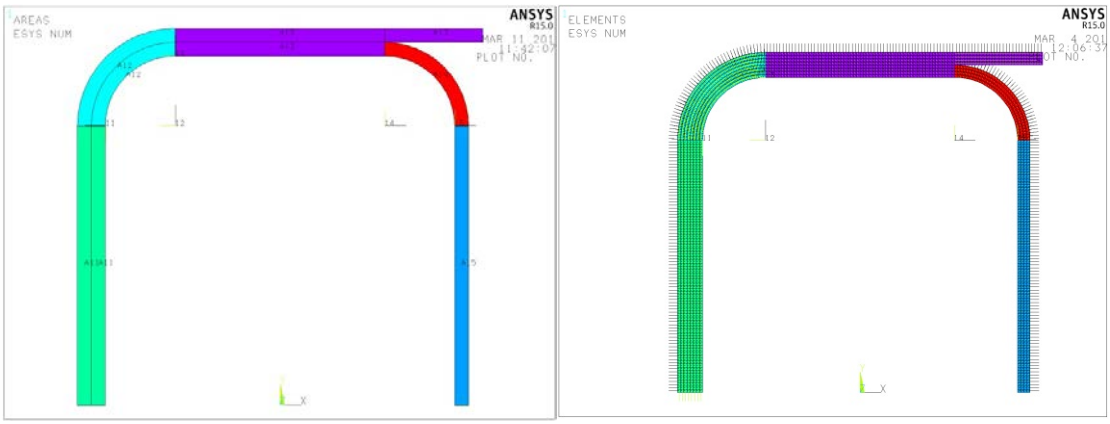

Figure 8.13: local element coordinate system, in black the X-axis

The element reference system of high insulation and bandage is built to follow the exact path of the wrapping direction. Material properties for the insulation and the bandage relate to the reference system in Fig. 12.3. The relation between this reference system and the model reference system is explained below.

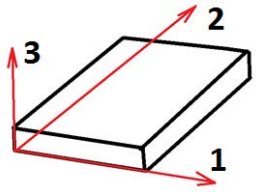

Figure 8.14 : Orientation of the reference system for material properties

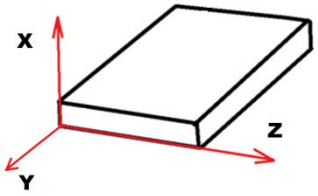

Figure 8.15 : Final orientation of the reference system

Fig. 12.4 shows that the direction “3” is corresponding to X-axis and direction “1” and “2” are corresponding to Z and Y axis respectively in the model element reference system.
The same procedure has been used to define the local reference system for the 3-D model. In *Fig 12.5* the plot of the element reference system in the 3-D model is shown.

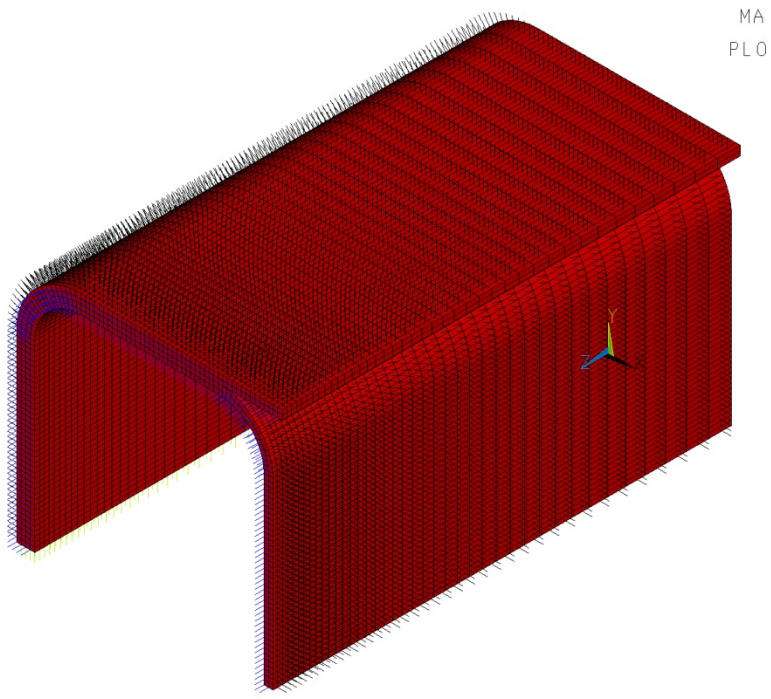

Figure 8.16

8.4 2-D Structural analysis

Knowing the temperature field in the whole model, now we can go through the structural analysis to calculate displacement, strain and stress results.
The geometry and the mesh is the same of the thermal analysis, but the mechanical analysis was held without the casing and the spacers. In fact we do the hypothesis that the casing and the separator will not modify the behaviour and the stresses on the insulation under thermal loads.
The spacers are located only under the steel clamps and the supports.
The casing is pressed in contact with the Busbar only where there are the steel clamps and the supports.
For this reasons the section we are considering in this structural analysis is not influenced by the behaviour of the casing and the separators.
The mesh is the same of the corresponding thermal analysis and the element type is just switched from thermal to structural element type using command: 'ETCHG'.
Element PLANE182 was used for this analysis.
Keyoption k1: full integration
Keyoption k1: plane stress
The element geometry is shown in *Fig.8.12*.

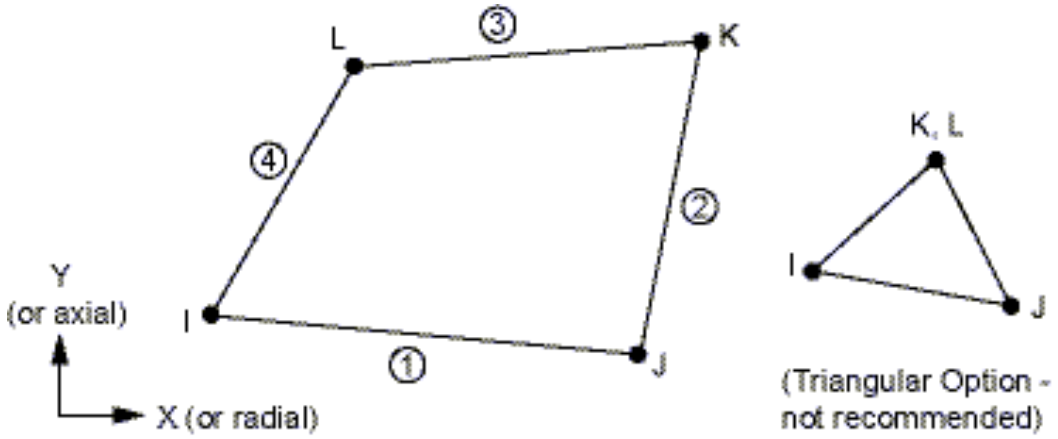

Figure 8.17: PLANE182 Geometry

For example CC Busbar model the number of elements is now reduced to 12739 elements (Fig. 8.13).

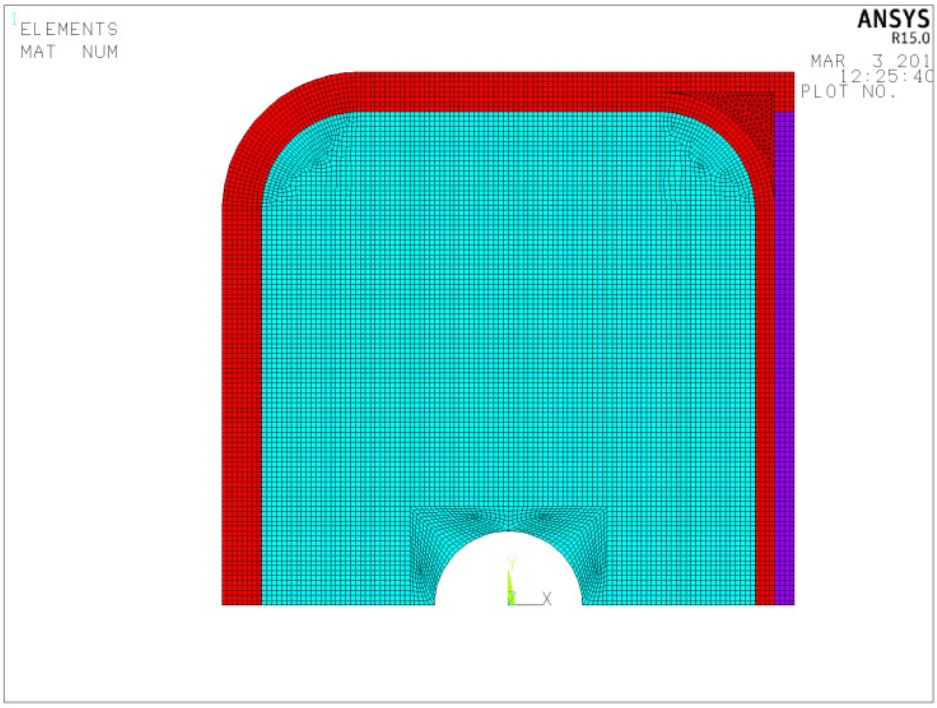

Figure 8.18: Model for mechanical analysis

8.4.1 Boundary conditions

The boundary conditions are :

- Reference temperature 20°C (TREF,20,).
- Thermal analysis results (LDREAD,TEMP,,, , ,'thermalsolutionname','rth',' ').
- Symmetry boundary condition (X-Z plane and Z-Y plane) (Fig.8.14).

In Fig.8.14 the symmetry boundary condition are shown with light blue triangles.

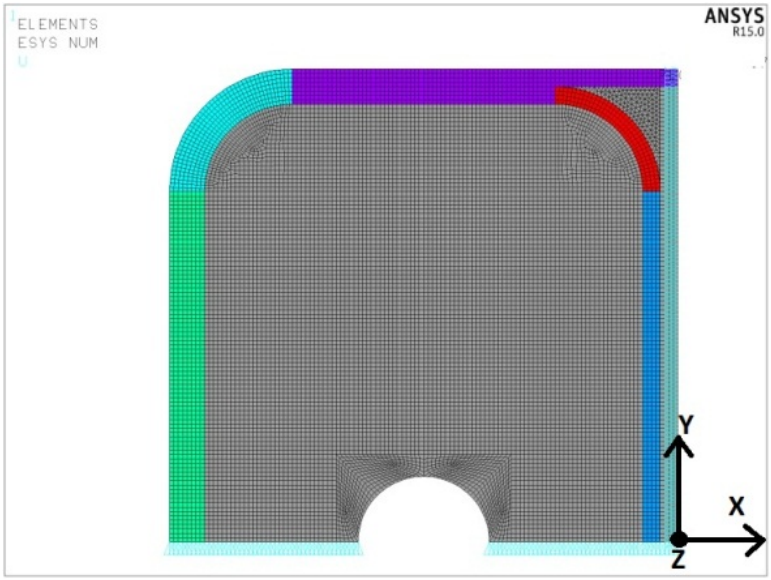

Figure 8.19: Symmetry boundary condition

8.4.2 Stress and strain result on high voltage insulation

In this paragraph we check the stresses in the high voltage insulation layer. The properties of this layer are orthotropic.
All stress and strain results are given in the element reference system this means that X-direction is equivalent to through thickness direction and Y-direction is the in-plane direction. (See Chapter 11)
The throught thinkness stress concentration are in the bend parts of the insulation.
For CC Busbar in the bandage the stress are three times lower than in the high voltage insulation.
The following *Fig. 8.15 - Fig. 8.16* are the plots of the through thickness stress in CC Busbar insulation. The higher compressive-stress zone is in the left round and is around 3MPa for high voltage insulation and around 1MPa for the bandage.

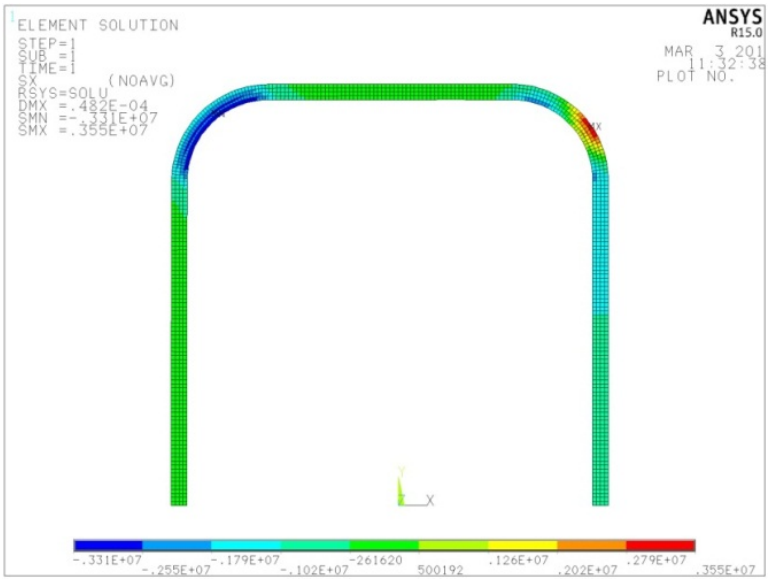

Figure 8.20: Through thickness stress on high voltage insulation

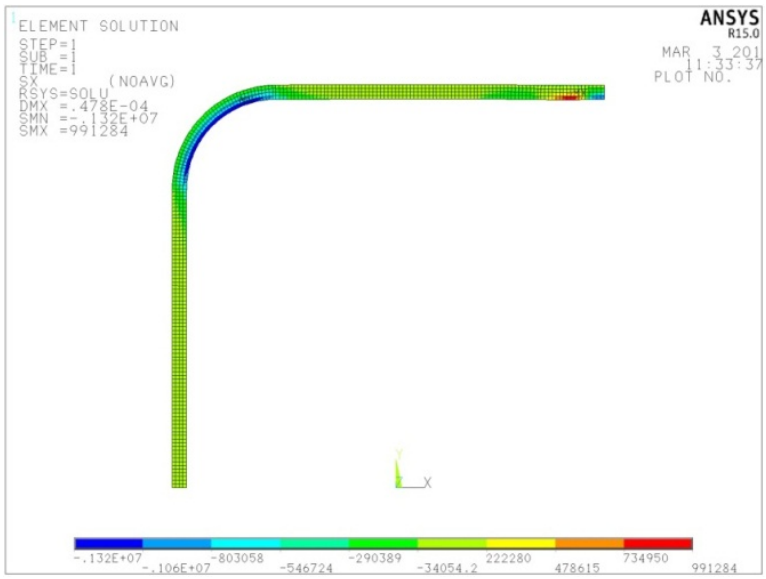

Figure 8.21: through thickness stress of bandage

Tensile stress in Y-direction in the high voltage insulation of CC Busbar reaches the value of 13 MPa. (*Fig. 8.17*)

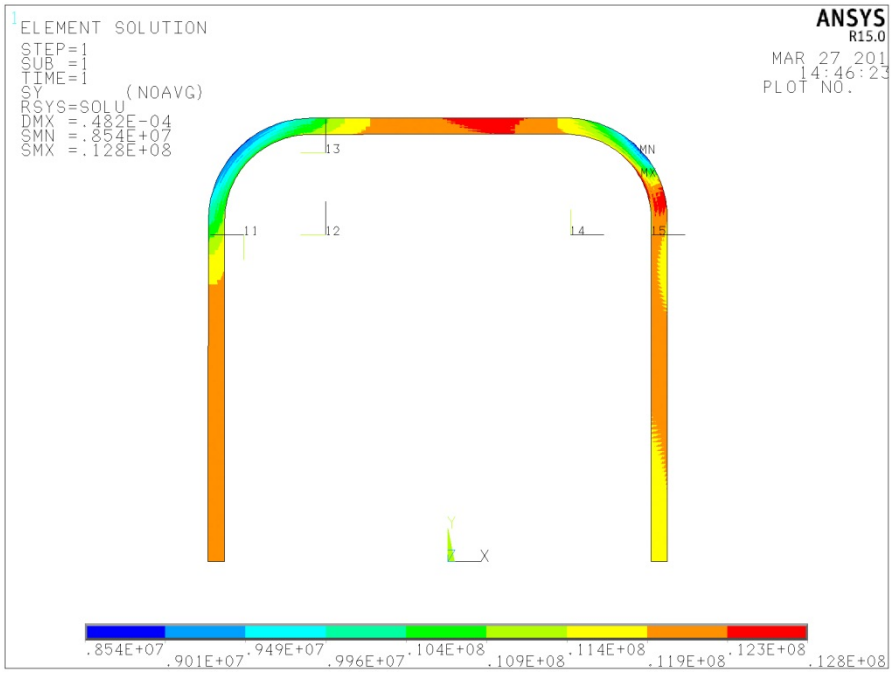

Figure 8.22

X-Y Shear stress for CC Busbar insulation is shown in *Fig. 8.18* and reaches values around 2 MPa. The maximum values are near the changing of curvature (n.1 in Fig. 8.18) and near the area where the separator produces some geometrical discontinuity.

Figure 8.23: Shear xy stress on high voltage insulation and bandage

In following *Fig. 8.19* and *Fig. 8.20* show the plot of CC Busbar strain results, both in through thickness and in reinforcing plane.

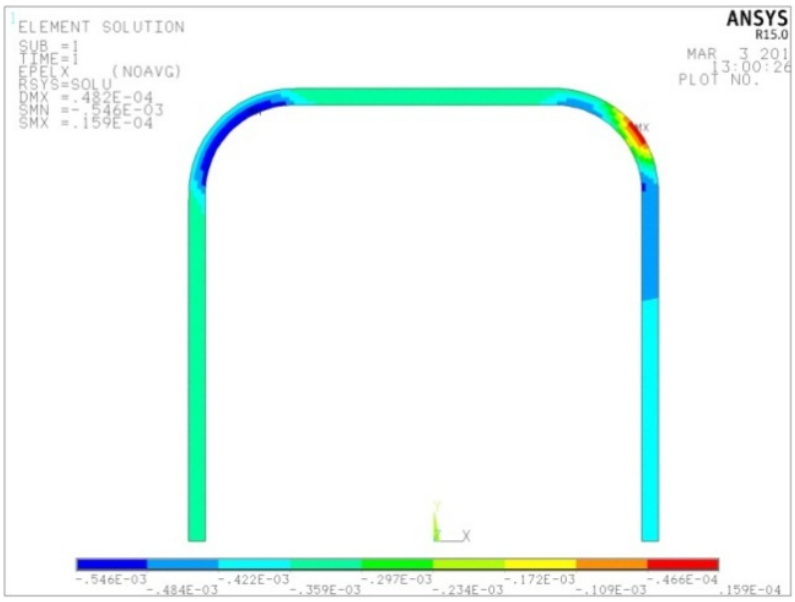

Figure 8.24: through thickness strain

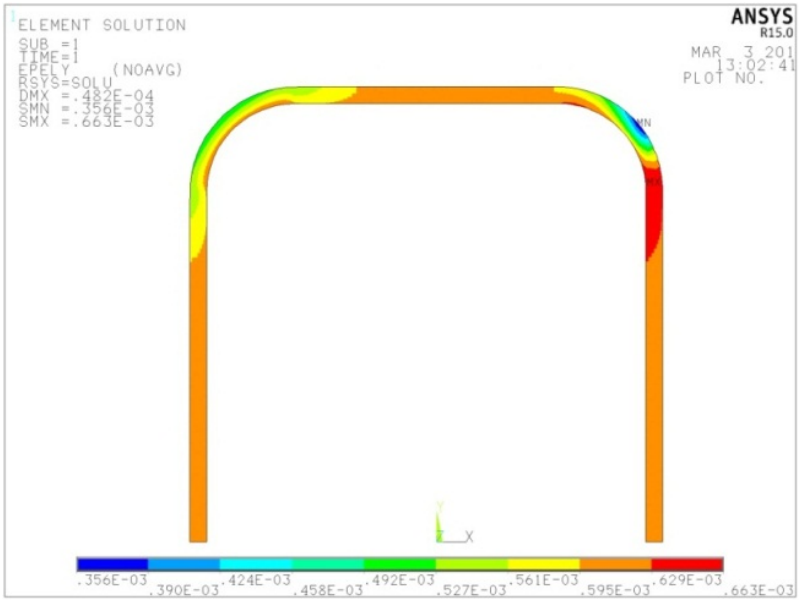

Figure 8.25: strain parallel to reinforcing plane (or in-plane strain)

The following figures show the TF Busbar high voltage inulation stress results. The through-thickness stress on high voltage insulation reaches -4.5 MPa in left round (the side where there is no separator. On the side where the separator is located, the max tensile through-thickness stress.

is 3.6 MPa.

Figure 8.26: through thickness stress on high voltage insulation

The in-plane tensile stress on the reinforcing reaches the maximum value of 13.6 MPa in the TF Busbar high voltage insulation, as shown in *Fig. 8.22.*

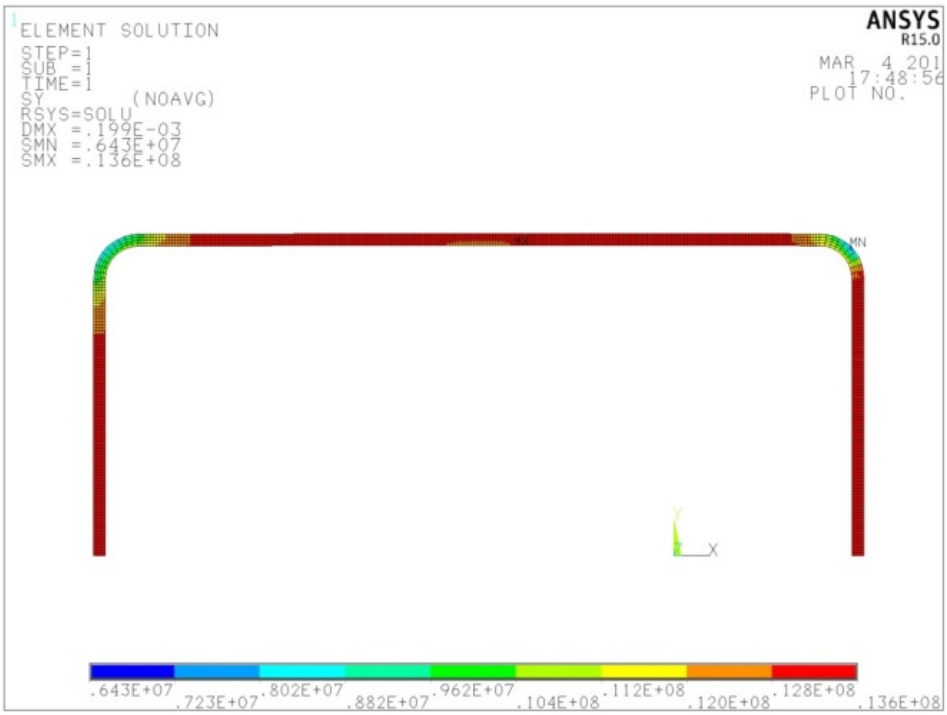

Figure 8.27: in plane stress/parallel to reinforcing plane

The maximum X-Y shear stress value is about 3 MPa and is reached near the change of curvature.

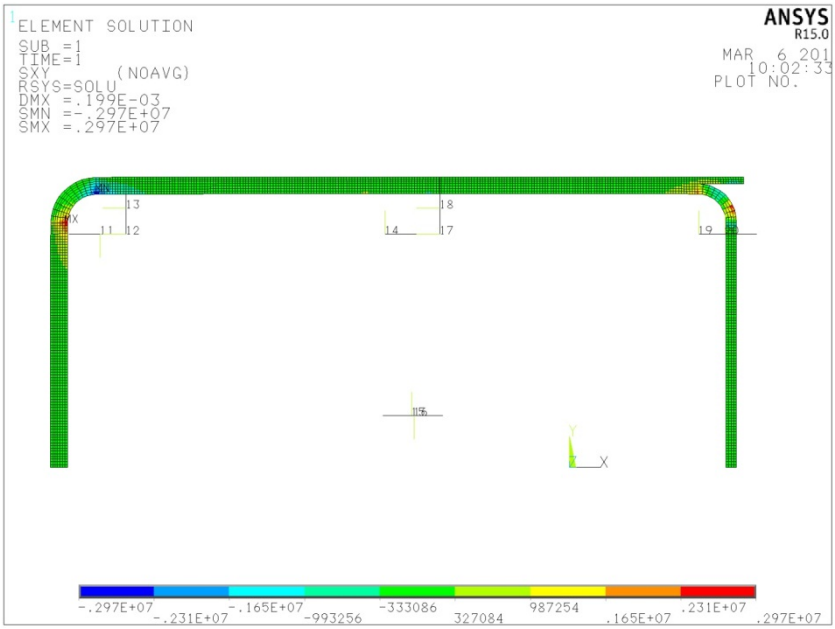

in the TF Busbar.

Figure 8.28: shear xy stress TF Busbar

The following *Fig. 8.24* and *Fig. 8.25 show* the plot of TF Busbar strain results, both in through-thickness plane and in reinforcing plane.

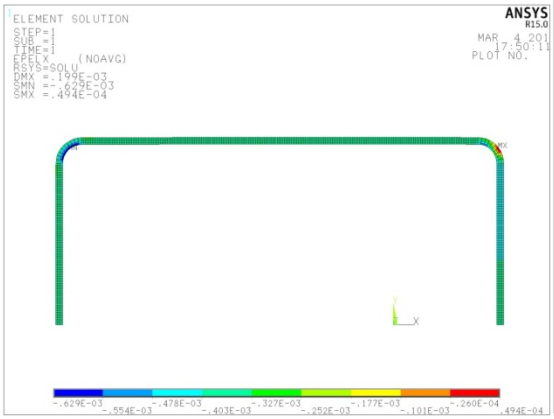

Figure 8.29: through thickness strain

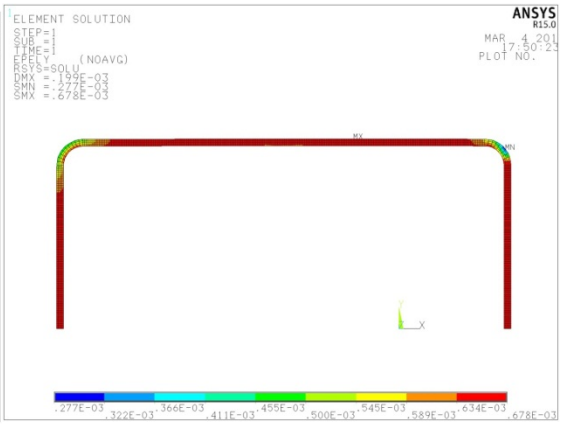

Figure 8.30: strain parallel to reinforcing plane (or in-plane strain)

In the following figures PF&CS Busbar high voltage insulation stress results.
The through thickness stress on high voltage insulation reaches -6 MPa in left round (the side where there isn't the separator). On the side where there is the separator the max tensile through thickness stress is 4.2 MPa.

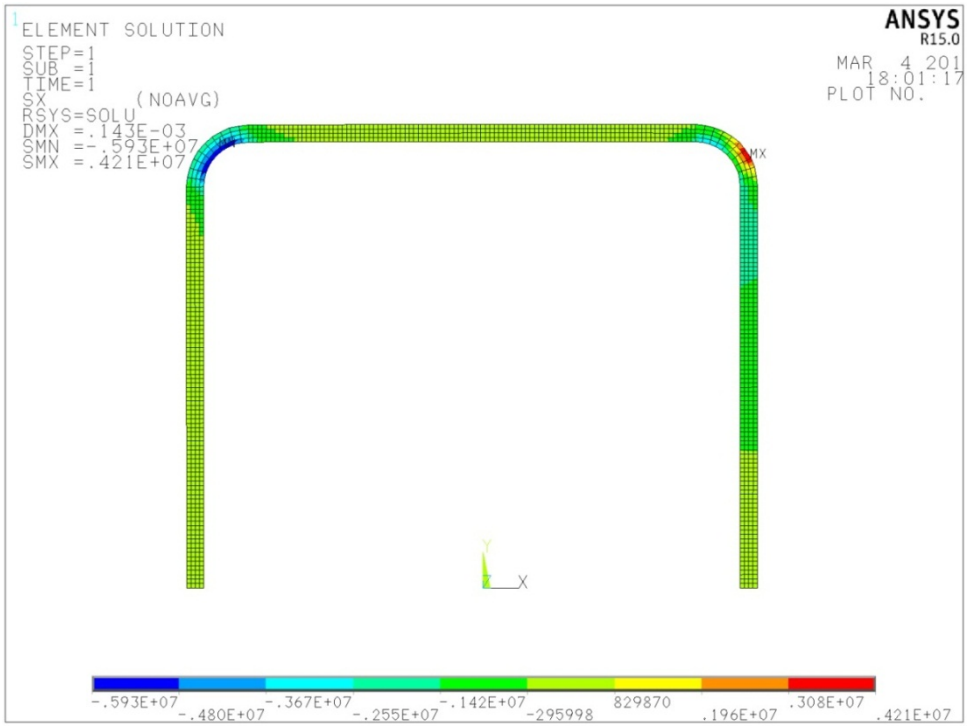

Figure 8.31: through thickness stress on high voltage insulation

In the plane of reinforcement the stress reaches the value of 16.5 MPa in the PF Busbar insulation.

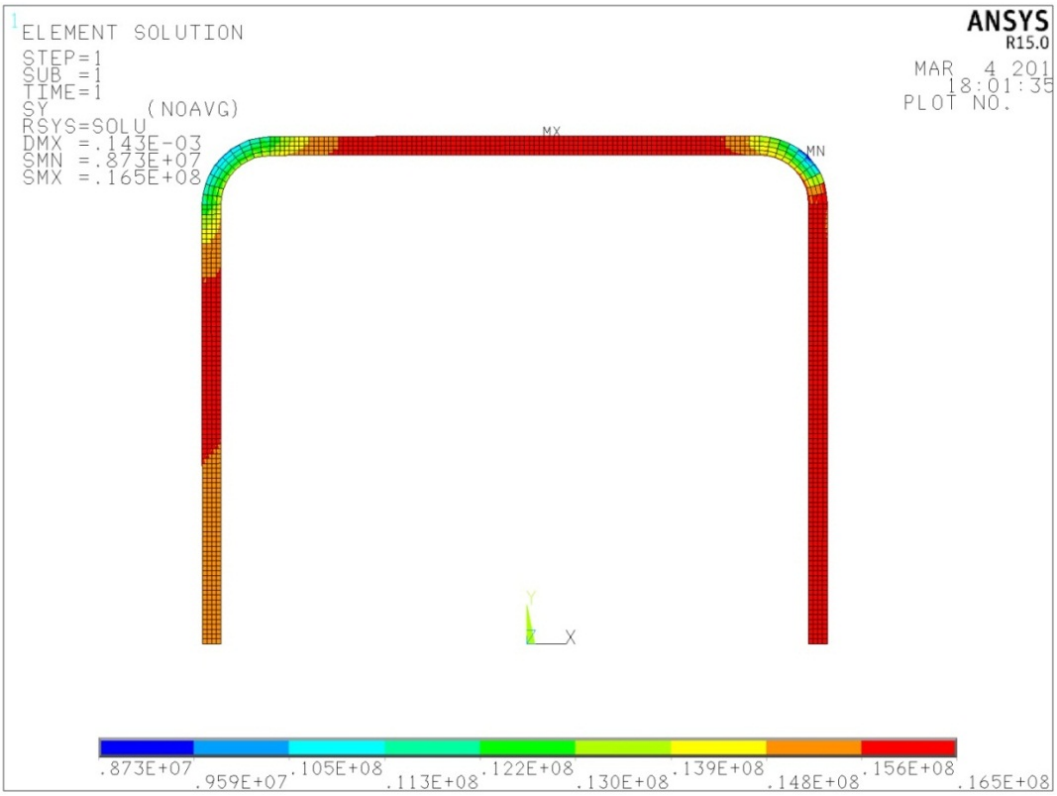

Figure 8.32: in plane stress/parallel to reinforcing plane

The maximum X-Y shear stress value is about 3.8 MPa and is reached near the change of curvature in the TF Busbar.

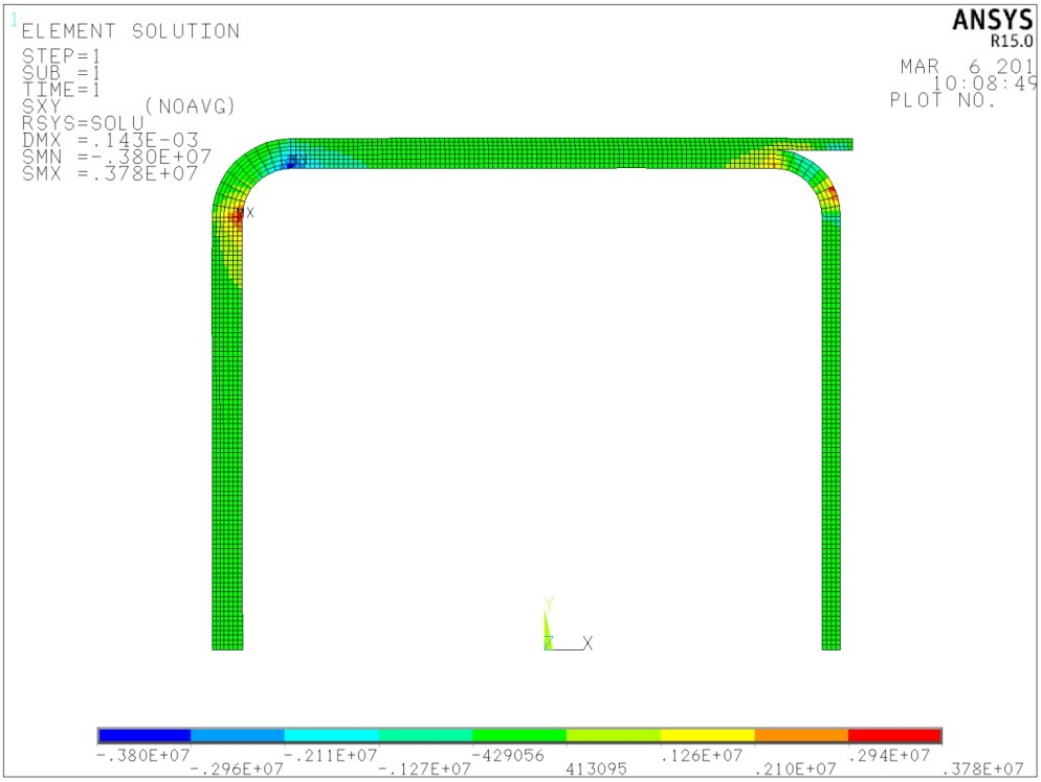

Figure 8.33: shear stress xy

The following Fig. 8.29 and Fig. 8.30 show the plot of TF Busbar strain results, both in through-thickness and in reinforcing plane.

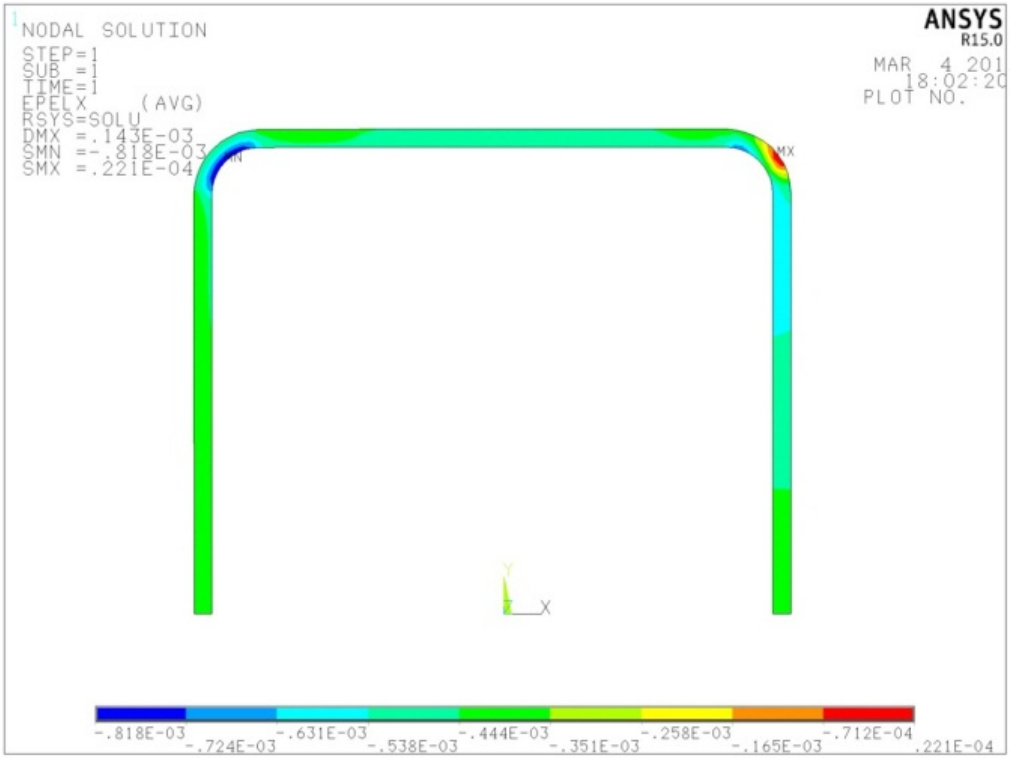

Figure 8.34: through thickness strain

Figure 8.35: strain parallel to reinforcing plane (or in-plane strain)

8.5 2-D Results

The 2-D analyses are intended to check:

- Through-thickness stress stress compressive stress in the insulation material
- In-plane strain (y-direction) in insulation material (for z-direction 3-D analysis is needed)
- X-Y Shear stress

Compressive-Stress Fatigue limit Allowable Normal to Reinforcing Plane is -200MPa considering magnets criteria but, considering aged mica/epoxy insulation material (see *Chapter.7.4*), the allowable fatigue stress value for 30000 cycles is -70 MPa. The values archived from the analysis (reported In *Table 8.4)* show that the safety coefficient is higher than 10.

Table 8.4

High voltage max compressive stress normal to renforcing plane	
CC Busbar	-3.31 MPa
PF Busbar	-5.93 MPa
TF Busbar	-4.48 MPa

-Tensile-Strain Normal to Reinforcing Plane in the surface between the aluminum conductor and the insulation must be zero for the criteria in *Chapter 7.2.3.*
All CC, TF, PF Busbar has compressive-strain in the surface between aluminum and insulation.

-Strain parallel to reinforcing plane must be less than +/- 0.5% according to the magnets insulation criteria. On the other hand, according to the data on aged mica/epoxy insulation, the max tensile strain shall not exceed 0.58% and the max compressive strain shall not exceed 0.1%.

Table 8.5

Max Strain parallel to reinforcing plane (Y-direction)	
CC Busbar	0.066%
PF Busbar	0.085%
TF Busbar	0.068%

This values aren't the total in-plane values: total strain values will be calculated in *Chapter 9.5* considering the Z-component of the strain.

-Fatigue shear stress allowable is 25MPa for magnet insulation

Table 8.6

Max Shear stress X-Y	
CC Busbar	2.26 MPa
PF Busbar	3.8 MPa
TF Busbar	2.97 MPa

The model is 2-D model so we don't know stress and strain in Z-direction, Z-X shear stress and Z-Y shear stress.

9. 3-D Thermo-structural analysis

The same cross-section of the 2-D model is extruded to build the 3-D model with ANSYS preprocessor extrusion capabilities.
The 3-D analysis uses the same symmetry properties of the 2-D analysis. For this reason, the model is always a quarter of Busbar. There are two borderline cases considered and the difference between them will be illustrated now.
The first case assumes that the busbar is of an infinite length. This hypothesis involves that the extremity of the Busbar, considering also the insulation extremity surface, will stay in a plane parallel to X-Y plane. Under this hypothesis no shear stress is found in the plane of contact between insulation and the aluminum conductor.
Considering this, another model is built in order to point up the shear stress generated by geometric singularity in the end of the Busbar.

9.1 3-D 'Infinite Busbar' Model and considerations on boundary conditions

Optimal 3-D model generation was found using element MESH200.
MESH200 is a "mesh-only" element, contributing nothing to the solution. This element can be used for multistep meshing operations, such as extrusion, that require a lower dimensionality mesh be used for the creation of a higher dimensionality mesh.
In our case a 2-D mesh was done with element MESH200 using where possible mapped mesh and the KEYOPT(1) used were 4 and 6 . Using command for extrusion (VEXT) the 3-D model for thermal analysis is built with elements SOLID278.

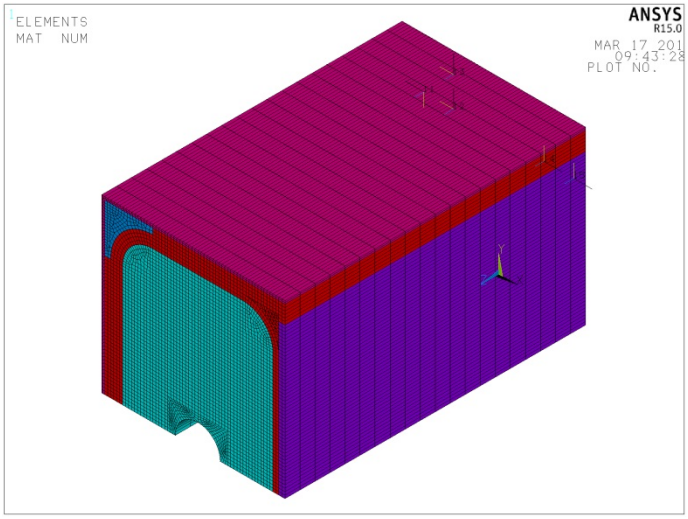

Figure 9.1: 3-D Model- CC Busbar

The thermal loads in the 3-D models are the same as in the 2-D models, but the convection is applied to surfaces and heat generation is applied to volumes. The following Fig. 9.2 shows in red the water convection surface and in blue the air convection surface.

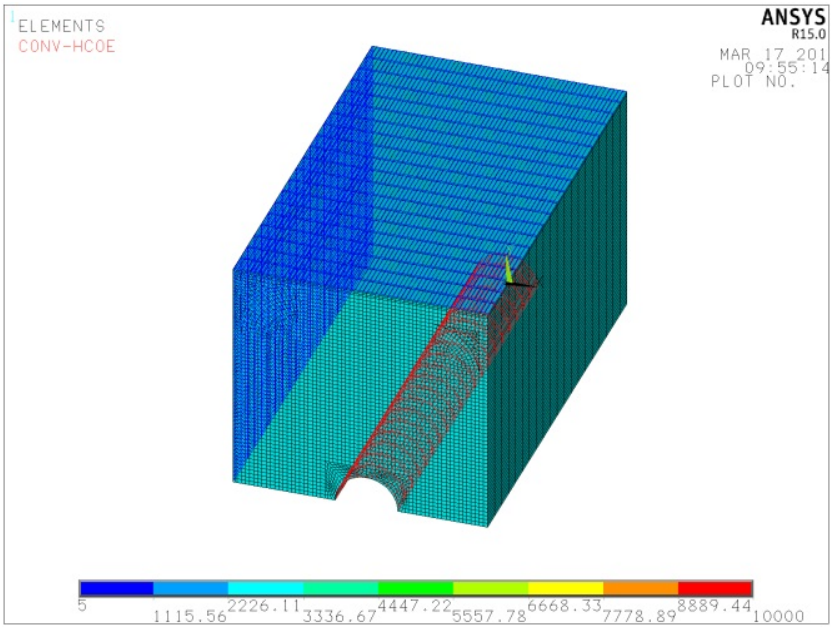

Figure 9.2: Convection loads-CC Busbar

In the *Fig. 9.3* below the heat generation volume is shown in red.

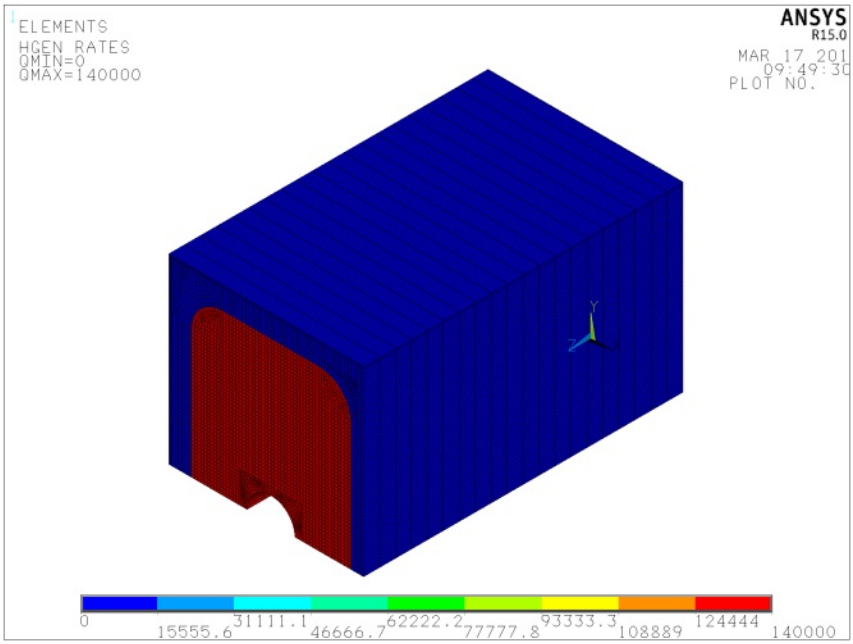

Figure 9.3: Heat generation-CC Busbar

This is the same for all the CC, PF, TF Busbar models.
In the following *Fig. 9.4* the thermal solution is shown for the CC Busbar and as was expected the temperature distribution is the same in each section and confirms the 2-D results.

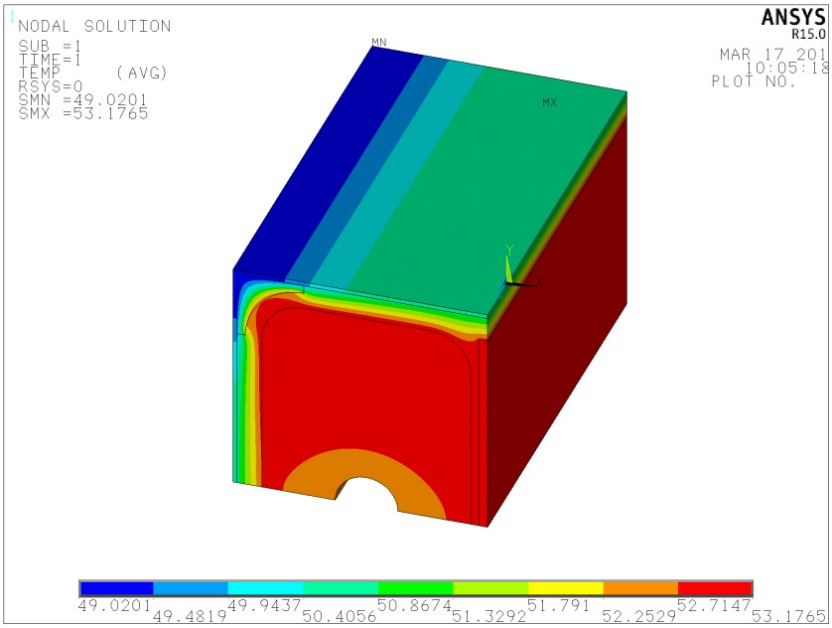

Figure 9.4: Thermal solution for CC Busbar

After obtaining the thermal solution, the elements are switched from thermal to structural. For the structural analysis element SOLID185 is used with:
Keyopt 2 = full integration
Keyopt 3 = structural solid
Keyopt 4 = pure displacement

The same thermal boundary condition has been used in structural 2-D and 3-D analysis:
-Reference temperature 20°C (TREF,20,)
-Thermal analysis results (LDREAD,TEMP,,, , ,'thermalsolution','rth',' ')

Symmetry conditions are not enough to constrain properly the 3-D model.
The first hypothesis considered is that the Busbar is straight and infinite. This hypothesis lead to two simple boundary conditions on the Busbar model end-surfaces. On one end-face, a symmetry boundary condition is applied. On the other end-face, the deformation in Z-direction is free, but we impose that the differential displacement in z- direction shall be zero.

This kind of boundary can be implemented through the use of coupled DOF of the nodes in that face.
So we do a coupling of Z-displacements of all the nodes in that end face.
In the following *Fig. 9.5* in blue are shown the symmetric boundary condition and in green the coupled DOF boundary.

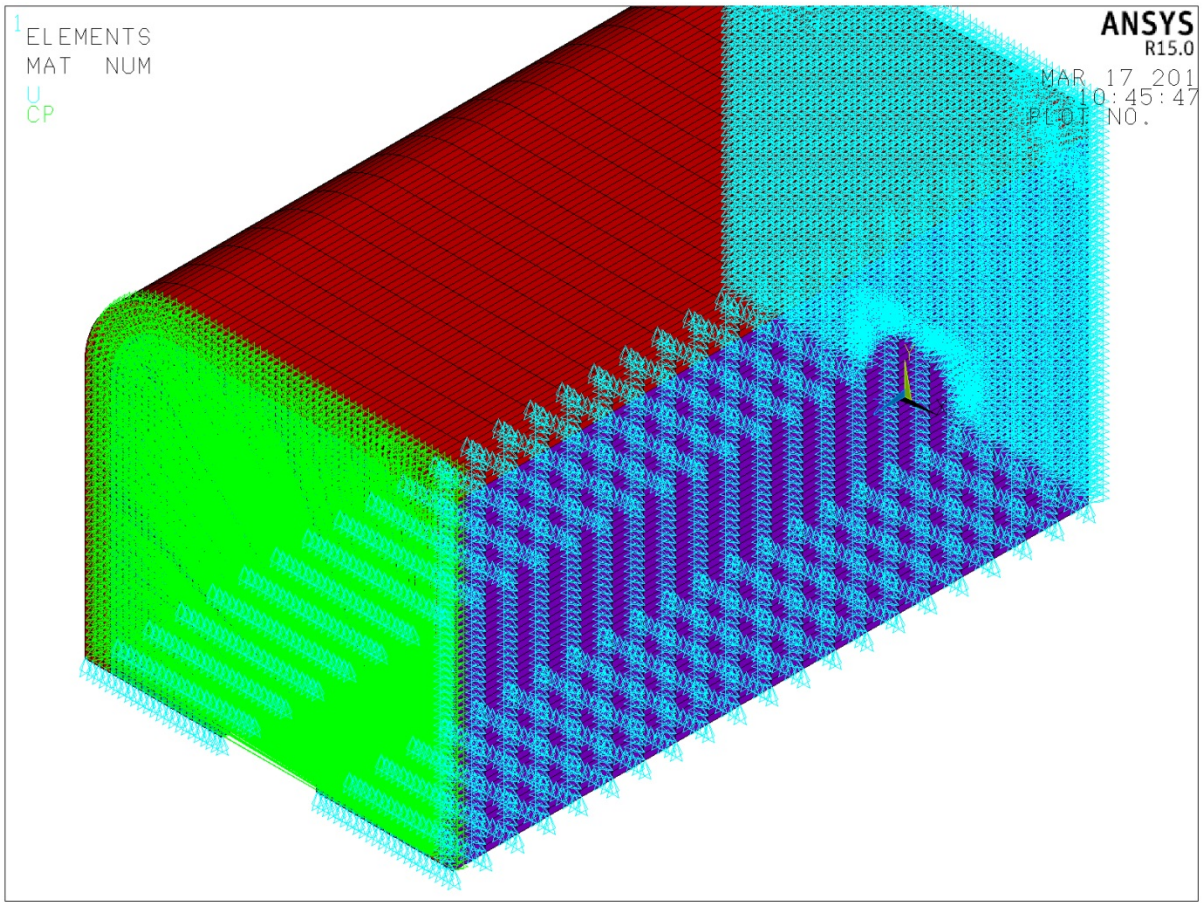

Figure 9.5: Coupled DOF nodes (Z-direction) in green and symmetry boundary condition in light blue.

From the analysis of the high voltage insulation in his reference system (see Chapter 12) we can deduce that:
-With this kind of boundary conditions we have a negligible shear stress on ZX and ZY plane.
-Stress and strain on XY plane are the same of the 2-D model
-Furthermore we obtain stress and strain on Z-direction that are roughly the same of the ones in Y-direction in the 2-D model.

The conclusion means that the 3D "infinite" Busbar hypothesis doesn't provide more information compared to the 2D model.
To obtain more information from our model, we need to understand where the areas of maximum stress are located.
No shear stress is foreseen in the central part of the Busbar in the plane between aluminium conductor and high voltage insulation, whereas near the point where the insulation finishes there is a shear stress concentration zone.
To understand the magnitude of shear stress in the vicinity of the insulation borders, a new model is created making this hypothesis:
-no external forces or boundary conditions acts on the Busbar end
-the high voltage insulation finishes in the same place where the bandage finishes
-also the separator ends in the same place
-the aluminium conductor is longer than the insulation and in the area without insulation there is direct air convection on the aluminium surface.
-other thermal load are the same that where always considered
-the Busbar is considered straight

It is important to highlight that in reality the geometrical discontinuity is much lower than the one considered. In the real busbar end the bandage will finish before the end of the high insulation layer.

This higher geometrical discontinuity will lead to higher stress and will make our analysis conservative.
The final 3-D model will be the one in Fig. 9.6 for CC Busbar.

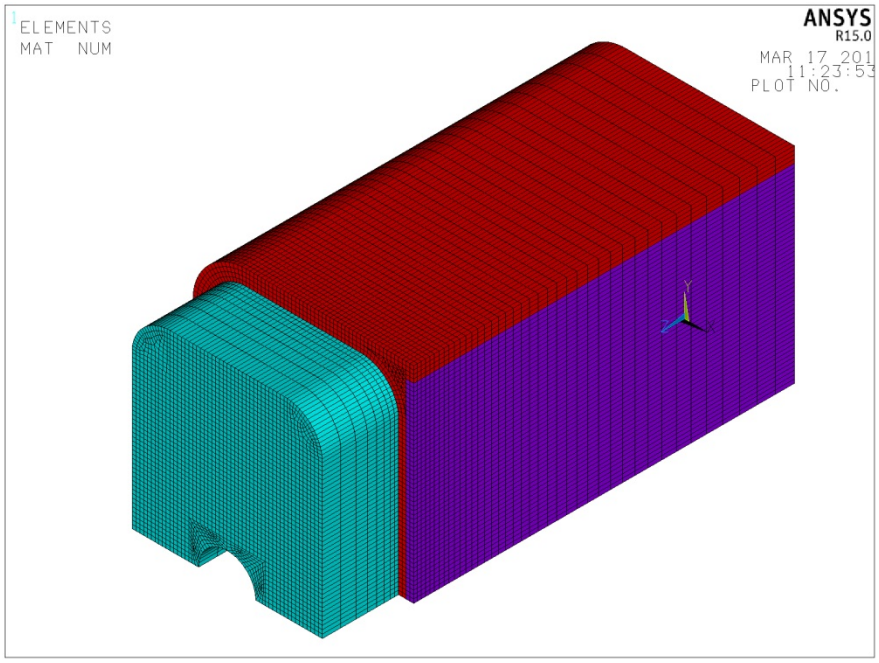

Figure 9.6: CC Busbar end 3-D model

9.2 3-D Steady state thermal analysis

The software used for thermal analysis is ANSYS Multiphysics.
The loads considered for this analysis are the uniform heat generation in the aluminum conductor, convection of cooling water and air natural convection on the casing and on the conductor.
The objective is to calculate nodal temperatures in order evaluate the whole field of temperature. Knowing these temperatures, a structural analysis will be done considering the ΔT temperature.
The thermal analysis is done on a quarter of Busbar for the same reasons explained in Chapter 8.1

9.2.1 Element Types

For this analysis were used:
-MESH200 (two types with different keyoptions)
-SOLID278

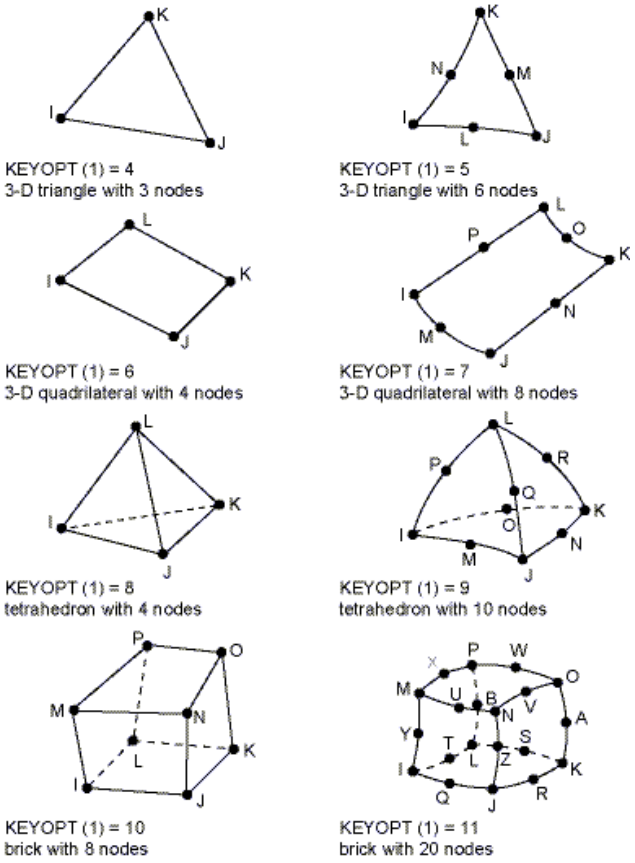

Figure 9.7: MESH200

2-D mesh was done with element MESH200 using where possible mapped mesh and the KEYOPT(1) used were QUAD 4-NODE and TRIA 3-NODE.
Using command for extrusion (VEXT) the 3-D model for thermal analysis is built with elements SOLID278 that has a 3-D thermal conduction capability. The element has eight nodes with a single degree of freedom, temperature, at each node. SOLID278 is designed to be a companion element for SOLID185 for the following structural analysis.
The length of the total extrusion for the conductor is more than the length of the rest of the model in this way is obtained a geometrical discontinuity (see Fig. 9.6).

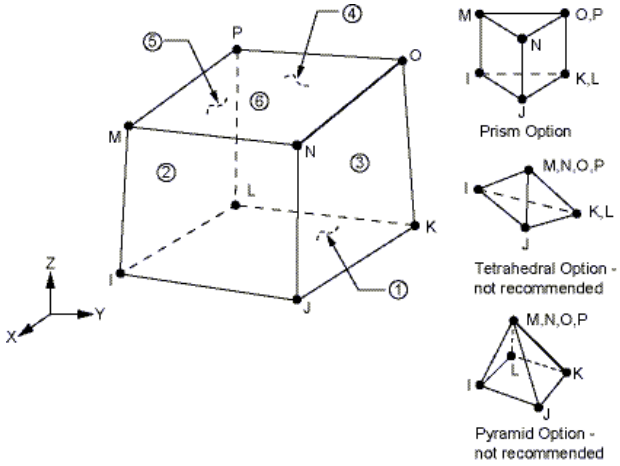

Figure 9.8: SOLID289

9.3 CC, PF, TF Busbar 3-D FEM model

The geometry used for each model is the same of the 2-D model because the 3-D model is obtained through extrusion (command VEXT).
In Fig.9.9 and Fig 9.10 there are the FEM model for CC and PF Busbars.

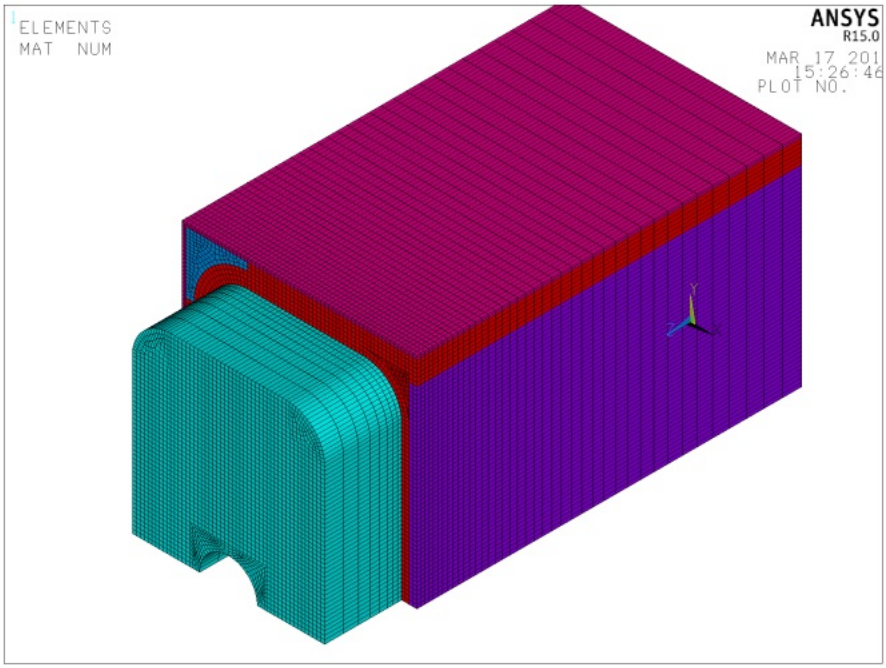

Figure 9.9: CC Busbar thermal analysis model

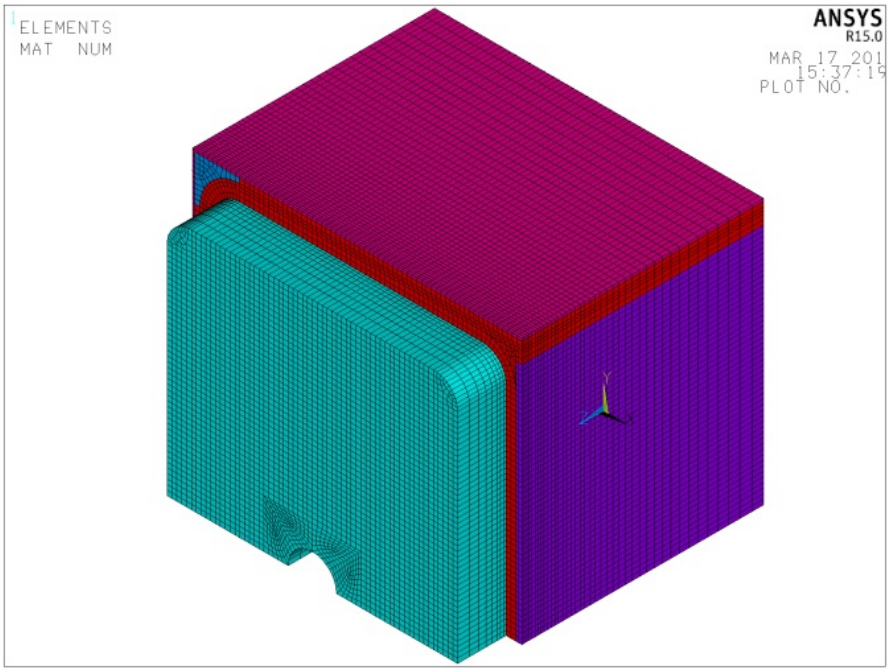

Figure 9.10: PF Busbar thermal analysis model

For CC Busbar and PF Busbar models the number of elements is 172805 and 191480.

In Fig.9.11 the FEM model for TF Busbars.

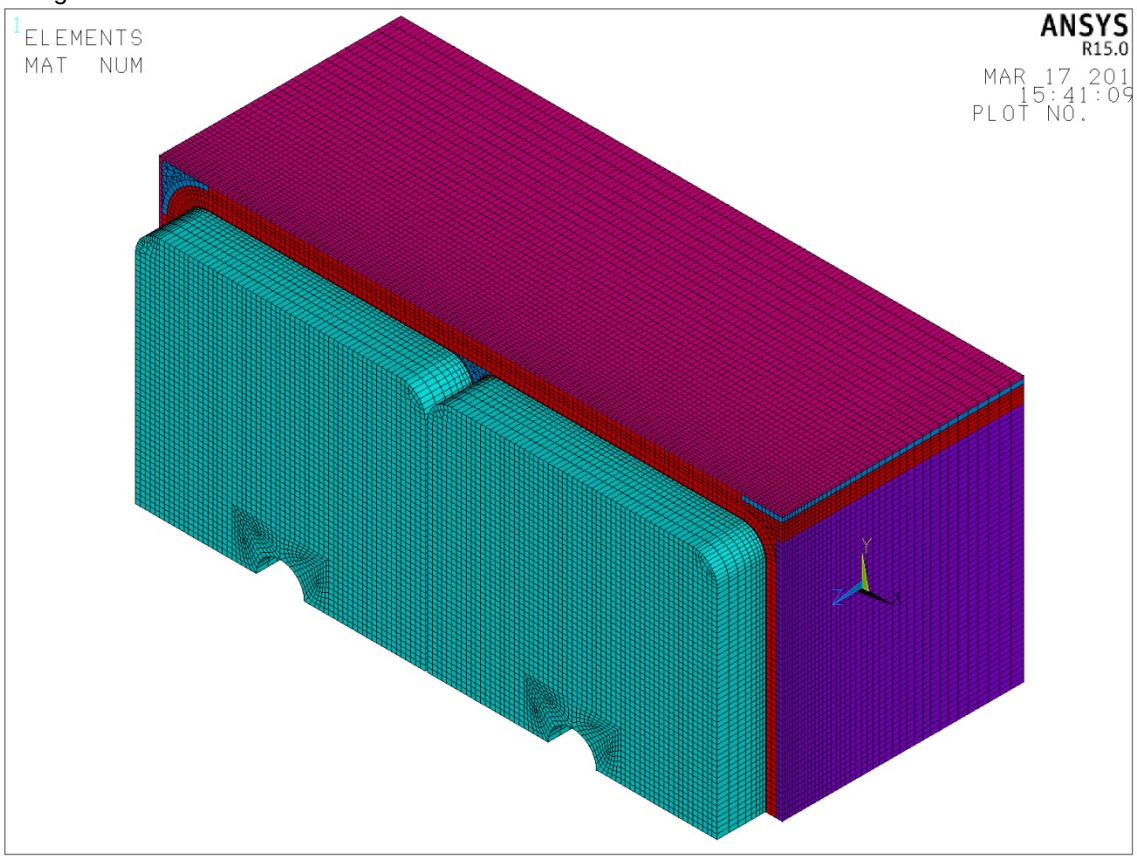

Figure 9.11 : PF Busbar thermal analysis model

For the TF Busbar model the number of elements is 375237.

9.3.1 Thermal loads on CC, PF/CS , TF Busbar 3-D model

As written for the previous analyses, uniform thermal loads, uniform heat generation, uniform water convection and air convection have been assumed.
The values of the uniform heat generation applied to the model are written in *Table 8.1* and in *Table 8.2* are written the convection loads and applied to the volume that represents the aluminium conductor.
The following Fig. 9.12 shows the water convection surface in red and the air convection surface in blue.

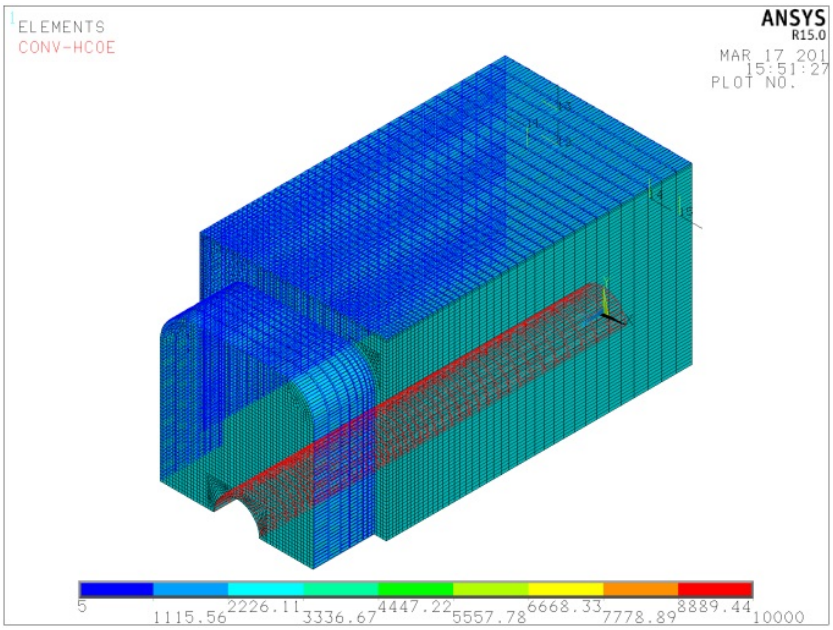

Figure 9.12: CC Busbar convection loads

The uniform heat generation volume is shown in red in Fig. 9.13.

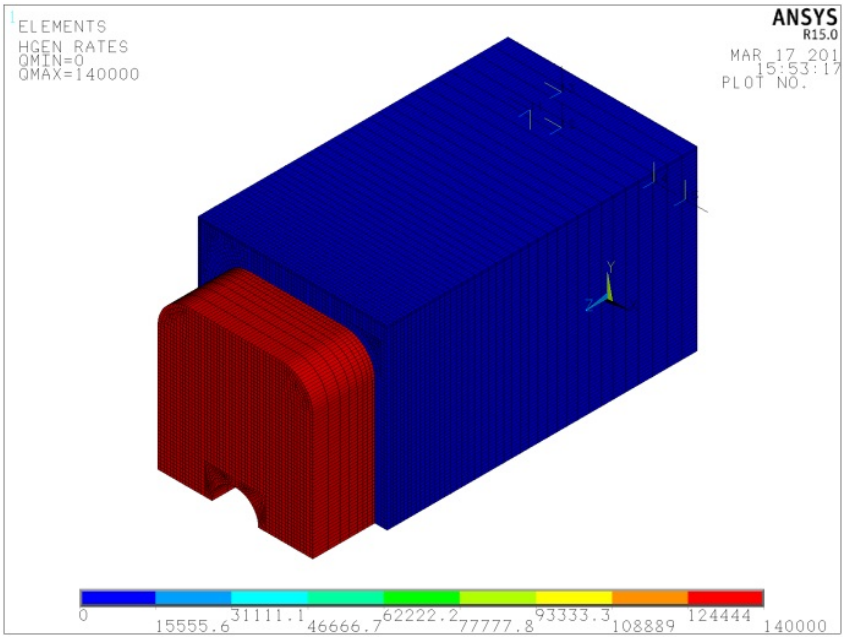

Figure 9.13: CC Busbar heat generation

9.3.2 Thermal results

The thermal results differs slightly from the 2-D thermal analysis only in the end part of the Busbar but the maximum and minimum temperatures are the same.

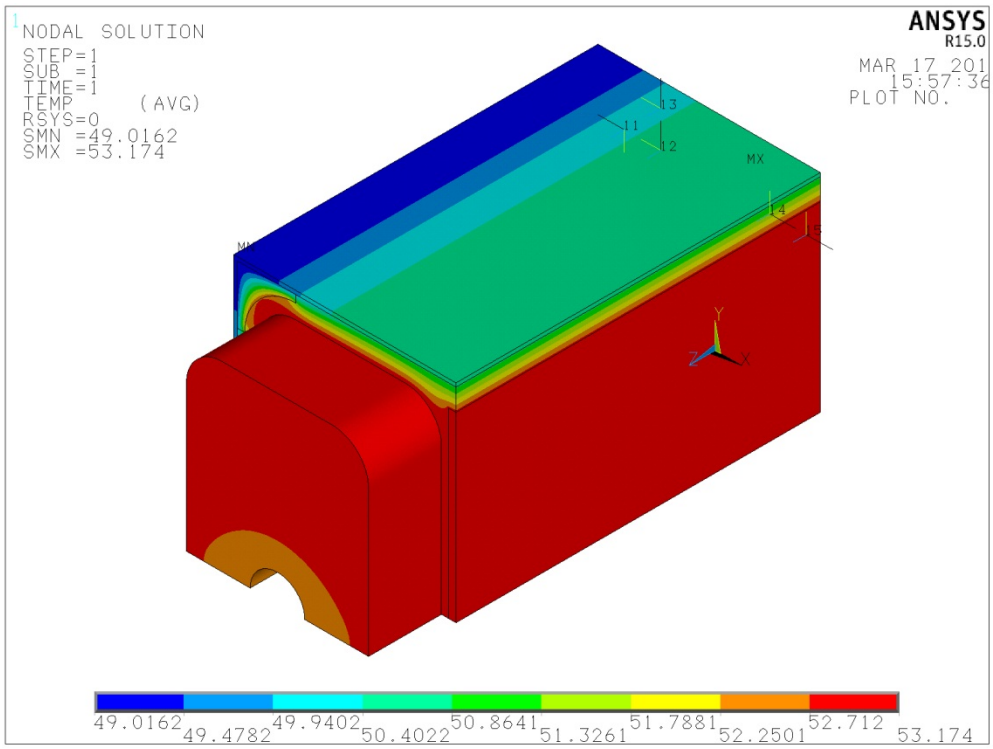

Figure 9.14:CC Busbar temperature distribution

9.4 3-D Structural analysis

The geometry and the mesh is the same of the thermal analysis the only difference is that the mechanical analysis was held without the casing and the spacers. The mesh is the same of the corresponding thermal analysis and the element type is just switched from thermal to structural element type using command: “ETCHG”.
Element SOLID185 was used for this analysis. This Structural Solid element is suitable for modeling general 3-D solid structures. It allows for prism, tetrahedral, and pyramid degenerations when used in irregular regions. Various element technologies such as uniformly reduced integration, and enhanced strains are supported.

Keyoption k2: Element technology = full integration
Keyoption k3:Layer construction = structural solid
Keyoption k6: Element formulation = Pure displacement

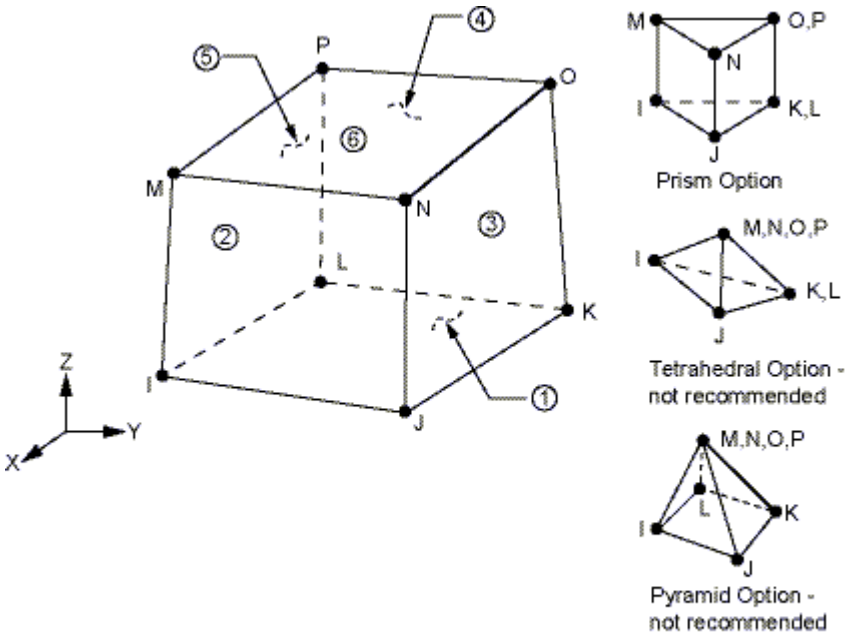

Figure 9.15: PLANE185 Geometry

9.4.1 Boundary conditions

The boundary conditions (Fig. 9.16) are:
-Reference temperature 20°C (TREF,20,)
-Thermal analysis results (LDREAD,TEMP,,,, , ,'thermalsolution','rth',' ')
-Symmetry boundary condition (X-Z plane and Z-Y plane)
-Symmetry boundary condition on the area X=0

In Fig. 9.16 the symmetry boundary condition are plotted on the model in light blue.

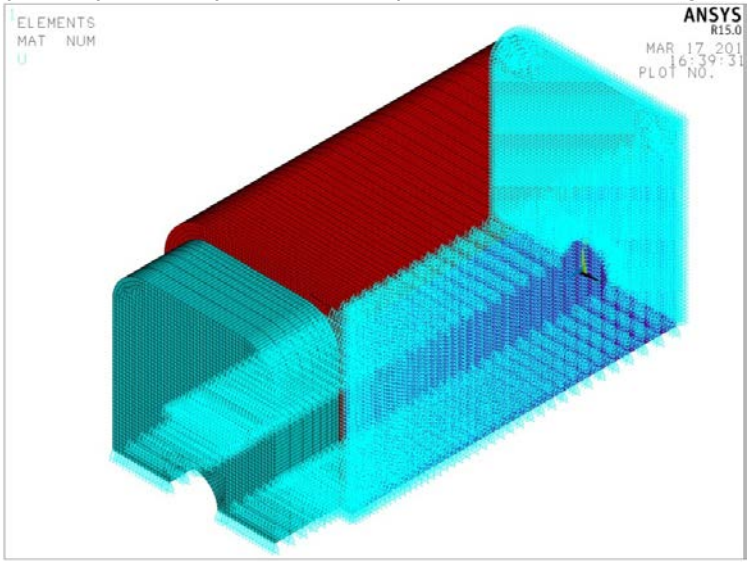

Figure 9.16: Boundary condition

9.4.2 Shear stress result on high voltage insulation

These 3-D analyses are necessary to evaluate the magnitude of peak shear stress in the borders, where the high voltage insulation finishes.
In the figure below (Fig. 9.17) Z-X shear stress are shown in the element reference system (see Chapter 12). The peak of shear stress is in the surface between the aluminium conductor and the high voltage insulation. This kind of stress is important because can lead to debonding between aluminium and insulation.
For the CC Busbar the zone with the higher peak is in the border between the high voltage insulation and the aluminium in the right bent part (n.1 in Fig. 9.17). The right vertical part of the insulation (n.2 in Fig.9.17) is the zone attached to the separator and this area has the lower shear stresses. In the rest of the model, distant for the border the shear stress is negligible.

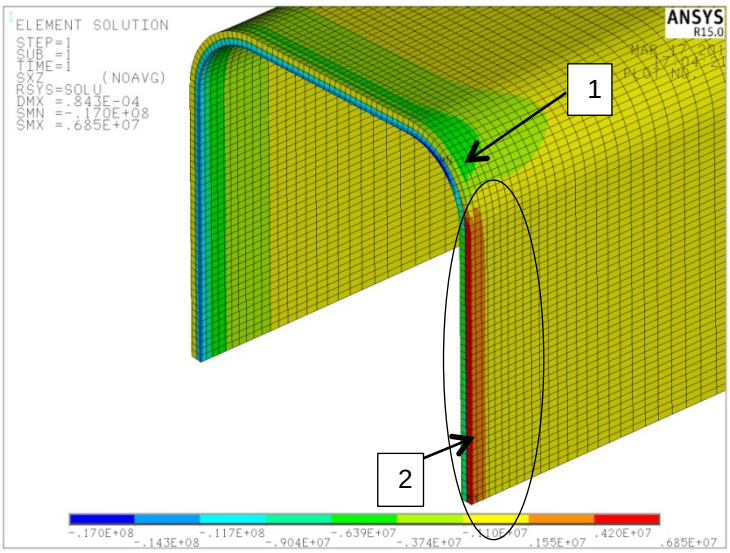

Figure 9.17:CC Busbar Z-X shear stress

For PF Busbar the situation is different; there isn't any stress concentration zone in the bent parts of the insulation but the value of shear stress reach 17 MPa in all the border zone in the straight parts (n.1 in Fig. 9.18). In the zone near the separator shear stress is lower like in CC Busbar.

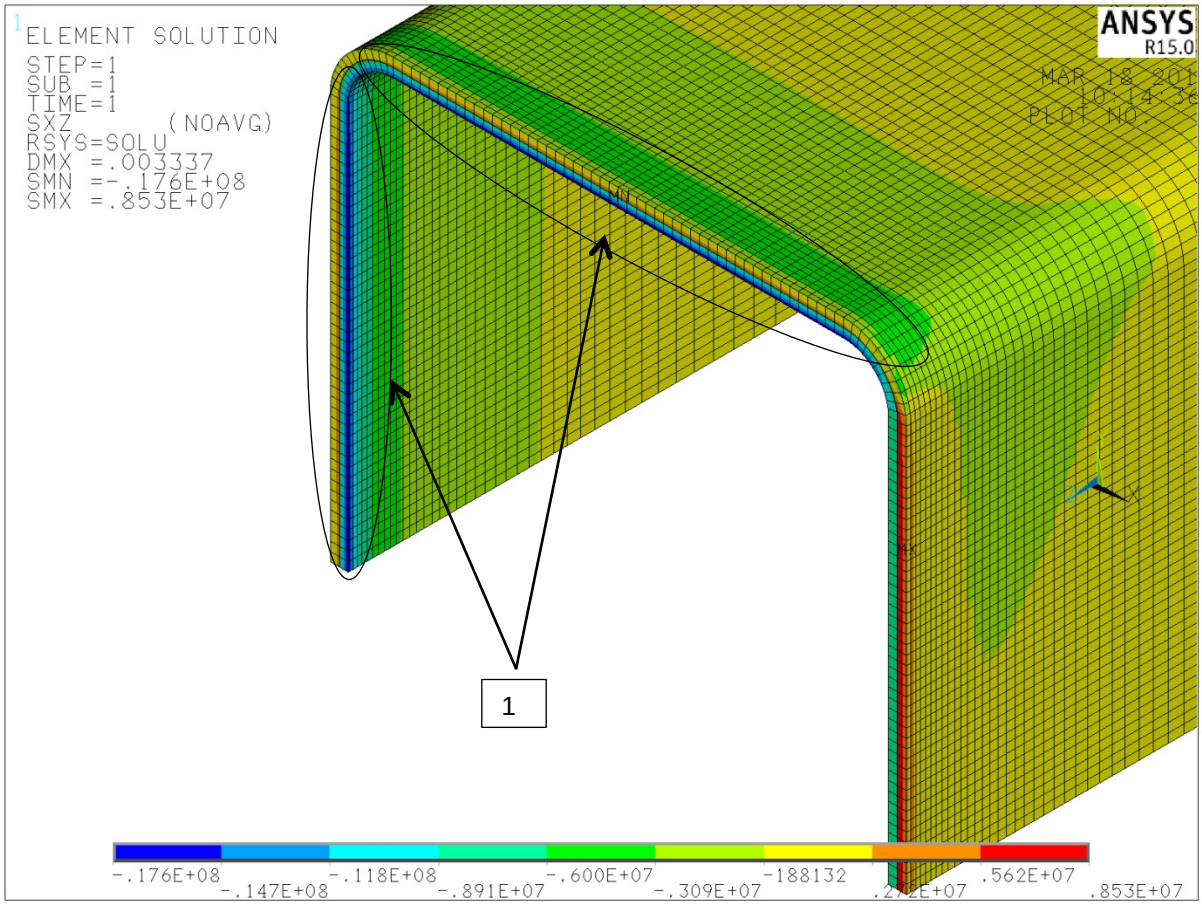

Figure 9.18: PF Busbar X-Z shear stress

In the PF Busbar there is a thin layer of fiberglass between the high voltage insulation and the aluminium conductor. The aim of this layer is to provide a better bonding between the aluminium surface and the high voltage insulation. This layer lowers down the shear stress in the high voltage insulation to maximum 10 MPa.
There is another stress concentration zone in the area between the two aluminium bars that in the TF Busbars form one polarity of the Busbar (n.1 Fig. 9.19 and Fig. 9.20).
Also in PF Busbar the right side of the high voltage insulation has lower shear stress because there is the effect of the separator.

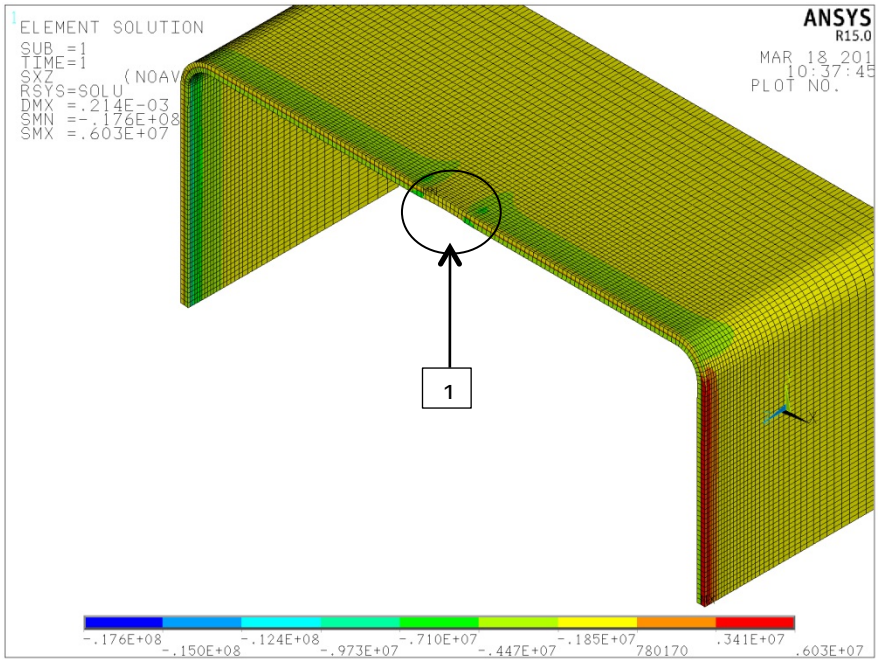

Figure 9.19

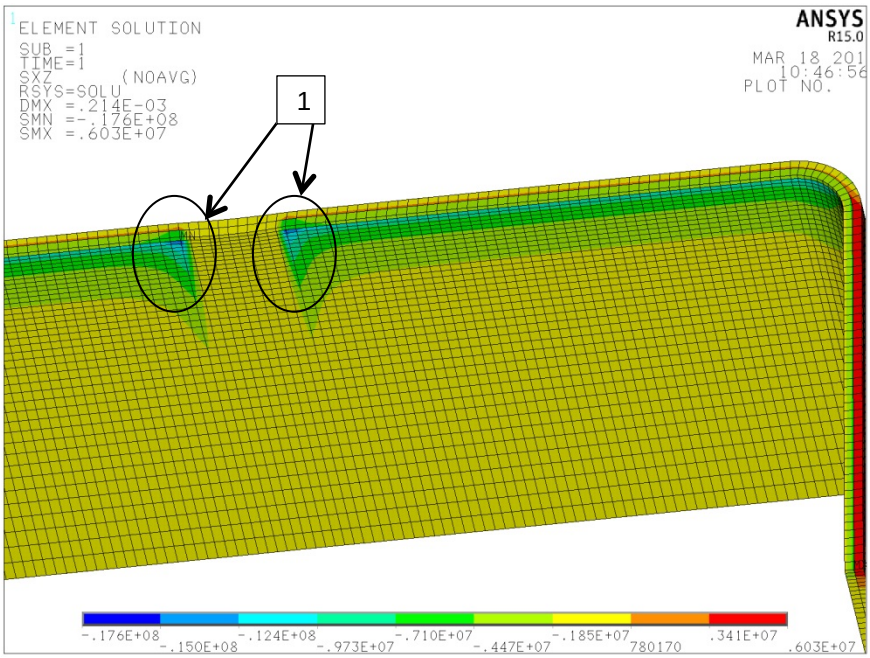

Figure 9.20

9.4.3 Strain in Z-direction

Using the 3D the “infinite” Busbar model, we see that the maximum value of strain will be distant from the end of the Busbar and near to the symmetry condition on the other face of the model. In the zone near to the symmetry boundary condition there isn’t any effect of the end of the Busbar caused by geometrical discontinuity. The results in this zone are the same of the straight 3D "infinite" Busbar model.
This value of strain is the same found for the ‘straight Busbar model’ in Cap. 9.1.
In figure 9.21 the plot of the Z-direction strain for CC Busbar.

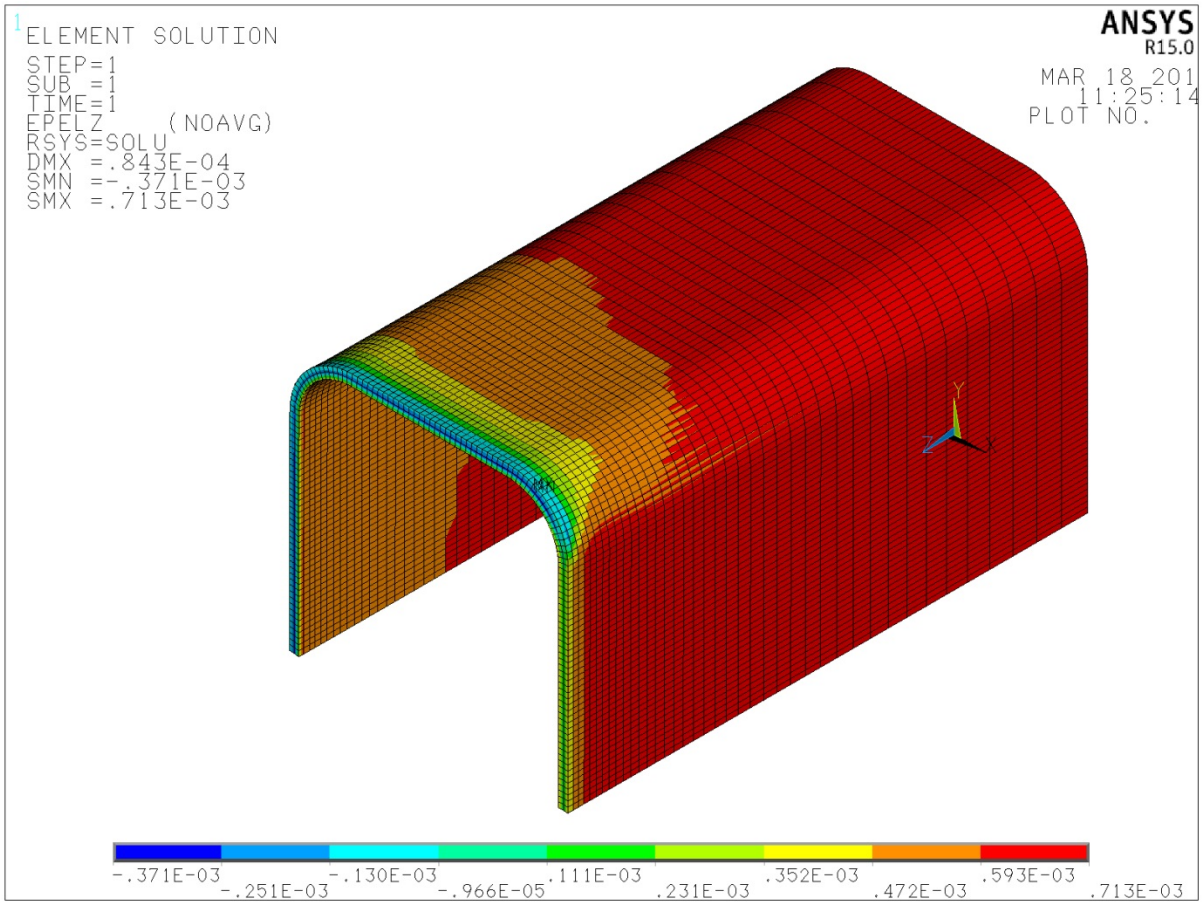

Figure 9.21: Strain Z-component for PF Busbar

Table 9.1

Max Strain parallel to reinforcing plane (Z-direction)	
CC Busbar	0.071%
PF Busbar	0.087%
TF Busbar	0.069%

9.5 3-D results

The purpose of the 3-D analyses is the accurate estimation of the stress/strain level in the insulating material as follows:
-values of the shear stress in the plane between the insulation and the conductor (Z-X plane in element reference system)
-values of in plane strain in the Z-direction that we didn't have from the 2-D analysis

In all the models we have the maximum interlaminar shear stress in the plane between the high voltage insulation and the aluminium conductor in the zone where the high voltage insulation ends (border zone).
In this area there is a negligible compressive through-thickness stress. From criteria for the insulation in magnets we can consider in our case a limit value of 25MPa for fatigue shear stress.

Table 9.2

Shear stress X-Z Plane	
CC Busbar	17.0 MPa
PF Busbar	17.6 MPa
TF Busbar	10 MPa

Strain parallel to reinforcing plane must be less than +/- 0.5% for the criteria magnets insulation and in tests for aged mica/epoxy insulation material the max tensile strain is 0.58% and max compressive strain is 0.1%. In our case there is only tensile strain. We need to take in consideration the whole strain in the Z-X plane.

Table 9.3

Max Strain parallel to reinforcing plane (Z-direction)	
CC Busbar	0.071%
PF Busbar	0.087%
TF Busbar	0.069%
Max Strain parallel to reinforcing plane (Y-direction)	
CC Busbar	0.066%
PF Busbar	0.085%
TF Busbar	0.068%

Taking in account both the contributions the total strain value parallel to the reinforcing plane will be:

$$\varepsilon_{tot} = \sqrt{\varepsilon_Y{}^2 + \varepsilon_z{}^2}$$

Table 9.4

ε_{tot} strain parallel to reinforcing plane (Y-Z Plane)	
CC Busbar	0.097%
PF Busbar	0.12%
TF Busbar	0.097%

Von Mises stress for High voltage insulation CC Busbar is 15MPa for straight hypothesis and 30 MPa the maximum values in the edge zone.
Von Mises stress for High voltage insulation PF Busbar is 19MPa for straight hypothesis and 31 MPa the maximum values in the edge zone.

The static limit allowable is σ_{id}=85 MPa.

9.6 Comments on 3-D model

The 3D model used so far does not consider that in the reality the high voltage insulation doesn't finish abruptly in the same place of the bandage, but there is a more smooth transition. The results are for this reason overestimated. The reason of this is that the geometrical discontinuity in the reality is less than the one considered in the model (Fig. 9.22).

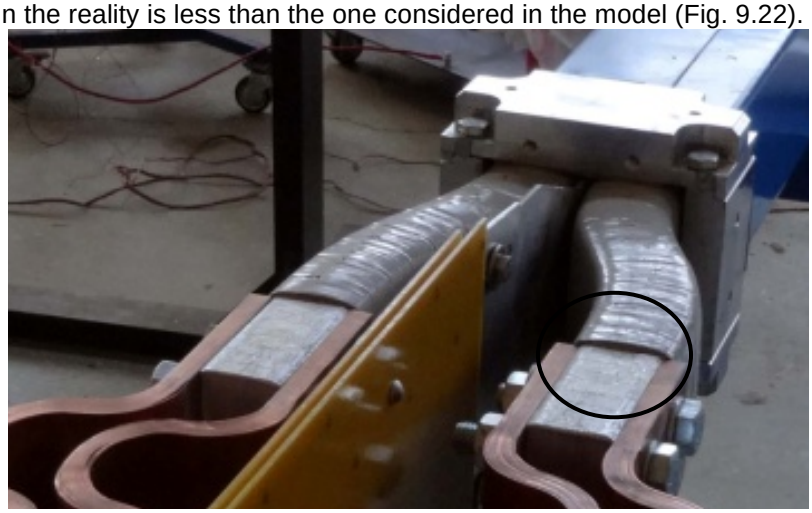

Figure 9.22: Edge zone

For a more accurate estimation of the shear stress in x-z plane another structural model is build considering only the high voltage insulation and the aluminium conductor. The results for this model must be lower in terms of stress compared the previous model because the geometrical discontinuity is lower.
The "reduced" model of the CC Busbar, which includes only the conductor and the high-voltage insulation, is represented in *Fig. 9.23.* Since the PF and TF Busbars have the same type of high-voltage insulation at the ends near the thermal expansion compensator, the model in Fig. *9.24* represents both.

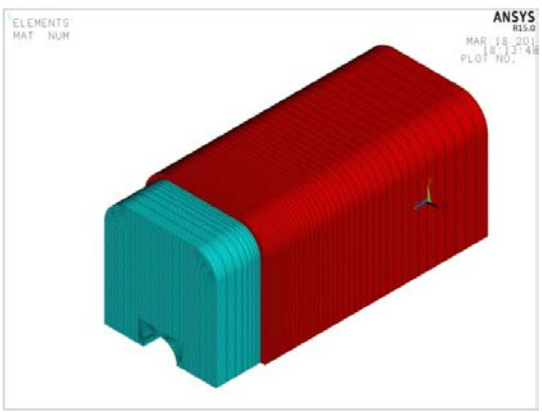

Figure 9.23

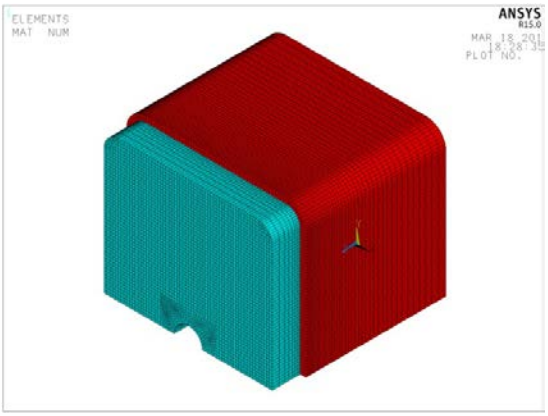

Figure 9.24

Figure 9.25 shows the results of the "reduced" models in terms of x-z shear stress on the PF and TF busbar ends.

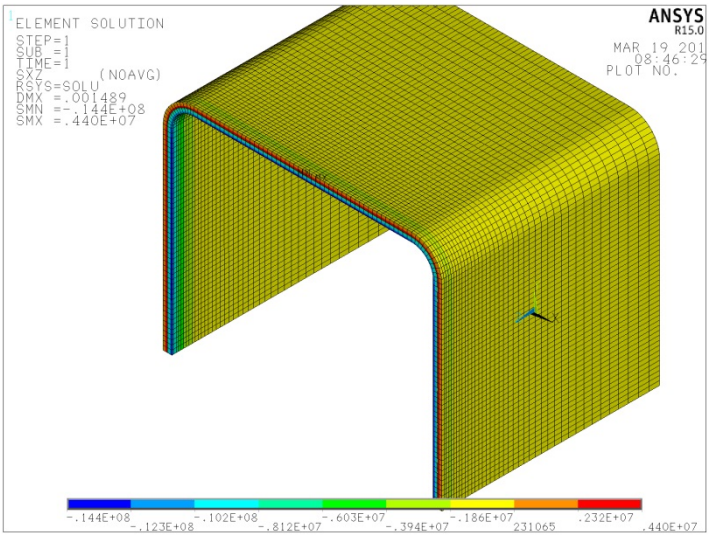

Figure 9.25

The max shear and von Mises stress calculated with the "reduced" model are given in Table 9.5 and Table 9.6 respectively.

Table 9.5

Busbar Type	Max Shear Stress
CC Busbar	10.6 MPa
PF/CS & TF Busbar	14.4 MPa

Table 9.6

Busbar Type	Max Von Mises Stress
CC Busbar	20 MPa
PF/CS & TF Busbar	26.5MPa

10. Contact analysis for insulation detachment study

10.1 Description of FEM model

This model has been developed for studying the possibility of insulation detachment, which can lead to the formation of air gaps in the insulation. The model used in this analysis is a 2-D model, in which "unidirectional' contact elements are implemented on the interface between the aluminium conductor and the high voltage insulation and also on the surface between the high voltage insulation and the aluminium separator.
Even though in the real Busbars these interface surfaces should be bonded (by epoxy or other resin), in the model an ideal contact with no bonding has been used. This means that the in the model there isn't any "glue" between aluminium and insulation. This rough approximation is considered in order to highlight the areas where the formation of air gaps is theoretically possible. For this reason no detailed contact definition and description the contact/detachment behaviour has been used. Only the PF Busbar was investigated, the model is shown in *Fig. 10.1.*

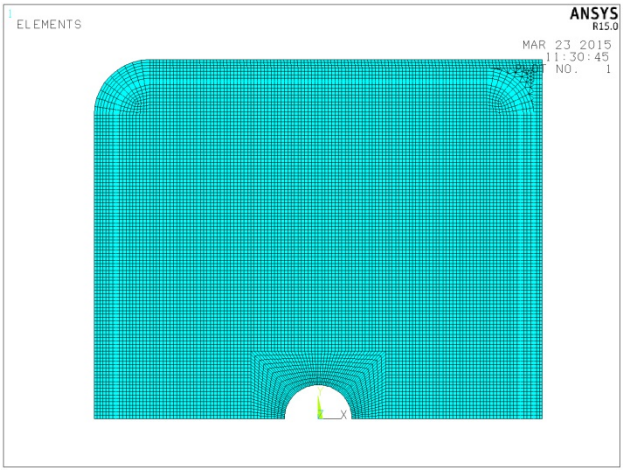

Figure 10.1

Four different contact surfaces are defined. One contact surface is for the area around the separator; Fig. 10.2 shows the target elements with the normals for this area. Target elements are associated with aluminium separator and contact elements with the insulation.

Figure 10.2: Target element of the separator with normals

In the surface between the high voltage insulation and the conductor three different contact surfaces are defined. These surfaces have different ID numbers so as to reduce the computation time. The three contact surfaces are partially overlapped (Fig. 10.3) in order to implement a real contact also after sliding of the elements in the border between the two surfaces. Target elements are associated with aluminium conductor and contact elements with the insulation.

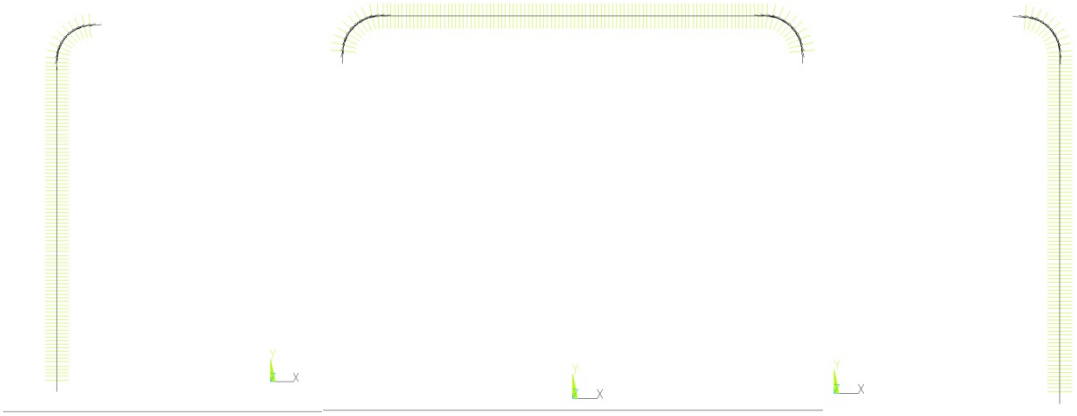

Figure 10.3: Contact and Target elements with normals

10.1.1 Element Types

The model was created using 2-D plane elements. Contact and target elements were used to define contact interfaces. Table 10.1 lists the used elements.

Table 10.1

Element type	Key option	Value	Description
TARGE169	2	0	Automatically constrained by ANSYS

Element type	Key option	Value	Description
CONTA172	2	1	Penalty function
	5	3	Close gap/reduce penetration with auto CNOF
	7	2	Change in contact predictions made to maintain a reasonable time/load increment
	9	2	Exclude initial penetration/gap
	12	0	Standard contact
PLANE182	3	2	Axisymmetric

10.1.2 Real Constants and Debonding Definition

As above discussed, the model assumes an ideal contact with zero bonding between the aluminium conductor and the insulation. With this hypothesis, the solution will indicate the region where the formation of a gap in the insulation could be possible.
The default values were used for the real constants on the contact interface between the high voltage insulation and the aluminium conductor.

10.1.3 Sliding Surfaces and Coefficient of Friction

According to the ITER magnet structural design criteria [11] we assume that::

-Insulation layers are frequently in sliding contact with metallic or non-metallic surfaces. The behaviour of the sliding interface must be strictly assessed.
The allowable coefficient of friction (μ) must always be determined in a conservative manner. In some cases it is conservative to permit a coefficient of friction higher than the average measured value and, in some cases, lower than the measured value. The guidelines are:

$$\mu_{max} = 0.4$$
$$\mu_{min} = 0.1$$

These guidelines may be adjusted for interfaces where specific materials and requirements are defined and justified by test data. Friction values outside the range 0.1-0.4 require exceptional justification. The cases of frictionless slip (μ=0) and no slip (but allowing gaps to open) must be considered as extremely unlikely events in the assessment (Criteria Level C or D shall be applied, depending on the potential consequences of the event).

In the event of cyclic displacements or loads being applied to a sliding interface (including thermal cycling) then ratcheting effects must be considered. Generally positive effects must be taken to prevent ratcheting. In a ratcheting analysis, the effect of variable friction in each sliding direction must also be considered, with a friction factor difference of at least 0.1 in each direction.

For this reason, we consider different friction coefficient and we compare the results.

10.2 Material properties, loads and boundary condition

The material properties in this model are the same as in Chapter 7.3 and the temperature field is the same as in Chapter 8.2.2. (Fig. 10.2).

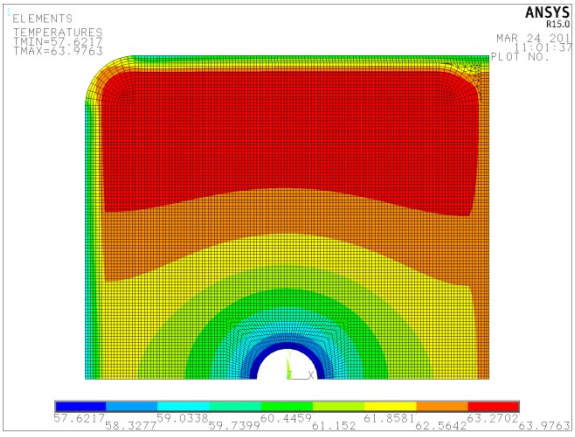

Figure 10.4

Symmetric boundary conditions are the same of the model in Cap. 9.3.1

10.3 Results with different friction coefficients

The analyses are carried out considering three values of friction coefficient, equal to 0.4, 0.2, 0.0 respectively. In all cases, 8 substeps where sufficient to obtain convergence of the solution. The time at the end of the loadstep used in the simulation is at least 500.
The trend is similar for all the coefficient of friction considered. The maximum dimension of the gaps is around 0.01 mm. The highest gap values are always in the external side of the model (opposite to the separator) and the maximum value near the separator reaches 0.002 mm. *Figures 10.5, 10.6, 10.7* show the profile of the gap width in the three cases considered.

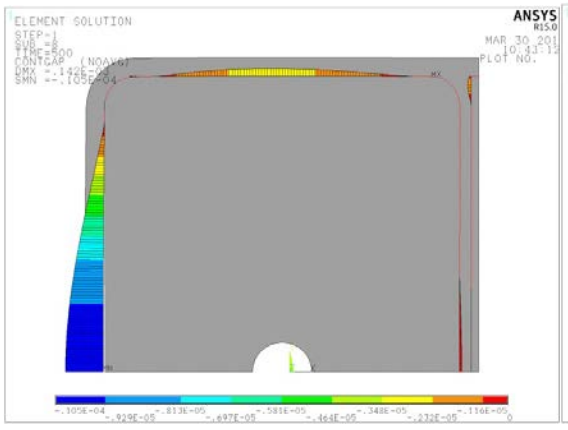

Figure 10.5:Gap distance-0.4 friction coefficient

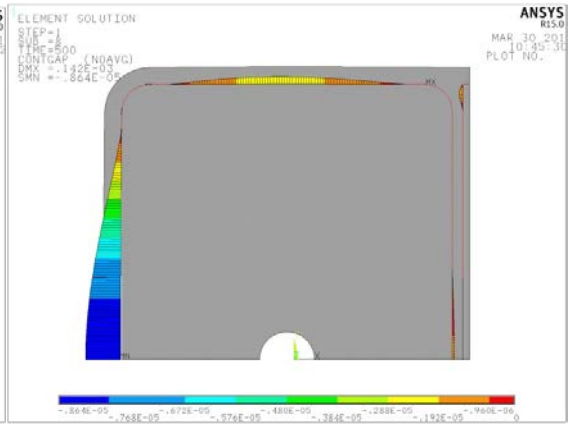

Figure 10.6: Gap distance-0.2 friction coefficient

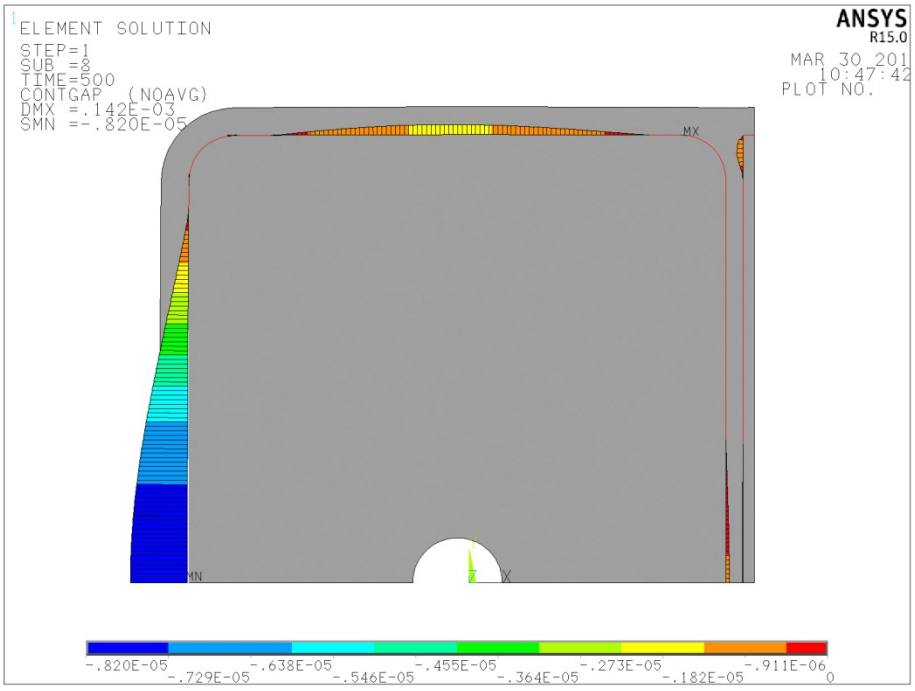

Figure 10.7: Gap distance-0.0 friction coefficient

11. Conclusion and advice for the manufacturing

Thermo-structural analysis on CC, TF and PF&CS Busbar has proved that stress and strain on the high voltage insulation do not exceed the criteria for magnet insulation [11]. The most critical zone is the end of the Busbar, where the geometrical discontinuity of the end of the insulation layer leads to relatively high shear stresses (Fig. 11.1).

Figure 11.1: Edge zone [8]

Since the DC Busbar insulation is made of a very peculiar material, for which the fatigue stress criteria are not well established, we cannot exclude that the cyclic thermal load could lead to damage in this zone due to shear stress.
Fortunately, the electrical field in this area is not critical and can't lead to partial discharges, because the separator is far from the conductor. This fact substantially reduces the possibility of failure.
Nevertheless, in order to reduce the stresses in the zone of the busbar end, it is advisable that, during manufacturing, the thickness of the insulation should be progressively reduced by the reducing the number of wrapped layers.
The contact analysis doesn't evidence any critical area, in fact, even a complete debonding of the high voltage insulation from the aluminium surface will not lead to considerable gaps. The maximum gap width will be lower than 0.01 mm.

Another possible critical point could be identified in the area around the edge of the separator in *Fig. 11.2.* This point is outside of the high voltage insulation of the conductors *and* wasn't analysed adequately because there isn't sufficient information about the mechanical properties of the material (pure epoxy resin) used in this zone.
This area is filled with a high viscosity resin during the assembly of the two insulated busbars with the separator. This point can be critical because a slight increase of the electric field and a mechanical stress concentration can be present at the same time around the separator edge. The levels of electric field and of mechanical stress are certainly low in absolute terms, however, the mechanical properties of the high-viscosity epoxy resin should be verified and a local stress analysis could be carried out. In any case, the radius of curvature of the separator edge is the leading variable for both phenomena. The smaller the radius of curvature, the larger will be the electrical field and the mechanical stress. For this reason, it is advisable to keep the radius as large as possible (2.5 mm is the maximum value possible because the thickness of the separator is 5 mm).

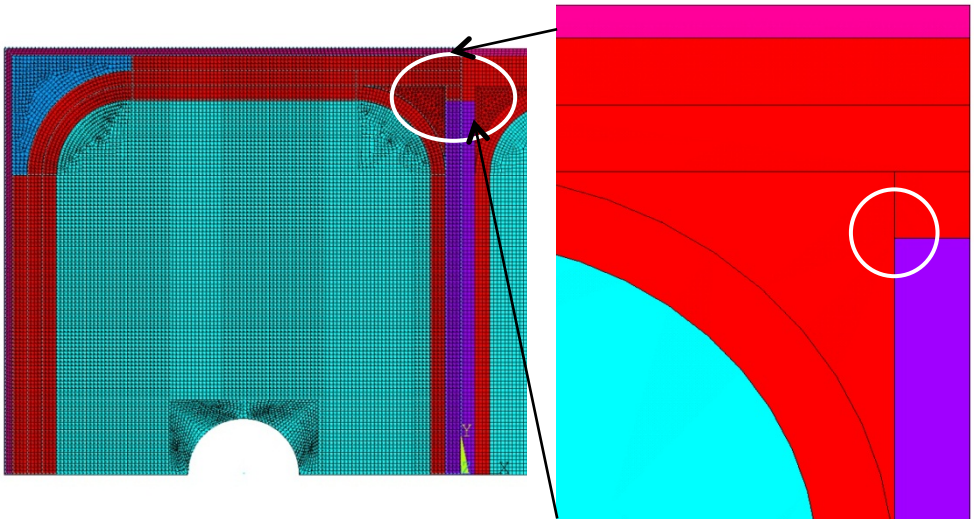

Figure 11.2

12. Bibliography

[1] R. Haange, "*The ITER Project" (presentation)*, Saint Paul les Durance, September, 2013.

[2] "www.Iter.org," [Online].

[3] R. Haange, "*ITER Project - Specific Goals, Progress and present status of Construction" (presentation) ,* Saint Paul Les Durance, September 2013.

[4] S. Orlandi, "*ITER Project: Lesson for Nuclear Engineer-Enter Fusion Technology in ITER after thirty three years of experience in an industrial system on fission technology in Chernobyl and Fukushima" (presentation)*, Lecture Slides, Pisa University, May 2013.

[5] Inho Song, "*System Design Description Document of Coil Power Supply System"*, ITER document 33JWDM, July 2010.

[6] J.C. Gascon, J. Hourtoule, I. Benfatto, S. Nair, J. Tao, J. Goff, "*Design, Chellenges and key Features for the ITER Electrical Power Distribution" (presentation)*, Saint Paul Lez Durance, Iter Organization, France, Jun 2011.

[7] J. Goff, J. Gascon, A. Mankani, I. Song, "*The ITER Magnet Power Supplies and Control System"*, Saint Paul Les Durance, France, ITER document 34M45C.

[8] V. Lokiev, A. Shabanov, S. Kovalev, "*System Design Description Document for SN, FDU, DC Busbars and Instrumentation. Part V. DC Busbars*", ITER Document NCKS64, December 2014.

[9] S. Beteev, D.V. Efremov Institute of Electrophysical Apparatus, "*Analysis of the TF Busbars Electric Field Distribution*", ITER Document PJRDGR, November 2014.

[10] D.V. Efremov Istitute of Electrophysical Apparatus, *Stress analysis of the PF, CS, TF and CC Busbars*, ITER Document PGDM3A, Jun 2014.

[11] "*Properties of magnets insulation: Structural Design Criteria for ITER Magnet Components* (SDC-MC)", Annex A, Iter Document 222RGU, May 2004

[12] H. D. Kim, H. G. Kim, J. J. Park, T. W. Kim and J. H. Kim, "*Mechanical and Electrical Properties of Mica/Epoxy Composite*", in Proceedings of the 5" International Conference on Properties and Applications of Dielectric Materials, Seoul, Korea, May 25-30,1997.

[13] W. J. Nuttall, "*Fusion as an Energy Source: Challenges and Opportunities*", IOP Istitute of Physics, IOP Publication, September 2008.

[14] M. Kikuchi, K. Lackner, M. Q. Tran, "*Fusion Physics"*, International Atomic Energy Agency, Vienna, 2012.

[15] G. Meneghetti, M. Manzolaro, Introduzione all'analisi termica con il codice di calcolo ANSYS, Libreria Progetto, Padova, 2012.

[16] G. Meneghetti, M. Manzolaro, M. Quaresimin, Introduction to static structural analysis with ANSYS numerical code, Libreria Progetto, Padova 2013.

[17] E. Madenci, I. Guven, "*The Finite Element Method and Applications in Engineering Using ANSYS*" , Springer, New York, 2006.

[18] ASM International. Hanbook Commiittee, "*Engineered materials handbook"*, Volume 1 - Composites, Materials Park, OH, 1995.

13. Annex I : LSM tape (ТУ 16-88 И79.0168.001 ТУ)

The LSM tape used for the insulation of the Busbars is a three-layer composition of fiberglass, mica paper and lavsan polyester film impregnated and glowed between each other with a modified epoxy-novolac binder. Heat resistance class F (155 ^{0}C). The LSM type tape is used for the insulation in electric machines with voltage up to 13,8 kV. Hardened state: 3 – 5 hours at the temperature 160 ^{0}C.

Technical characteristics:

Table 13.1 : Technical characteristics LSM Tape

Parameter	Test type	Unit	LSM	
Rated thickness	IEC 371-2, GOST 26103, DIN 53111	mm	0.14+0.02-0.01	0.16±0.02
Mass fraction of components: Mica, not less than Binder, not more than	IEC 371-2, GOST 26103	%	30 35±5 1,5	33 35±5 1,5
Electric strength, not less than	GOST 26103 GOST 6433.3, IEC 371-2, 243 DIN 53481 ASTM D-149-75	kV/mm	35	35
Specific breaking load	IEC 371-2, GOST 26103	H/cm	120	120
Surface density	IEC 371-2, GOST 26103	g/m^2	230±30	155±30
Dielectric loss tangent, not more than: in initial state at t= 130^{0}C at t= 155^{0}C	GOST 26103 GOST 6433.3, IEC 371-2, 243 DIN 53481 ASTM D-149-75	-	 - 0,25 0,45	 - 0,25 0,45
Binder fluidity, not less than	IEC 371-2, GOST 26103	%	45	45

The tape is delivered in rolls: 100±10 mm in diameter, from 15 to 870 mm in width, taped with film out on a rigid bush with inner diameter 36±1 mm. The shelf life is 4 months from the date of manufacturing. Transport packing is in accordance with GOST 26103.

14. Annex II : Geometry APDL scripts

CC Busbar cross section geometry

```
/PREP7
k,1,0,0,0
k,2,0.0075,0,0
K,3,-0.0075,0,0
K,4,0,0.0075,0
K,5,0.025,0,0
K,6,0.025,0.04,0
K,7,0.015,0.05,0
K,8,0.015,0.04,0
K,9,-0.025,0,0
K,10,-0.025,0.04,0
K,11,-0.015,0.05,0
K,12,-0.015,0.04,0
K,13,0.027,0,0
K,14,0.027,0.04,0
K,15,-0.027,0,0
K,16,-0.027,0.04,0
K,17,0.015,0.052,0
K,18,-0.015,0.052,0
K,19,0.029,0,0
K,20,0.029,0.05,0
K,21,-0.029,0,0
K,22,-0.029,0.04,0
K,23,0.015,0.054,0
K,24,-0.015,0.054,0
k,25,0.01,0,0
K,26,0,0.01,0
K,27,0.01,0.01,0
K,28,-0.01,0.01,0
K,29,-0.01,0,0
K,30,0.025,0.01,0
K,31,-0.025,0.01,0
K,32,0.029,0.054,0
K,33,0.029,0.052,0
K,34,0.027,0.05,0
K,35,0.027,0.052,0
K,36,-0.031,0,0
K,37,-0.031,0.04,0
K,38,-0.015,0.056,0
K,39,-0.032,0,0
K,41,0.029,0.056,0
K,42,0.029,0.057,0
K,44,-0.032 ,0.057,0
K,45,-0.031,0.056,0

LSTR,5,30
LSTR,30,6
LSTR,5,13
LSTR,13,14
LSTR,19,20
LSTR,8,12
LSTR,7,11
LSTR,17,18
LSTR,23,24
LSTR,2,25
LSTR,2,25
LSTR,25,27
LSTR,26,27
LSTR,28,26
LSTR,28,29
LSTR,3,29
LSTR,29,9
LSTR,9,15
LSTR,15,21
LSTR,9,31
LSTR,31,10
LSTR,15,16
LSTR,21,22
```

```
LSTR,22,16
LSTR,16,10
LSTR,4,26
LSTR,31,28
LSTR,30,27
LSTR,5,25
LSTR,8,6
LSTR,6,14
LSTR,8,7
LSTR,7,17
LSTR,17,23
LSTR,12,11
LSTR,11,18
LSTR,18,24
LSTR,12,10
LSTR,13,19
LSTR,14,34
LSTR,20,33
LSTR,33,32
LSTR,23,32
LSTR,17,35
LSTR,35,33
LSTR,34,20
LSTR,34,35
LSTR,21,36
LSTR,36,37
LSTR,37,45
LSTR,37,22
LSTR,32,41
LSTR,41,42
LSTR,36,39
LSTR,44,42
LSTR,39,44
LSTR,45,38
LSTR,38,41
LSTR,38,24
LSTR,44,45

LARC,2,4,1,0.0075,
LARC,3,4,1,0.0075
LARC,6,7,8,0.01
LARC,14,17,8,0.012
LARC,10,11,12,0.01
LARC,16,18,12,0.012
LARC,22,24,12,0.014

AL,28,1,27,11
AL,10,11,12,25,60
AL,15,61,25,13,14
AL,16,14,26,19
AL,26,13,12,27,2,29,6,37,20
AL,29,62,31
AL,6,31,7,34
AL,37,34,64
AL,3,4,30,2,1
AL,30,63,32,62
AL,7,32,8,35
AL,24,64,35,65
AL,17,19,20,24,21
AL,38,5,45,39,4
AL,45,40,44,46
AL,63,39,46,43
AL,43,44,41,42,33
AL,8,33,9,36
AL,23,65,36,66
AL,18,21,23,22
AL,47,22,50,48
AL,9,42,51,57,58
AL,66,58,56,49,50
AL,53,48,49,59,55
AL,56,57,52,54,59
!local coordinate system
CSKP,11,0,10,16,31,1,1,
CSKP,12,1,12,11,10,1,1,
CSKP,13,0,11,18,45,1,1,
CSKP,14,1,8,6,7,1,1,
```

CSKP,15,0,6,14,35,1,1,

PF&CS Busbar cross section geometry

```
/PREP7
k,1,0,0,0
k,2,0.01,0,0
K,3,-0.01,0,0
K,4,0,0.01,0
K,5,0.02,0,0
K,6,0.02,0.02,0
K,7,-0.02,0.02,0
K,8,-0.02,0,0
K,9,0,0.02,0
K,10,0.06,0,0
K,11,0.06,0.09,0
K,12,0.05,0.09,0
K,13,0.05,0.1,0
K,14,-0.05,0.1,0
K,15,-0.05,0.09,0
K,16,-0.06,0.09,0
K,17,-0.06,0,0
K,18,0.064,0,0
K,19,0.064,0.09,0
K,20,0.05,0.104,0
K,21,-0.05,0.104,0
K,22,-0.064,0.09,0
K,23,-0.064,0,0
K,24,0.0665,0,0
K,25,0.0665,0.1,0
K,26,0.064,0.1,0
K,27,0.0665,0.104,0
K,28,0.0665,0.1065,0
K,29,-0.05,0.1065,0
K,30,-0.0665,0.09,0
K,31,-0.0665,0,0
K,32,0.0665,0.1085,0
K,33,0.0665,0.1095,0
K,34,-0.0695,0.1095,0
K,35,-0.0685,0.1085,0
K,36,-0.0685,0,0
K,37,-0.0695,0,0

LSTR,    10,    11
LSTR,    13,    14
LSTR,    16,    17
LSTR,    23,    22
LSTR,    21,    20
LSTR,    19,    18
LSTR,    24,    25
LSTR,    25,    26
LSTR,    26,    19
LSTR,    31,    30
LSTR,    36,    35
LSTR,    37,    34
LSTR,    29,    28
LSTR,    35,    32
LSTR,    34,    33
LSTR,    16,    15
LSTR,    15,    14
LSTR,    16,    22
LSTR,    22,    30
LSTR,    14,    21
LSTR,    21,    29
LSTR,    12,    13
LSTR,    12,    11
LSTR,    11,    19
LSTR,    13,    20
LSTR,     6,     9
LSTR,     9,     7
LSTR,     7,     8
LSTR,     8,     3
LSTR,     2,     5
LSTR,     5,     6
LSTR,     4,     9
LSTR,    20,    27
```

```
LSTR,      25,      27
LSTR,      28,      32
LSTR,      27,      28
LSTR,      32,      33
LSTR,      20,      27
LSTR,      25,      27
LSTR,      28,      32
LSTR,      27,      28
LSTR,      32,      33

LARC,16,14,15,0.01,
LARC,13,11,12,0.01,
LARC,22,21,15,0.014,
LARC,20,19,12,0.014,
LARC,3,4,1,0.01,
LARC,4,2,1,0.01,
LARC,30,29,15,0.0165,

LSTR,      20,      27
LSTR,      25,      27
LSTR,      28,      32
LSTR,      27,      28
LSTR,      32,      33
LSTR,      37,      36
LSTR,      36,      31
LSTR,      31,      23
LSTR,      23,      17
LSTR,      17,       8
LSTR,       3,       1
LSTR,       1,       2
LSTR,       5,      10
LSTR,      10,      18
LSTR,      18,      24
LSTR,      15,      12
LSTR,      15,      12
LANG,      14,      29,90, ,
LANG,      11,      30,90, ,
LANG,      33,      26,90, ,
LANG,       3,       7,90, ,
LANG,       1,       6,90, ,
LSTR,35,34
```

TF Busbar Cross section geometry

```
/PREP7
k,1,0,0,0
k,2,0.01,0,0
K,3,-0.01,0,0
K,4,0,0.01,0
K,5,0.02,0,0
K,6,0.02,0.02,0
K,7,-0.02,0.02,0
K,8,-0.02,0,0
K,9,0,0.02,0
K,10,0.06,0,0
K,11,0.06,0.09,0
K,12,0.05,0.09,0
K,13,0.05,0.1,0
K,14,-0.05,0.1,0
K,15,-0.05,0.09,0
K,16,-0.06,0.09,0
K,17,-0.06,0,0
K,18,0.0645,0,0
K,19,0.0645,0.09,0
K,20,0.05,0.1045,0
K,210,0.05,0.107,0
K,220,0.05,0.109,0
K,230,0.05,0.11,0
K,24,0.0670,0,0
K,25,0.0670,0.1,0
K,26,0.0645,0.1,0
K,40,0.0645,0.1045,0
K,27,0.0670,0.1045,0
K,28,0.0670,0.1070,0
K,29,0.0670,0.109,0
K,30,0.0670,0.11,0
```

```
LSTR,      10,      11
LSTR,      13,      14
LSTR,      16,      17
LSTR,      16,      15
LSTR,      15,      14
LSTR,      12,      13
LSTR,      12,      11
LSTR,       6,       9
LSTR,       9,       7
LSTR,       7,       8
LSTR,       8,       3
LSTR,       2,       5
LSTR,       5,       6
LSTR,       4,       9
LARC,16,14,15,0.01,
LARC,13,11,12,0.01,
LARC,3,4,1,0.01,
LARC,4,2,1,0.01,
LANG,       3,       7,90, ,
LANG,       1,       6,90, ,
LSTR,      15,      12
LSTR,       3,       1
LSTR,       1,       2
LSTR,       5,      10
LSTR,      17,       8
LSTR, 28,29
LSTR,29,30

k,100,-0.121,0,0
k,200,-0.111,0,0
K,300,-0.131,0,0
K,400,-0.121,0.01,0
K,500,-0.101,0,0
K,600,-0.101,0.02,0
K,700,-0.141,0.02,0
K,800,-0.141,0,0
K,900,-0.121,0.02,0
K,1000,-0.061,0,0
K,1100, -0.061,0.09,0
K,1200, -0.071,0.09,0
K,1300, -0.071,0.1,0
K,1400, -0.171,0.1,0
K,1500, -0.171,0.09,0
K,1600, -0.181,0.09,0
K,1700,-0.181,0,0


LSTR,      1000,      1100
LSTR,      1300,      1400
LSTR,      1600,      1700
LSTR,      1600,      1500
LSTR,      1500,      1400
LSTR,      1200,      1300
LSTR,      1200,      1100
LSTR,       600,       900
LSTR,       900,       700
LSTR,       700,       800
LSTR,       800,       300
LSTR,       200,       500
LSTR,       500,       600
LSTR,       400,       900
LARC,1600,1400,1500,0.01,
LARC,1300,1100,1200,0.01,
LARC,300,400,100,0.01,
LARC,400,200,100,0.01,
LANG,       32,       700,90, ,
LANG,       30,       600,90, ,
LSTR,      1500,      1200
LSTR,       300,       100
LSTR,       100,       200
LSTR,       500,      1000
LSTR,      1700,       800
LSTR,      18,      24
LSTR,      18,      19
```

```
LSTR,      19,      26
LSTR,      26,      25
LSTR,      24,      25
K,101,0.0605,0,0
K,111,0.0605,0.09,0
K,131,0.05,0.1005,0
K,161, -0.0605,0.09,0
K,171,-0.0605,0,0
K,141,-0.05,0.1005,0
K,1310,-0.071,0.1005,0
K,1410,-0.171,0.1005,0
K,1610, -0.1815,0.09,0
K,1710,-0.1815,0,0
K,1720,-0.1855,0,0
K,1620,-0.1855,0.09,0
K,1420,-0.171,0.1045,0

K,1730,-0.188,0,0
K,1740,-0.190,0,0
K,1750,-0.191,0,0

K,1630,-0.188,0.09,0
K,1640,-0.190,0.09,0
K,1650,-0.191,0.09,0
K,1550,-0.191, 0.11,0
K,1540,-0.190, 0.109 ,0

K,1430,-0.171,0.107,0
K,1440,-0.171,0.109,0
K,1450,-0.171,0.11,0

LSTR,      101,      111
LSTR,      131,      141
LSTR,      161,      171
LSTR,      1000,      171
LSTR,      17,      171
LSTR,      10,      101
LSTR,      18,      101
LSTR,      1310,     1410
LSTR,      1710,      1610
LSTR,      1730,      1630
LSTR,      1740,      1640
LSTR,1700,1710
LSTR,1710,1720
LSTR,1720,1730
LSTR,1730,1740
LSTR,1440,220
LSTR,220,29
LSTR,1620,1720
LSTR,1420,20
LSTR,1430,210
LSTR,20,40
LSTR,25,27
LSTR,27,28
LSTR,210,28
LSTR,230,30
LSTR,230,1450
LSTR,1550,1450
LSTR,1650,1550
LSTR,1540,1440
LSTR,1540,1640
LSTR,1650,1750


LARC,161,141,15,0.0105,
LARC,111,131,12,0.0105,
LARC,1310,161,1200,0.0105,
LARC,1310,161,1200,0.0105,
LARC,1410,1610,1500,0.0105,
LARC,1420,1620,1500,0.0145,
LARC,19,20,12,0.0145,
LARC,1430,1630,1500,0.017,
LARC,1640,1440,1500,0.019,
LSTR,40,27
LSTR,26,40
LSTR,1650,1640
```

LSTR,1630,1640
LSTR,1630,1620
LSTR,1620,1610
LSTR,1610,1600
LSTR,1550,1540
LSTR,1400,1410
LSTR,1410,1420
LSTR,1420,1430
LSTR,1430,1440
LSTR,1440,1450
LSTR,1300,1310
LSTR,14,141
LSTR,13,131
LSTR,131,20
LSTR,20,210
LSTR,210,220
LSTR,220,230
LSTR,11,111
LSTR,111,19
LSTR,1750,1740
LSTR,1310,141
LSTR,16,161
LSTR,161,1100